Chemical and Genetic Analysis of the Mitochondrial Unfolded Protein Response (UPR^{mt})

by

MUSTAFI RAISA AMIN

DISSERTATION

Submitted in partial fulfillment of the requirements

for the degree of Doctor of Philosophy at

The University of Texas-Arlington

August 2021

Arlington, Texas

Supervising Committee:

Dr. Mark W. Pellegrino, Supervising Professor

Dr. Todd A. Castoe

Dr. A. Clay Clark

Dr. Subhrangsu S. Mandal

Dr. Laura D. Mydlarz

Copyright © by Mustafi Raisa Amin 2021

All Rights Reserved

Acknowledgments

The last five years of my life have often been hectic and challenging, but I believe they have allowed me to grow as a person. For this, I would like to thank my friends, colleagues, and mentors in the Biology department at UTA who have supported and encouraged me in the last few years and made the Ph.D. experience a bit more fun along the way. I would like to thank my supervising professor, Dr. Mark Pellegrino, who allowed me to work in his lab and provided me with the knowledge and guidance needed to complete my work. I am also thankful for my other committee members, Dr. Clay Clark, Dr. Laura Mydlarz, Dr. Todd Castoe, and Dr. Subhrangsu Mandal, who have provided their insight and support into my projects. The opportunities and experiences gained in the last few years have helped pave the path for my future.

Dedication

I would like to dedicate this dissertation to all my loved ones, especially my parents and brother, who have encouraged and supported me from the beginning. To my friends, who were always there for my grievances and my joy. Lastly, I would like to thank those individuals who have impacted my life from near and far, for all the ways they have helped shape my life.

Abstract

Mitochondria are essential for energy production, metabolic signaling, calcium homeostasis, and other roles. Consequently, mitochondrial dysfunction can result in cellular decline and the onset of disease. Cells use the mitochondrial unfolded protein response (UPR^{mt}) to facilitate the recovery of damaged mitochondria to restore homeostasis. Recent studies have shown that the UPR^{mt} plays a vital role in tumorigenesis and cancer survival. Therefore, UPR^{mt} inhibition may be used as an anticancer strategy with great therapeutic results. Moreover, a known paradigm exists between mitochondrial stress signaling and the regulation of organismal lifespan. Since the UPR^{mt} is activated during mitochondrial stress, it is believed to be involved in the process of aging, albeit with some controversy. In addition to organismal aging, the UPR^{mt} is associated with protecting the host during infection via the regulation of innate immunity. Understanding the mechanisms associated with UPR^{mt} activation, therefore, has relevance to our fundamental understanding of mitochondrial recovery, as well as having potential practical applications in the biomedical field. With these implications in mind, my dissertation aims to investigate the regulation of the UPR^{mt} using genetic and chemical means, using the model organism *Caenorhabditis elegans*.

Contents

Chapter 1: Introduction

I. Origin of mitochondria

Mitochondria are double-membraned intracellular organelles found in eukaryotic cells. They are most commonly known as the powerhouse of the cell as they are responsible for the vast majority of ATP production. Evidence indicates that mitochondria arise from the bacterial phylum α-Proteobacteria (alphaproteobacteria) that were engulfed by a eukaryotic progenitor cell [1] [2]. Similar to their bacterial ancestor, mitochondria have functionally distinct outer and inner membranes surrounding the intermembrane space (IMS) and internal matrix. Likewise, they contain a circular genome that is approximately 16-kb long in several mammalian species. The mitochondrial genome encodes a small number of proteins (13 in mammals) consisting of subunits of the electron transport chain (ETC) and ATP synthase, as well as mitochondrial rRNAs and tRNAs needed for mitochondrial translation [1].

The mtDNA is associated with several proteins in discreet nucleoids and anchored to the mitochondrial inner membrane. Transcription factor A of mitochondria (TFAM), the mtDNA helicase Twinkle, and mitochondrial single-stranded DNA-binding protein (mtSSB) are co-localized within nucleoids along with the mtDNA [3, 4]. The binding of TFAM to mtDNA helps with condensation and packaging into nucleoids, suggesting that TFAM is essential for both the transcription and maintenance of mtDNA. Moreover, TFAM is also expressed in the nucleus and regulates nuclear genes [4].

II. Mitochondrial structure

The outer mitochondrial membrane separates the mitochondria from the cytoplasm. It is a porous structure that allows for the transfer of ions and small uncharged molecules through mitochondrial porins, also known as voltage-dependent anion channels (VDACs) [5]. Larger molecules,

including proteins, are imported with the help of special translocases. The inner mitochondrial membrane encapsulates the mitochondrial intermembrane space and the matrix components and has a more tightly regulated diffusion mechanism. Ions and molecules are transported across the inner membrane using transport proteins, each specific for particular molecules. The ETC complexes (I to IV) are located in the inner membrane and function in coupling electron flow with the pumping of protons from the matrix to the intermembrane space. This creates an electrochemical gradient across the inner membrane which is used to drive ATP synthesis via the ATP synthase complex. The intermembrane space (IMS) is enclosed by the outer and the inner membrane. The inner membrane encapsulates the matrix, which drives the tricarboxylic acid (TCA) cycle. The TCA cycle is a series of enzymatic reactions that metabolizes pyruvate and fatty acids for energy production, producing high energy electron donors (NADH and $FADH_2$) for ETC-mediated energy production [5] (Figure 1).

III. Mitochondrial functions

Mitochondria are multifunctional organelles that help maintain and regulate cellular homeostasis. Their primary function is energy production through oxidative phosphorylation (OXPHOS). In addition, mitochondria contain several enzymes involved in the TCA cycle and the metabolism of amino acids, carbohydrates, and fatty acids. Mitochondria generate metabolic byproducts such as reactive oxygen species (ROS) under several conditions such as cellular respiration and pathological conditions, including mild ischemia or ionizing radiation [6]. ROS also plays vital roles in cell signaling, calcium homeostasis, and the regulation of apoptosis [7].

The powerhouse of the cell:

Cellular respiration is a metabolic pathway employed by cells to generate energy (ATP) using oxygen for some of its reactions. Energy production in cells is dependent on nutrient availability,

tissue type, and mitochondrial respiratory capacity. In healthy cells, pyruvate is produced from glycolysis, one of the main pathways involved in cellular respiration [8]. Glycolysis is a multi-step pathway occurring in the cytoplasm that generates pyruvate from the oxidation of glucose, which is then transported across the IMM and further metabolized through the TCA cycle to generate energy. However, mitochondrial respiration is repressed during periods of low oxygen (also known as hypoxia) since it is needed for further oxidation of pyruvate and NADH produced in glycolysis [8]. Instead, NAD+ is regenerated from NADH by the reduction of pyruvate to lactate using lactate dehydrogenase in the cytoplasm. This pathway is commonly used in muscles during long periods of exercise, as well as the intestine and renal medulla of the kidneys [9] (Figure 2).

Glutamine is one of the most abundant amino acids present. Its catabolism usually starts within mitochondria to carry electrons onto NADH and $FADH_2$ carriers. Glutamine metabolism releases carbon and nitrogen atoms which are needed to synthesize intermediates involved in the TCA cycle and biosynthesis of nucleotides, glutathione, and other nonessential amino acids [10]. Glutamine is converted to α-ketoglutarate via glutaminase [8]. This conversion is necessary for glutamine anaplerosis, which is used to maintain the TCA cycle during periods of limited glucose [11]. Glutamine anaplerosis is vital for sustaining energy needs in proliferative cells (e.g., T cells during their transition from naïve T cells to effector cells).

Similarly, branched-chain amino acids (BCAAs – leucine, valine, and isoleucine) are essential amino acids and vital cellular energy sources. Cells such as myocytes and adipocytes activate mitochondrial aminotransferases to catabolize BCAAs to support ATP production via the TCA cycle during exercise and fasting [8]. However, the mechanism of BCAA import into mitochondria and their transport is still lesser understood.

Fatty acids are a significant energy source in cells, especially during nutrient-poor conditions, that are broken down during the process known as β-oxidation. The import of fatty acids into mitochondria is a vital rate-limiting step of β-oxidation. Fatty acids are first converted into an acyl-CoA derivative by acyl-CoA synthetase at the mitochondrial outer membrane. Carnitine palmitoyl transferase (CPT-1), present in the mitochondrial outer membrane, conjugates the acyl-CoA derivative to carnitine (producing acylcarnitine) which is necessary for transport across the membrane. Acyl-carnitines are then translocated into the mitochondrial matrix via carnitine-acylcarnitine transferases present at the inner mitochondrial membrane. The fatty acid is liberated from the carnitine by a second carnitine palmitoyltransferase, CPT-2, which then initiates β-oxidation. The acetyl-CoA produced during the oxidation of fatty acids can then be used as a substrate for the TCA cycle [8] (Figure 2).

Biosynthetic hubs:

Mitochondria are critical organelles involved in biosynthetic pathways, including nucleotides, amino acids, glucose, etc. (Figure 3). The following is an overview of some of these biosynthetic pathways.

1. One-carbon metabolism

The one-carbon metabolic pathway involves reactions that produce and transfer activated one-carbon units for *de novo* nucleotide synthesis. Tetrahydrofolate (THF) is a cofactor that functions as a carrier to mediate one carbon reaction for *de novo* nucleotide synthesis. THF is imported into mitochondria using the carrier SLC25A32, where it is converted into 5,10 methylene-THF and glycine by the enzyme serine hydroxymethyltransferase (SHMT2). SHMT2 is bidirectional and favors the generation of glycine and 5,10 methylene-THF. The 5,10 methylene-THF is converted

to 10-formyl THF by the mitochondrial methylenetetrahydrofolate dehydrogenase (MTHFD2). 10-formyl THF can then be used for multiple purposes, including its conversion to THF, formation of formyl-methionine for mitochondrial translation, or hydrolyzation to formate. Mitochondrial formate is a vital source for cytosolic 1 C catabolism. Dihydroorotate dehydrogenase (DHODH) is an enzyme of the inner mitochondrial membrane used to produce orotate needed for *de novo* pyrimidine synthesis [8] [12].

2. Amino acid synthesis

Mitochondria are sites of amino acid synthesis, including glutamine, glutamate, aspartate, alanine, and proline. Glutamine synthetase catalyzes the metabolism of nitrogen by condensing glutamate and ammonia to produce glutamine. Mitochondrial enzymes and transmembrane carriers tightly regulate glutamate metabolism. Glutamate is created and used as a nitrogen source for several reactions involved in metabolic and signaling functions [8].

Pyrroline-5-carboxylate (P5C) is produced from pyrroline-5-carboxylate synthase (P5CS), which can be utilized for proline and ornithine production. The reduction of P5C by P5C reductase creates proline, while ornithine is made from ornithine aminotransferase [13]. Both proline and ornithine metabolism occur within mitochondria.

Aspartate can be produced from oxaloacetate, an intermediate of the TCA cycle, using glutamate-mediated transaminases. When cells lack a direct mode of transport for NAD, they depend on the compartmentalized flux of metabolites to maintain the balance of reducing equivalents NAD/NADH and NADP/NADPH. One of the fundamental mechanisms to compartmentalize these reducing equivalents is through the malate-aspartate shuttle. This shuttle is key to cell survival during stress conditions like exercise when cytosolic NAD^+ is necessary to initiate glucose

catabolism, and mitochondrial NADH is needed for ATP production [14]. As a result, aspartate metabolism is tightly regulated by mitochondrial activity. Also, aspartate and glutamine are precursor molecules for asparagine, synthesized by asparagine synthetase in the cytosol [8] [15].

Alanine is produced via alanine transaminase, which transfers the amino group between glutamate and pyruvate. This reaction generates alanine and α-ketoglutarate, providing both proteogenic alanine and a source of α-ketoglutarate, which can be used for the TCA cycle [15].

3. Gluconeogenesis

Gluconeogenesis is a metabolic pathway involved in the production of glucose. While most of the steps of gluconeogenesis occur in the cytosol, the first step is initiated by the conversion of pyruvate to oxaloacetate via pyruvate carboxylase (PC) in mitochondria. Oxaloacetate is then converted to malate and exported to the cytosol. In the cytosol, oxaloacetate is then converted into phosphoenolpyruvate (PEP) by the phosphoenolpyruvate carboxykinase (PCK) for gluconeogenesis [8] [15].

Calcium homeostasis:

Calcium serves many purposes, including its role as a secondary messenger in signal transduction. Intracellular calcium levels must be tightly controlled to promote optimal cell physiology and ensure accurate signaling. Intracellular calcium is predominantly stored in the endoplasmic reticulum (ER) and can be released either to the cytosol or into mitochondria through defined contact sites. Disruption to calcium homeostasis could lead to cellular toxicity and death and thus needs to be tightly controlled. Mitochondria regulate calcium homeostasis by acting as a storage site to buffer intracellular ion levels and fuel metabolic reactions. Calcium transfer between the ER and mitochondria occurs through defined microdomains known as ER-mitochondrial contact

sites. Calcium is first transported across the mitochondrial outer membrane through VDACs and followed by the mitochondrial inner membrane via the mitochondrial calcium uniporter (MCU). The close contact between the cellular calcium (Ca^{2+}) gates present in the endoplasmic reticulum (ER) and mitochondria forms microdomains that facilitate the increase in calcium concentration in mitochondria [16]. These microdomains allow the entry of extracellular calcium through the plasma membrane into mitochondria, facilitating a link between cellular signaling and mitochondrial function [17]. This rapid diffusion of calcium avoids organelle overload and maintains mitochondrial calcium homeostasis [18] [19].

Innate immunity

The innate immune response is the first line of defense in mammals against disease-causing pathogens. This arm of the immune response consists of physical, chemical, and cellular mechanisms to fight off pathogens before an active infection occurs. Mitochondria act as a central hub in orchestrating various innate immune responses, notably the NLR family pyrin domain-containing 3 (NLRP3) inflammasome and retinoic acid-inducible gene (RIG-I)-like receptor (RLR) pathways. Mitochondria damage-associated molecular patterns (DAMPs) such as mtDNA, ROS, and cardiolipin, are released during host tissue damage that acts as signals for pathogen infection (Figure 4). These molecules are recognized as alarmins that activate the innate immune receptors and initiate the formation of the NLRP3 inflammasome complex. Once formed, the inflammasome complex then activates caspase-1 and ultimately leads to the secretion of IL-1β and IL-18 that promotes an innate immune response [20].

Mitochondria also defend against viral infections via the RLR signaling mechanism using MAVS (Mitochondrial-associated viral signaling) pathway (Figure 5). MAVS, a membrane protein

anchored at the mitochondrial outer membrane, acts as an adaptor of the pattern recognition receptors (PRRs) RIG-I, and MDA-5. These PRRs activate NF-κB or IRF-3/7, resulting in the production of pro-inflammatory cytokines and Type-I interferons during the early phase of infection [20].

Moreover, mitochondria also promote an antibacterial response through the generation of ROS. ROS can be used directly as an antibacterial agent or indirectly in the production of interferon-β (IFN-β). Consistently, a recent study has shown that mice deficient in ROS production showed increased susceptibility to bacteria [21].

Apoptosis:

Apoptosis is a regulated form of cell death occurring naturally during development in the formation of digits and during neurite pruning. However, unregulated apoptosis is often detrimental to organismal fitness and associated with several diseases. Mitochondria are critically involved in the regulation of apoptosis. The mitochondrial apoptotic pathway requires the mitochondrial permeability transition pore (MPTP) complex [22, 23]. The MPTP complex is a transmembrane protein in the IMM which interacts with VDAC at the OMM. The pore is closed under physiological conditions; however, during mitochondrial stress, such as reduced fatty acid oxidation, increased ROS production, or calcium overload, this large complex opens at the IMM. Opening of the MPTP increases the inner membrane permeability allowing for the transport of molecules less than 1.5kDa into the mitochondrial matrix [23], disrupting the metabolic gradients between the cytosol and mitochondria. As a result, there is an influx of water into the mitochondria, causing osmotic swelling until the OMM eventually bursts. This releases cytochrome c and other pro-apoptotic proteins such as apoptosis-inducing factor (AIF), endonuclease G (endoG), and

second mitochondria-derived activator of caspases/direct inhibitor of apoptosis (IAP)-binding protein with low pI (Smac/Diablo) into the cytosol and death of the cell [24].

In the cytosol, cytochrome c forms an apoptosome complex with apoptosis activating factor-1 (Apaf-1) and procaspase-9, which activates caspase-9. Caspase-9, in turn, activates effector caspases such as caspase-3, -6, and -7 [24]. This results in the cleavage of cellular proteins and apoptotic cell death. In addition, AIF and Endo G translocate to the nucleus to cause DNA fragmentation [24, 25].

Additionally, the mitochondrial apoptotic pathway is induced as a cellular response to mtDNA damage, infection, or cytokine deprivation. This results in activation of the pro-apoptotic BH-3 only proteins, e.g., Bid, Bim, Puma, etc. These BH-3 only proteins act as sensors for different cellular stress and may directly bind and induce the pore-forming Bax and Bak proteins. Once activated, the Bax and Bak proteins oligomerize to produce pores in the OMM that releases cytochrome c oxidase. Cytosolic cytochrome c leads to caspase activation and subsequent cell death.

IV. Mitochondrial stress and human diseases

The mitochondrial network is essential for ATP production, synthesizing essential cofactors and amino acids, and serves as a signaling hub for innate immune and apoptotic pathways [26]. However, there are various perturbations to mitochondria homeostasis, including misfolded proteins, calcium overload, deleterious mtDNA accumulation, and increased ROS generation. All these factors can disrupt mitochondrial function, compromising several essential mitochondrial processes that result in cellular decline and disease onset, including neurodegenerative, cardiovascular, metabolic disorders, and cancer.

1. mtDNA and disease

Mitochondrial genome mutations account for many human diseases, including neurodegenerative disorders, metabolic diseases, cardiovascular diseases, gastrointestinal disorders, skin disorders, and cancer. With regards to cancer, one study has shown that more than 50% of mtDNA mutations are associated with carcinogenesis and are located in the 22 mitochondrial tRNA genes. The most common mtDNA mutation is the single nucleotide polymorphism (SNP), 3243A > G transition, that alters leucine mt-tRNA and affects translation of the 13 respiratory subunits. This mutation results in a lesser number of mitochondrial subunits and impaired OXPHOS. In addition, individuals who acquire 10–30% faulty copies of $tRNA^{Leu}$ may develop maternally inherited diabetes and deafness. Furthermore, individuals with 50–90% defective copies can develop mitochondrial encephalomyopathy, lactic acidosis, and stroke-like episodes (MELAS). In addition to mtDNA mutations associated with faulty $tRNA^{Leu}$, other mutations resulting in defective $tRNA^{Ser}$ or $tRNA^{Ile}$ have been associated with deafness and cardiomyopathies, respectively [4].

Interestingly, some evidence shows that both an increased and decreased copy number of mtDNA have been associated with increased cancer incidence, with contradictory findings between some studies for the same type of tumor. For example, both increased and decreased copy numbers caused an increase in the incidence of renal cancer [4].

2. Mitochondrial dysfunction and neurodegeneration

Extensive evidence from animal and clinical studies suggests that mitochondria are crucial in aging, cancer, diabetes, and several neurodegenerative diseases, like Alzheimer's, Parkinson's, and Huntington's disease. Several studies have shown that mitochondrial oxidative damage causes a

cellular change in most late-onset neurodegenerative disorders. Structural changes in mitochondria, including increased mitochondrial fragmentation and decreased mitochondrial fusion, are major factors related to mitochondrial dysfunction and death in aging and age-related diseases [27].

Alzheimer's disease is a late-onset, progressive neurodegenerative disease that is characterized by progressive loss of memory, cognitive functions, and changes in personality and behavior [28, 29]. Two key pathological characteristics are found in the postmortem brains of Alzheimer's patients that include intracellular neurofibrillary tangles and deposits of extracellular neurotoxic amyloid-beta (Aβ) in the brain regions responsible for memory and learning. Alzheimer's disease is also related to the loss of synapses, synaptic function, mitochondrial abnormalities, inflammatory responses, and neuronal loss [27]. The Aβ peptide is generated from the sequential cleavage of amyloid precursor protein (APP), a single-pass transmembrane protein expressed in high levels in the brain. Neuronal studies conducted in postmortem brains of Alzheimer's patients suggest that amyloid precursor protein (APP) derivatives, including Aβ monomers and oligomers, are associated with mitochondrial membranes [30, 31, 32]. One study discovered that full-length APP and C-terminal truncated APP species accrue in mitochondria of progressive AD patients. Some *in vitro* and *in vivo* studies have found APP to accumulate specifically in mitochondrial membranes as the disease progresses. This suggested that APP is associated with mitochondria and disease progression [33, 32]. Another study conducted by Reddy et al. showed decreased activities of several mitochondrial enzymes, including cytochrome oxidase activity, pyruvate dehydrogenase, and α-ketodehydrogenase in the fibroblasts, lymphoblasts, and postmortem brains from AD patients, compared to those of healthy subjects [34]. Several lines of evidence show an increase in lipid peroxidation, free radical production, and oxidative protein and DNA damage in postmortem

brains of AD patients in contrast to healthy individuals [32, 35, 36, 37]. Lastly, postmortem brains of AD patients had a higher number of mutated mtDNA than age-matched control subjects, suggesting an accumulation of deleterious mtDNA in AD pathogenesis that is age-related [38, 39].

Parkinson's disease (PD) is a progressive, age-related neurodegenerative disorder characterized by rigidity, resting tremor, postural instability, and bradykinesia [40]. The hallmark of PD is the degeneration of dopaminergic neurons of the substantia nigra, the structure located in the midbrain that plays an essential role in reward and movement. In recent years, there have been multiple reports between PD and altered expressions of several genes, such as PARK7 (encoding DJ-1), α-synuclein, Parkin, or PINK1 kinase, which perturbs mitochondrial dynamics and function [41]. For example, specific mutations in α-synuclein can lead to its aggregation, delaying the fusion of phagosomes with lysosomes during mitophagy, a selective mechanism used to degrade damaged mitochondria. Also, α-synuclein causes mitochondrial dysfunction by modifying mitochondrial dynamics, inhibiting respiration, and generating excessive ROS [42, 43]. On the other hand, the deletion of PINK1 causes an increase in oxidative stress within mitochondria [44].

Huntington's disease is another neurodegenerative disease characterized by uncontrolled movements, psychiatric disturbances, and dementia. HD typically develops between ages 30-40. It is caused by CAG triplet repeat expansions (>35 CAGs) in the huntingtin (*htt*) gene [45]. This increases the length of the polyglutamine (polyQ) tract in the N-terminal of the HTT protein, causing it to aggregate. The aggregation of proteins has adverse effects on mitochondrial dynamics and impairs mitochondrial transport along the axons and dendrites [46, 47]. There is also an increase in ROS production in HD patients and mouse models, causing mitochondrial damage [48]. In normal cells, oxidized glyceraldehyde 3-phosphate dehydrogenase (GAPDH), an enzyme in the glycolytic pathway, is needed to activate lysosomes to engulf damaged mitochondria for

degradation. However, Hwang *et al*. have shown that polyQ repeats in HD cell models can interact abnormally with GAPDH and prevent GAPDH-mediated mitophagy [49].

3. Diabetes

Diabetes mellitus is a major metabolic disorder that prevents individuals from regulating their blood glucose levels due to impaired insulin function. This disease can be divided into two groups: Type 1 diabetes mellitus, whereby patients lack insulin-producing beta cells in the pancreas due to self-attack by their own immune system; and Type 2 diabetes mellitus (T2DM), whereby patients continue to produce insulin but become resistant to its effects.

Studies have linked mitochondrial stress to insulin resistance in T2DM. For example, reduced mitochondrial OXPHOS was associated with age-related declines in insulin sensitivity and increased fat build-up in intramyocellular and intrahepatic cells [50]. These findings suggested a relationship between mitochondrial function and insulin resistance. Transcriptomics has confirmed the association between mitochondrial homeostasis and insulin resistance, showing that genes involved in OXPHOS were significantly downregulated in T2DM [51] [52]. Also, research has shown that diabetic patients with mtDNA mutations have impaired pancreatic β-cell insulin secretory function. ATP energy generated from mitochondria is critical for the coupling of blood glucose and insulin secretion. When blood glucose enters the pancreatic β-cells, the increased ATP/ADP ratio depolarizes the plasma membrane. This causes voltage-gated calcium channels to open, causing an increased influx of calcium that initiates the fusion of the plasma membrane with insulin-containing granules, leading to insulin secretion. Hence, any disruption to mitochondrial function can impair insulin secretion and cause T2DM [53, 54]. Lastly, a study has shown that mitochondrial dysfunction is linked with pancreatic β-cell failure, causing a reduction in β-cell mass and function. Diabetic-prone, obese mice had increased pancreatic β-cell mass at an early

stage in life, but the cell mass was significantly reduced in older age. In addition, there were significant changes in mitochondrial structure and function in T2DM human pancreatic cells, including an increase in mitochondria size, decreased ATP levels, and an increase in uncoupling proteins, suggesting a role of mitochondrial dysfunction in the pathogenesis of β-cell failure in T2DM [55].

4. Cardiovascular disease

Multiple studies have suggested a link between mitochondrial damage and cardiovascular disease (CVD) development. For example, increased mtDNA damage has been observed in the aortas and hearts of CVD patients when compared to healthy individuals [56]. mtDNA accumulations can cause altered mitochondrial appearance and functional changes, which can be observed in atherosclerotic lesions in patients. One study compared the entire aortic intima areas and lipofibrous plaques in twelve postmortem aorta samples to identify the average number of mtDNA mutations. It was shown that these heteroplasmic mtDNA mutations were more common in lipofibrous plaques compared to healthy aortic intimas, substantiating the association between atherosclerosis development and mitochondrial mutations [57]. Another study utilized parallel sequencing to compare mtDNA levels from myocardial tissues of patients with coronary artery disease (CAD) and control individuals. Consistently, there was a comparatively higher level of mtDNA heteroplasmy in myocardial tissues of CAD patients. In addition, patients with CAD had more mtDNA deletions than healthy individuals. These results suggest an increased accumulation of mtDNA mutation in atherosclerotic plaques compared to healthy tissues [58]. In addition, deficiencies in mitochondrial antioxidants and uncoupling proteins (UCPs) that regulate antioxidant production have been associated with the onset of CVD *in vivo* and are needed for atherogenesis [59].

V. Mitochondrial recovery mechanisms

Mitochondria are indispensable for cellular function and survival. Accordingly, several mechanisms have evolved to sense and mitigate mitochondrial dysfunction to reestablish homeostasis (Figure 7).

1. Mitochondrial dynamics and mitophagy:

Mitochondria are not static organelles but instead are constantly shifting their size, structure, and distribution. There are two general phases associated with mitochondrial dynamics: fusion and fission. Specific GTPases regulate both mitochondrial fusion and fission process: mitochondrial fusion being regulated by Mitofusin GTPases Opa1, Mff1, and Mff2, and mitochondrial fission regulated by dynamin-related protein Drp1 [60].

Mitochondrial fusion during stress promotes the mixing of internal contents, thus allowing compensation for defective constituents through the sharing of resources. Conversely, when the mitochondrial network is badly damaged, defective portions are isolated through fission. This enables the removal of the damaged mitochondria while producing new organelles and facilitating quality control [61].

However, the process of mitophagy is engaged when mitochondria are severely damaged and beyond repair. As mentioned earlier, mitophagy is a specialized form of autophagy, referring to the regulated removal and recycling of cellular components. This form of mitochondrial degradation involves two players: PINK1 kinase and the ubiquitin ligase Parkin. PINK1 is usually imported into healthy mitochondria and degraded by PARL protease. Damaged mitochondria disrupt the import of PINK1, causing it to be sequestered on the outer mitochondrial membrane. PINK1 accumulation on the mitochondrial outer membrane recruits Parkin. PINK1 then phosphorylates Parkin leading to its activation. Phosphorylated Parkin then poly-ubiquitinates

multiple target proteins that enlist machinery to engulf the damaged organelle into an autophagosome. The autophagosome is then transferred to the lysosomes to be degraded [61, 26].

2.Integrated stress response (ISR):

There is a need to reduce protein translation rates during stress to prevent further proteotoxicity and promote cellular recovery. The ISR is activated during stress and involves a collection of four kinases that help reduce global protein translation: PERK (PKR-like ER kinase, GCN2 (General control non-depressible protein 2), PKR (Double-stranded RNA-dependent protein kinase), and HRI (Heme-regulated eIF2α kinase) [62]. These kinases phosphorylate the alpha subunit of the eukaryotic initiation factor-2 (eIF2α) at serine-51 to reduce global protein translation [63]. Interestingly, while the general synthesis of proteins reduces due to the ISR, other target mRNAs are preferentially translated to assist in cellular recovery. Translation of these target mRNAs occurs due to the presence of upstream open reading frames (uORFs) [64]. Three main target mRNAs undergo this preferential translation during stress due to the ISR: the transcription factors ATF4, ATF5, and CHOP. Both ATF4 and CHOP are known to regulate the transcription of ATF5. CHOP induces apoptosis via the regulation of ATF5 when stress levels are not controlled [65].

The ISR also operates during mitochondrial stress. Indeed, it is believed that GCN2 is activated by mitochondrial-derived ROS generated during stress [66]. In addition, ATF4, ATF5, and CHOP all play a role in mitigating mitochondrial stress, in part through the regulation of the retrograde stress response known as the mitochondrial unfolded protein response.

3. Mitochondrial unfolded protein response:

Cells use retrograde signaling mechanisms as one means to promote mitochondrial homeostasis, including the mitochondrial unfolded protein response (UPR^{mt}) (Figure 8). Retrograde signaling refers to inter-organelle communication to communicate functional status. UPR^{mt} retrograde

signaling occurs between mitochondria and the nucleus. During stress, damaged mitochondria signal to the nucleus to transcriptionally regulate several genes to promote mitochondrial repair, including genes involved in proteostasis (e.g., molecular chaperones and proteases), detoxification, metabolic rewiring, and mitochondrial dynamics [67].

The UPR^{mt} was first characterized in mammalian cell culture as a response to the accumulation of misfolded proteins in the mitochondrial matrix or the depletion of mtDNA. This resulted in increased expression of mitochondrial chaperones and proteases to assist in mitochondrial recovery. However, the mechanistic basis of the UPR^{mt} was more fully evolved using the nematode model organism *Caenorhabditis elegans*. *C. elegans* offers many advantages in the study of cell signaling pathways. It has a fast life cycle of 3-5 days depending on temperature, a completely annotated genome, easy lab maintenance, and straightforward genetic manipulations. It is also transparent, allowing for the use of fluorescent reporters to label cells of interest.

The key regulator for UPR^{mt} in *C. elegans* is a transcription factor known as activating transcription factor related to stress-1 (ATFS-1). ATFS-1 contains two signal sequences: one amino-terminal mitochondrial targeting sequence (MTS) and one nuclear localization signal (NLS). In healthy cells, ATFS-1 is efficiently imported into mitochondria and degraded by the protease Lon. However, during stress, mitochondrial import of ATFS-1 is reduced, leading to nuclear translocation of ATFS-1 and the regulation of gene expression needed for survival and recovery of the mitochondrial network. These activities essentially prevent the accumulation of misfolded or potentially damaging proteins in mitochondria, maintaining compartmentalized protein homeostasis critical for organelle function. In addition to stabilizing the protein folding environment in mitochondria, the UPR^{mt} is also involved in metabolic rewiring to produce alternative sources of energy during times of defective OXPHOS [65].

Organismal longevity

A decline in mitochondrial function is a sign of aging in most organisms and is often associated with reduced OXPHOS and increased levels of deleterious mtDNA. Interestingly, mild mitochondrial stress has been known to increase organismal lifespan, including flies, *C. elegans*, and mice. In *C. elegans,* knockdown of ETC components such as *cco-1*, which encodes cytochrome c oxidase, can robustly induce the UPR^{mt} and increase animal lifespan. However, the increased longevity in *C. elegans* is only observed when the mitochondrial stress preceded the juvenile developmental stage to induce the UPR^{mt}. Similarly, changes in the metabolic input can affect mitochondrial function and cause UPR^{mt} activation and affect lifespan; for example, controlling the amount of metabolic cofactor NAD+ or vitamin B_{12} can activate UPR^{mt} and increase the lifespan [68, 69].

Moreover, the UPR^{mt} can be activated by genetic or pharmacological means that impair mitochondrial ribosome function, resulting in reduced mitochondrial translation rates. Impairing mitochondrial translation results in a mitonuclear imbalance, whereby mitochondrial ETC proteins encoded by the nuclear genome are not matched with the synthesis of those encoded by the mitochondrial genome. This mitonuclear imbalance activates the UPR^{mt} and results in robust lifespan extension [70]. Although substantial data shows the association between induction of UPR^{mt} and extension of life span, the exact mechanism of how the UPR^{mt} regulates life span remains to be identified.

Host protection during infection:

Mitochondria are known to regulate innate immunity, but that can be compromised during bacterial infections. Bacteria have specific means to subvert mitochondrial functions to develop

and survive, including directly targeting virulence factors to mitochondria. So it is not surprising that mitochondrial recovery programs have coupled mitochondrial repair with antibacterial defense strategies to fight infection. Indeed, in *C. elegans*, the UPR^{mt} was found to regulate the expression of genes with both mitoprotective and innate immune properties. Pathogens such as *Pseudomonas aeruginosa*, which produce mitochondrial toxins such as hydrogen cyanide that target the ETC, can activate the UPR^{mt}. And consistent with the UPR^{mt} being protective during infection, loss of ATFS-1 renders animals more susceptible to infection.

In contrast, priming animals for the UPR^{mt} before infection increases their defenses against the pathogen and significantly extends host survival rates. Mechanistically, ATFS-1 and the UPR^{mt} promote innate immune gene expression through one of its targets, the mitochondrial chaperone HSP-60. Here, upregulation of HSP-60 by the UPR^{mt} was found to promote p38 MAPK signaling, the conserved and predominant innate immune pathway of *C. elegans*. Specifically, HSP-60 was found to stabilize SEK-1 MAPKK (Mitogen-activated protein kinase kinase), a component of the p38 signaling pathway, thus enhancing the efficacy of this immune response.

Further investigations into the regulation of the UPR^{mt} are thus warranted owing to the relationship this stress response has with organismal lifespan, host protection during infection, and various human diseases such as cancer. The objective of my dissertation is to unveil these mechanisms using a combined genetic and chemical approach. In my first research aim, I conducted a screen of a collection of clinically approved small molecule drugs for those that can inhibit the UPR^{mt}. In my second aim, I used an unbiased genetic screening approach to uncover novel repressors of the UPR^{mt}. In my third aim, I began a pilot investigation into the role of nutrient-sensing by methionine restriction in the regulation of the UPR^{mt} and lifespan.

References

[1] M. W. Gray, "Mitochondrial Evolution," *Cold Springs Harbor Perspective Biology,* 2012.

[2] A. J. Roger, S. A. Muñoz-Gómez and R. Kamikawa, "The Origin and Diversification of Mitochondria," *Current Biology,* vol. 27, no. 21, pp. PR1177-R1192, November 2017.

[3] N. Rajala, J. M. Gerhold, P. Martinsson, A. Klymov and J. N. Spelbrink, "Replication factors transiently associate with mtDNA at the mitochondrial inner membrane to facilitate replication," *Nucleic acids research,* vol. 42, no. 2, p. 952–967, 2014.

[4] P. M. Herst, M. R. Rowe, G. M. Carson and M. V. Berridge, "Functional Mitochondria in Health and Disease," *Frontiers in Endocrinology,* vol. 8, 2017.

[5] T. G. Frey and C. A. Manella, "The internal structure of mitochondria," *Trends in Biochemical Sciences,* vol. 25, no. 7, pp. 319-324, 2000.

[6] B. Mayer and R. Oberbauer, "Mitochondrial Regulation of Apoptosis," *American Physiological Society,* vol. 18, no. 3, pp. 89-94, 2003.

[7] R. B. Flavell, "Mitochondrion as a Multifunctional Organelle," *Nature,* vol. 230, p. 504–506, 1971.

[8] J. B. Spinelli and M. C. Haigis, "The multifaceted contributions of mitochondria to cellular metabolism," *Nature Cell Biology,* vol. 20, p. 745–754, 218.

[9] A. Farhana and S. L. Lappin, "Biochemistry, Lactate Dehydrogenase," StatPearls Publishing, [Online]. Available: https://www.ncbi.nlm.nih.gov/books/NBK557536/.

[10] C. T. DeBerardinis RJ, "Q's next: the diverse functions of glutamine in metabolism, cell biology and cancer.," *Oncogene,* vol. 29, no. 3, pp. 313-24, 2010.

[11] C. Yang, B. Ko, C. T. Hensley, L. Jiang, A. T. Wasti, J. Kim, J. Sudderth, M. A. Calvaruso, L. Lumata, Mitsche, M., J. Rutter, M. E. Merritt and R. J. DeBerardinis, "Glutamine oxidation maintains the TCA cycle and cell survival during impaired mitochondrial pyruvate transport," *Molecular cell,* vol. 56, no. 3, pp. 414-424, 2014.

[12] A. Basu, C. Desler, A. Lykke and L. J. Rasmussen, "The Effect of Mitochondrial Dysfunction on Cytosolic Nucleotide Metabolism," *Journal of Nucleic Acids,* vol. 2010, no. Article ID 701518, p. 9, 2010.

[13] I. Pérez-Arellano, F. Carmona-Alvarez, A. I. Martínez, J. Rodríguez-Díaz and J. Cervera, "Pyrroline-5-carboxylate synthase and proline biosynthesis: From osmotolerance to rare metabolic disease," *Protein Sci.,* vol. 19, no. 3, pp. 372-382, 2010.

[14] D. Hayes, D. Taylor, P. Bore, D. Hilton-Jones, D. Arnold, M. Squier, A. Gent and G. Radda, "An unusual metabolic myopathy: a malate-aspartate shuttle defect.," *J Neurol Sci.*, vol. 82, no. 1-3, pp. 27-39, 1987.

[15] C. Ahn and C. Metallo, "Mitochondria as biosynthetic factories for cancer proliferation.," *Cancer Metabolism*, vol. 3, no. 1, 2015.

[16] L. Jouaville, P. P. C. Bastianutto, G. Rutter and R. Rizzuto, "Regulation of mitochondrial ATP synthesis by calcium: Evidence for a long-term metabolic priming.," *Proc Natl Acad Sci USA*, vol. 96, p. 13807–13812, 1999.

[17] R. Rizzuto, P. Pinton, W. Carrington, F. Fay, K. Fogarty, L. Lifshitz, R. Tuft and T. Pozzan, "Close contacts with the endoplasmic reticulum as determinants of mitochondrial Ca2+ responses.," *Science*, vol. 280, no. DOI: 10.1126/science.280.5370.1763 , p. 1763–1766, 1998.

[18] S. Romero-Garcia and S. & Romero-Garcia, "Mitochondrial calcium: Transport and modulation of cellular processes in homeostasis and cancer (Review).," *International Journal of Oncology*, vol. 54, pp. 1155-1167, 2019.

[19] V. Paupe and J. Prudent, "New insights into the role of mitochondrial calcium homeostasis in cell migration," vol. 500, no. 1, pp. 75-86, 2018.

[20] K. Yasukawa and T. Koshiba, "Mitochondrial reactive zones in antiviral innate immunity," *Biochimica et Biophysica Acta (BBA) - General Subjects*, vol. 1865, no. 3, 2021.

[21] A. West, G. Shadel and S. & Ghosh, "Mitochondria in innate immune responses," *Nat Rev Immunol*, vol. 11, p. 389–402, 2011.

[22] P. Bernardi, "The mitochondrial permeability transition pore: a mystery solved?," *Front. Physiol.*, vol. 4, pp. 3377-3389, 2013.

[23] A. Halestrap, "What is the mitochondrial permeability transition pore?," *J. Mol. Cell. Cardiol.*, vol. 46, pp. 821-831, 2009.

[24] S. Orrenius, V. Gogvadze and B. Zhivotovsky, "Calcium and mitochondria in the regulation of cell death," *Biochem. Biophys. Res. Commun.*, vol. 460, pp. 72-81, 2015.

[25] M. Redza-Dutordoir and D. A. Averill-Bates, "Activation of apoptosis signalling pathways by reactive oxygen species," *Biochimica et Biophysica Acta (BBA) - Molecular Cell Research*, Vols. 1863,, no. 12, pp. 2977-2992, 2016.

[26] A. Melber and C. Haynes, "UPRmt regulation and output: a stress response mediated by mitochondrial-nuclear communication," *Cell Research*, vol. 28, p. 281–295, 2018.

[27] P. Reddy, "The role of mitochondria in neurodegenerative diseases: mitochondria as a therapeutic target in Alzheimer's disease," *CNS Spectr.*, vol. 14, pp. 8-18, 2009.

[28] D. Selkoe, "Alzheimer's disease: genes, proteins, and therapy.," *Physiol Rev.*, pp. 741-66, 2001.

[29] M. Mattson, "Pathways towards and away from Alzheimer's disease.," *Nature,* vol. 430, no. 7000, pp. 631-9, 2004.

[30] M. Manczak, T. Anekonda, E. Henson, B. Park, J. Quinn and P. Reddy, "Mitochondria are a direct site of A beta accumulation in Alzheimer's disease neurons: implications for free radical generation and oxidative damage in disease progression.," *Hum Mol Genet,* vol. 15, no. 9, pp. 1437-49, 2006.

[31] C. Caspersen, N. Wang, J. Yao, A. Sosunov, X. Chen, J. Lustbader, H. Xu, D. Stern, G. McKhann and S. Yan, "Mitochondrial Abeta: a potential focal point for neuronal metabolic dysfunction in Alzheimer's disease," *FASEB J.*, vol. 19, p. 2040–2041, 2005.

[32] L. Devi, B. Prabhu, D. Galati, N. Avadhani and H. Anandatheerthavarada, "Accumulation of amyloid precursor protein in the mitochondrial import channels of human Alzheimer's disease brain is associated with mitochondrial dysfunction," *J Neurosci,* vol. 26, no. 35, pp. 9057-68, 2006.

[33] H. Anandatheerthavarada, G. Biswas, M. Robin and N. Avadhani, "Mitochondrial targeting and a novel transmembrane arrest of Alzheimer's amyloid precursor protein impairs mitochondrial function in neuronal cells.," *J Cell Bio,* vol. 161, no. 1, pp. 41-54, 2013.

[34] P. Reddy and M. Beal, "Amyloid beta, mitochondrial dysfunction and synaptic damage: implications for cognitive decline in aging and Alzheimer's disease," *Trends Mol Med.,* vol. 14, no. 2, 2008.

[35] G. Gibson, K. Sheu and J. Blass, "Abnormalities of mitochondrial enzymes in Alzheimer disease.," *J Neural Transm (Vienna),* vol. 105, no. 8-9, pp. 855-70, 1998.

[36] W. J. Parker, F. CM and J. Parks, "Cytochrome oxidase deficiency in Alzheimer's disease.," *Neurology. Aug; 40(8):,* vol. 40, no. 8, pp. 1302-3, 1990.

[37] I. Maurer, S. Zierz and H. Möller, "A selective defect of cytochrome c oxidase is present in brain of Alzheimer disease patients.," *Neurobiol Aging,* vol. 21, no. 3, pp. 455-62, 2000.

[38] M. Lin, D. Simon, C. Ahn, L. Kim and M. Beal, "High aggregate burden of somatic mtDNA point mutations in aging and Alzheimer's disease brain," *Hum Mol Genet,* vol. 11, no. 2, pp. 133-45, 2002.

[39] P. Coskun, M. Beal and D. Wallace, "Alzheimer's brains harbor somatic mtDNA control-region mutations that suppress mitochondrial transcription and replication," *Proc Natl Acad Sci USA,* vol. 101, no. 29, pp. 10726-31, 2004.

[40] W. Poewe, K. Seppi, C. Tanner, G. Halliday, P. Brundin, J. Volkmann, A. Schrag and A. Lang, "Parkinson disease," *Nat Rev Dis Primers* , vol. 3, 2017.

[41] S. de la Monte, "Brain insulin resistance and deficiency as therapeutic targets in Alzheimer’s disease," *Curr Alzheimer Res,* vol. 9, p. 35–66, 2012.

[42] D. Hu, X. Sun, X. Liao, X. Zhang, S. Zarabi, A. Schimmer, Y. Hong, C. Ford, Y. Luo and X. Qi, "Alpha-synuclein suppresses mitochondrial protease ClpP to trigger mitochondrial oxidative damage and neurotoxicity," *Acta Neuropathol,* vol. 137, p. 939–960, 2019.

[43] D. Ordonez, M. Lee and M. Feany, "Alpha-synuclein induces mitochondrial dysfunction through spectrin and the actin cytoskeleton," *Neuron,* vol. 97, no. e106, p. 108–124, 2018.

[44] F. Menzies, A. Fleming, A. Caricasole and e. al., " Autophagy and neurodegeneration: pathogenic mechanisms and therapeutic opportunities," *Neuron,* vol. 93, no. 5, pp. 1015- 1034, 2017.

[45] "A novel gene containing a trinucleotide repeat that is expanded and unstable on Huntington's disease chromosomes. The Huntington's Disease Collaborative Research Group," *Cell,* vol. 72, no. 6, pp. 971-83, 1993.

[46] A. Orr, S. Li, C.-E. Wang and e. al., "N-terminal mutant huntingtin associates with mitochondria and impairs mitochondrial trafficking," *J Neurosci.,* vol. 28, no. 11, pp. 2783- 2792, 2008.

[47] P. Reddy and S. U. , "Mutant huntingtin, abnormal mitochondrial dynamics, defective axonal transport of mitochondria, and selective synaptic degeneration in Huntington's disease," *Biochim Biophys Acta,* vol. 1822, no. 2, pp. 101-110, 2012.

[48] Y. Choo, G. Johnson, M. MacDonald, P. Detloff and M. Lesort, "Mutant huntingtin directly increases susceptibility of mitochondria to the calcium-induced permeability transition and cytochrome c release.," *Hum Mol Genet,* vol. 13, no. 14, pp. 1407- 1420, 2004.

[49] S. Hwang, M. Disatnik and D. Mochly-Rosen, "Impaired GAPDH-induced mitophagy contributes to the pathology of Huntington's disease," *EMBO Mol Med,* vol. 7, no. 10, pp. 1307- 1326, 2015.

[50] K. F. Petersen, S. Dufour, D. Befroy, R. Garcia and G. I. Shulman, "Impaired Mitochondrial Activity in the Insulin-Resistant Offspring of Patients with Type 2 Diabetes," *N Engl J Med,* vol. 350, no. 7, pp. 664-671, 2004.

[51] V. Mootha, C. Lindgren, K. Eriksson, A. Subramanian, S. Sihag, J. Lehar, P. Puigserver, E. Carlsson, M. Ridderstråle, E. Laurila, N. Houstis, M. Daly, N. Patterson, J. Mesirov, T. Golub, P. Tamayo, B. Spiegelman, E. Lander, J. Hirschhorn, D. Altshuler and L. Groop, "PGC-1alpha-responsive genes involved in oxidative phosphorylation are coordinately downregulated in human diabetes," *Nat Genet,* vol. 34, no. 3, pp. 267-73, 2003.

[52] M. Patti, A. Butte, S. Crunkhorn, K. Cusi, R. Berria, S. Kashyap, Y. Miyazaki, I. Kohane, M. Costello, R. Saccone, E. Landaker, A. Goldfine, E. Mun, R. DeFronzo, J. Finlayson, C. Kahn and L. Mandarino, "Coordinated reduction of genes of oxidative metabolism in humans with insulin resistance and diabetes: Potential role of PGC1 and NRF1.," *Proc Natl Acad Sci U S A.,* vol. 100, no. 13, pp. 8466-71, 2003.

[53] J. Lang, "Molecular mechanisms and regulation of insulin exocytosis as a paradigm of endocrine secretion," *Eur J Biochem,* vol. 259, pp. 3-17, 1999.

[54] F. Ashcroft, P. Proks, P. Smith, C. Ammälä, K. Bokvist and P. Rorsman, "Stimulus-secretion coupling in pancreatic beta cells," *J Cell Biochem.,* vol. 55, pp. Suppl:54-65, 1994.

[55] S. Deng, M. Vatamaniuk, X. Huang, N. Doliba, M. Lian, A. Frank, E. Velidedeoglu, N. Desai, B. Koeberlein, B. Wolf, C. Barker, A. Naji, F. Matschinsky and J. Markmann, "Structural and functional

abnormalities in the islets isolated from type 2 diabetic subjects.," *Diabetes,* vol. 53, no. 3, pp. 624-32, 2004.

[56] S. W. Ballinger, "Mitochondrial dysfunction in cardiovascular disease," *Free Radical Biology and Medicine,* vol. 38, no. 10, pp. 1278-1295, 2005.

[57] A. V. Poznyak, E. A. Ivanova, I. A. Sobenin, S. F. Yet and A. N. Orekhov, "The Role of Mitochondria in Cardiovascular Diseases," *Biology,* vol. 9, no. 6, p. 137, 2020.

[58] I. Sobenin, M. Sazonova, P. A. Y. Bobryshev and A. Orekhov, "Changes of mitochondria in atherosclerosis: possible determinant in the pathogenesis of the disease.," *Aherosclerosis,* vol. 227, no. 2, pp. 283-8, 2013.

[59] S. Ballinger, C. Patterson, C. Knight-Lozano, D. Burow, C. Conklin, Z. Hu, R. J. Hu, C. Horaist, R. Lebovitz, G. Hunter, K. McIntyre and M. Runge, "Mitochondrial Integrity and Function in Atherogenesis," *Circulation,* vol. 106, no. 5, pp. 544-549, 2002.

[60] S. Hoppins, L. Lackner and J. Nunnari, "The machines that divide and fuse mitochondria," *Annu. Rev. Biochem,* vol. 76, no. 751, 2007.

[61] R. Youle and A. van der Bliek, "Mitochondrial Fission, Fusion, and Stress," *Science,* vol. 337, no. 6098, pp. 1062-1065, 2012.

[62] K. Pakos-Zebrucka, I. Koryga, K. Mnich, M. Ljujic, A. Samali and A. M. Gorman, "The integrated stress response," *EMBO Rep,* vol. 17, no. 10, p. 1374–1395, 2016.

[63] D. Ron, "Translational control in the endoplasmic reticulum stress response," *J Clin Invest,* vol. 110, pp. 1383-1388, 2002.

[64] D. Zhou, L. Palam, L. Jiang, J. Narasimhan, K. Staschke and R. Wek, "Phosphorylation of eIF2 directs ATF5 translational control in response to diverse stress conditions.," *J Biol Chem,* vol. 283, no. 11, pp. 7064-73, 2008.

[65] M. A. Qureshi, C. M. Haynes and M. W. Pellegrino, "The mitochondrial unfolded protein response: Signaling from the powerhouse.," *The Journal of biological chemistry,* vol. 292, no. 33, p. 13500–13506, 2017.

[66] B. Baker, A. S. T. Nargund and s. C. Hayne, "Protective coupling of mitochondrial function and protein synthesis via the eIF2α kinase GCN-2," *PLoS Genet,* vol. 8, no. 6, 2012.

[67] A. Schulz and C. Haynes, "UPRmt-mediated cytoprotection and organismal aging," *Biochimica et Biophysica Acta (BBA) - Bioenergetics,* vol. 1847, no. 11, pp. 1448-1456, 2015.

[68] N. Naresh and C. Haynes, "Signaling and Regulation of the Mitochondrial Unfolded Protein Response," *Cold Spring Harb Perspect Biol.,* vol. 11, no. 6, 2019.

[69] M. Amin, S. Mahmud, J. Dowgielewicz, M. Sapkota and M. Pellegrino, "A novel gene-diet interaction promotes organismal lifespan and host protection during infection via the mitochondrial UPR," *PLOS Genetics,* vol. 16, no. 12, 2020.

[70] R. Houtkooper, M. L, D. Ryu, N. Moullan, E. Katsyuba, G. Knott, R. Williams and J. Auwerx, "Mitonuclear protein imbalance as a conserved longevity mechanism," *Nature*, vol. 497, p. 451–457, 2013.

[71] R. Jennings and C. Premanandan, "Mitochondria," Ohio State Pressbooks, 2021. [Online]. Available: https://ohiostate.pressbooks.pub/vethisto/chapter/1-mitochondria/.

[72] M. Amin, S. Mahmud, J. Dowgielewicz, M. Sapkota and M. Pellegrino, "A novel gene-diet interaction promotes organismal lifespan and host protection during infection via the mitochondrial UPR.," *PLOS genetics*, vol. 16, no. 12, 2020.

[73] H. Otera, K. Mihara and L. Ghibelli, "Mitochondrial Dynamics: Functional Link with Apoptosis," *International Journal of Cell Biology*, 2012.

[74] J. Lopez and S. Tait, "Mitochondrial apoptosis: killing cancer using the enemy within," *British Journal of Cancer*, vol. 112, p. 957–962, 2015.

[75] C. Wang and R. J. Youle, "The Role of Mitochondria in Apoptosis," *Annual review of genetics*, vol. 43, pp. 95-118, 2009.

[76] S. H. Kwak, K. S. Park, K. U. Lee and H. K. Lee, "Mitochondrial metabolism and diabetes," *J Diabetes Investig*, vol. 1, no. 5, p. 161–169, 2010.

Figures

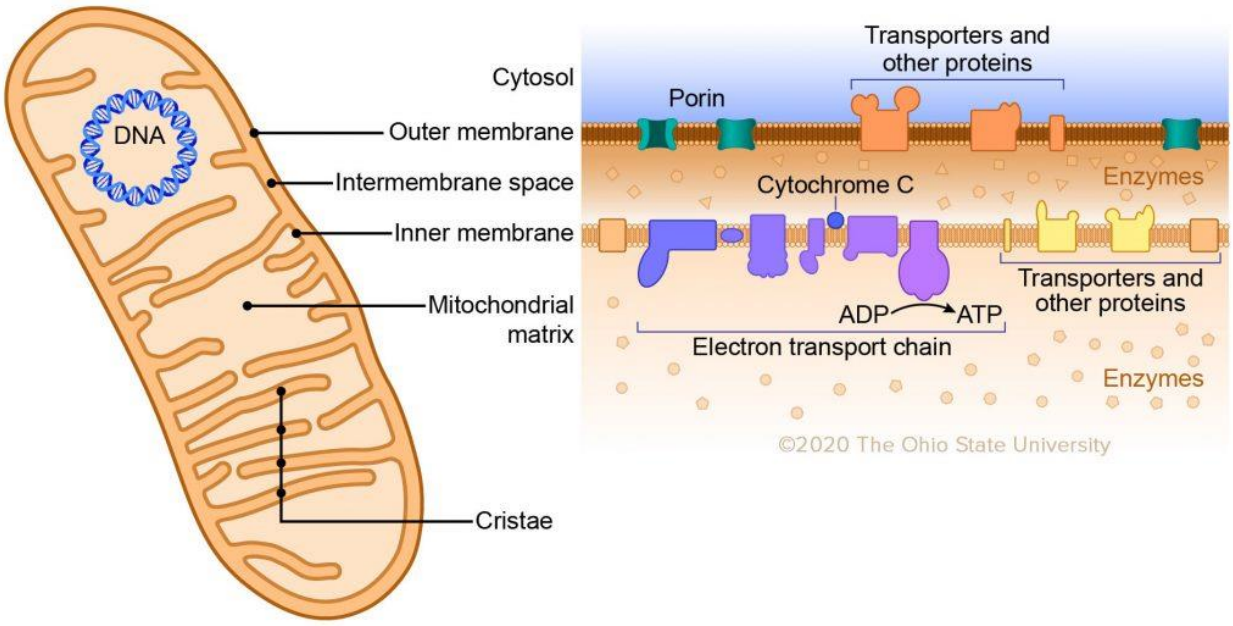

Figure 1. Basic structure of the mitochondrion *[71]*

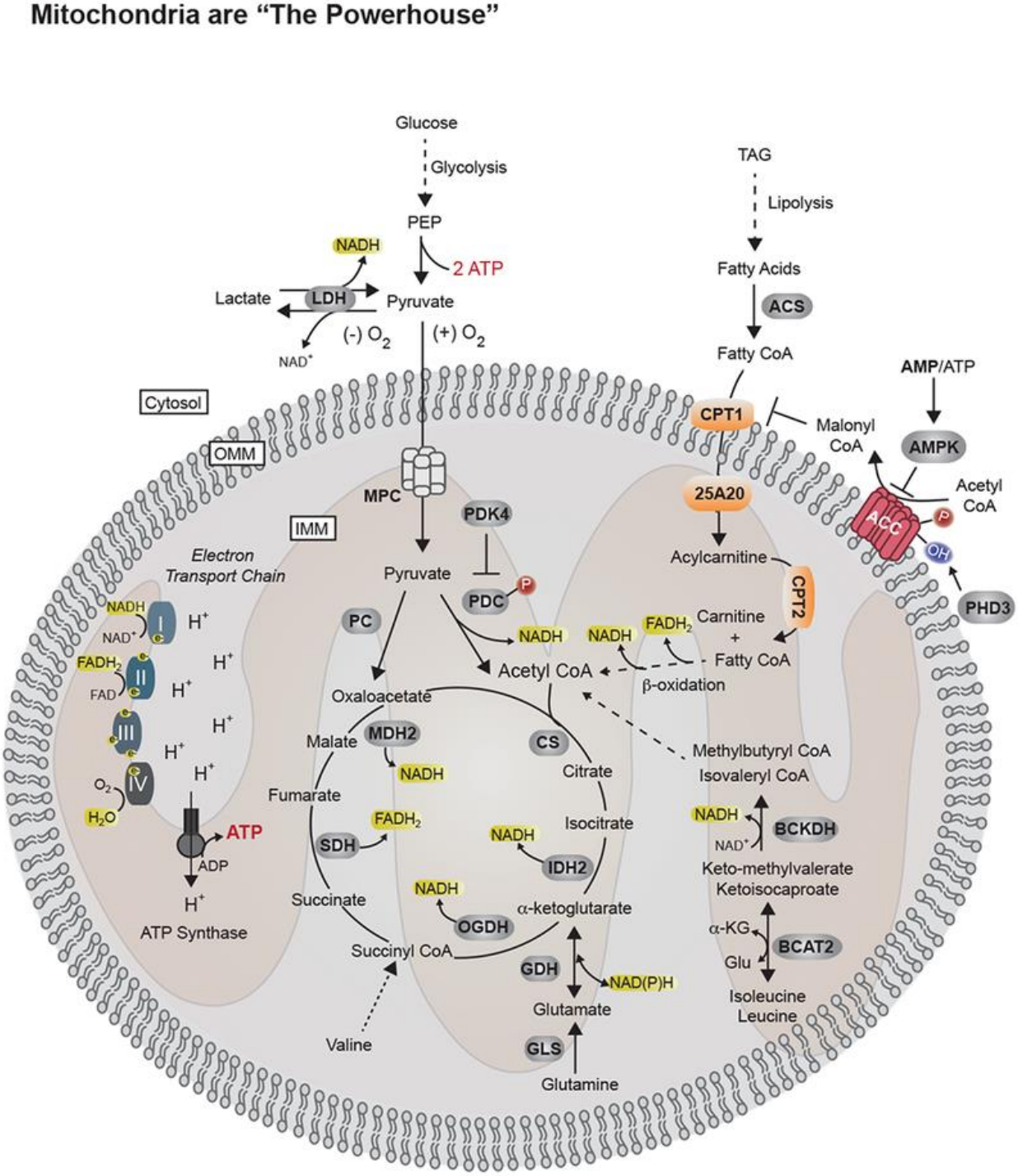

Figure 2. Mitochondria: the powerhouse of the cell *[8]*. Mitochondria integrate fuel metabolism to generate energy in the form of ATP. Mitochondria oxidize pyruvate (derived from glucose or lactate), fatty acids, and amino acids to harness electrons onto the carriers NADH and $FADH_2$.

NADH and $FADH_2$ transport these electrons to the electron transport chain, in which an electrochemical gradient is formed to facilitate ATP production through oxidative phosphorylation. Enzymes have the following abbreviations: LDH: lactate dehydrogenase, VDAC: Voltage-dependent anion channel, MPC: mitochondrial pyruvate carrier, PDC: pyruvate dehydrogenase complex, PC: pyruvate carboxylase, CS: citrate synthase, IDH2: isocitrate dehydrogenase 2, OGDH: α-ketoglutarate dehydrogenase, SDH: succinate dehydrogenase, MDH2: malate dehydrogenase 2, GLS: glutaminase, GDH: glutamate dehydrogenase, BCAT2: branched chain amino transferase 2, BCKDH: branched chain ketoacid dehydrogenase, PHD3: prolyl hydroxylase 3, AMPK: adenosine monophosphate kinase, ACC: Acetyl CoA Carboxylase, , ACS: acyl CoA synthetase, CPT1/2: carnitine palmitoyltransferase 1/2. Electrons and reducing equivalents are shown in yellow.

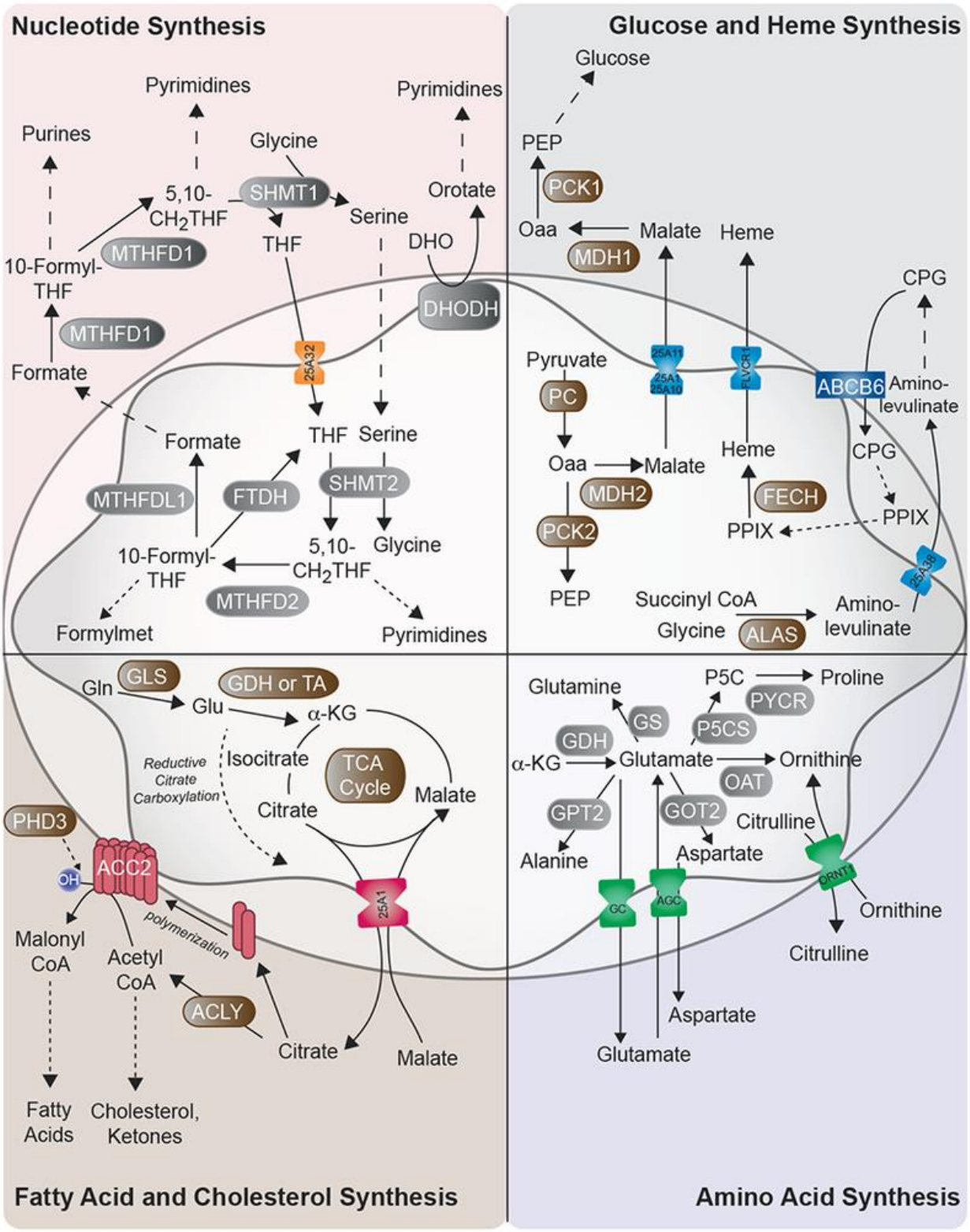
Nucleotide Synthesis
Glucose and Heme Synthesis
Pyrimidines
Pyrimidines
Purines
Glycine
5,10-
CH2THF
SHMT1
Serine
Orotate
THF
DHO
10-Formyl-
THF
MTHFD1
DHODH
MTHFD1
25A32
Formate
Formate
THF
Serine
MTHFDL1
FTDH
SHMT2
10-Formyl-
THF
5,10-
CH2THF
Glycine
MTHFD2
Formylmet
Pyrimidines
Glucose
PEP
PCK1
Oaa
Malate
Heme
MDH1
CPG
Pyruvate
25A11
25A1
25A10
FLVCR1
ABCB6
Amino-
levulinate
PC
Oaa
Malate
Heme
CPG
MDH2
FECH
PPIX
PCK2
PPIX
PEP
Succinyl CoA
Glycine
ALAS
Amino-
levulinate
25A38
Gln
GLS
GDH or TA
Glu
α-KG
Reductive
Citrate
Carboxylation
Isocitrate
TCA
Cycle
Malate
Citrate
PHD3
OH
ACC2
polymerization
Malonyl
CoA
Acetyl
CoA
ACLY
Citrate
Malate
25A1
Fatty
Acids
Cholesterol,
Ketones
Glutamine
P5C
Proline
PYCR
GS
P5CS
GDH
α-KG
Glutamate
Ornithine
OAT
GPT2
GOT2
Citrulline
Alanine
Aspartate
GC
AGC
ORNT1
Ornithine
Citrulline
Aspartate
Glutamate
Fatty Acid and Cholesterol Synthesis
Amino Acid Synthesis

Figure 3. Mitochondria as biosynthetic hubs *[8]*. Mitochondria are critical sources of the building blocks needed for biosynthetic pathways such as nucleotide synthesis, fatty acid and cholesterol synthesis, amino acid synthesis, and glucose and heme synthesis. Compartmentalization is a key feature of biosynthetic pathways. While many of the enzymes listed are bi-directional, arrows are drawn to highlight biosynthetic functions. Enzymes are circled in grey and brown with the following abbreviations: *Nucleotide Synthesis:* MTHFD1/2: methylenetetrahydrofolate dehydrogenase, SHMT1/2: serine hydroxymethyltransferase, DHODH: dihydroorotate dehydrogenase, FTDH: formate dehydrogenase. *Fatty Acid and Cholesterol Synthesis:* GLS: glutaminase, GDH: glutamate dehydrogenase, TA: transaminase, ACLY: ATP citrate lyase, ACC2: acetyl CoA carboxylase, PHD3: prolyl hydroxylase 3, MPC: mitochondrial pyruvate carrier. *Amino Acid Synthesis:* GDH: glutamate dehydrogenase, GS: glutamine synthetase, P5CS: Pyrroline-5-carboxylate synthase, PYCR1: Pyrroline-5-carboxylate reductase 1, OAT: ornithine aminotransferase, GOT2: glutamate oxaloacetate transaminase 2, GPT2: glutamate pyruvate transaminase 2, GC: glutamate carrier, AGC: aspartate-glutamate carrier, ORNT1: ornithine translocator. *Glucose and Heme Synthesis:* PCK1/2: phosphoenolpyruvate carboxykinase, MDH1/2: malate dehydrogenase, PC: pyruvate carboxylase, ALAS: aminolevulinate synthase, FECH: ferrochetolase, ABCB6: ATP binding cassette subfamily B member 6, FLVCR: feline leukemia virus subgroup C receptor 1.

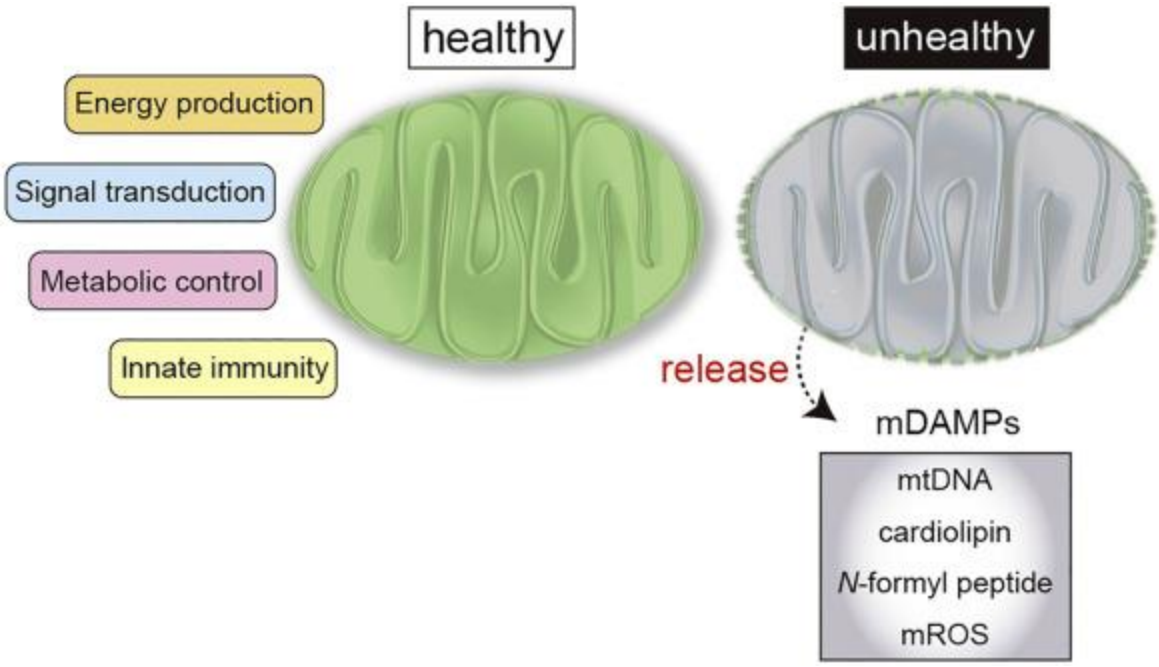

Figure 4. Physiological roles of mitochondria in mammals *[20]*. Mitochondria participate in a wide range of processes required for viability (left). While the key function of mitochondria is to generate cellular energy, it has many other roles such as in signal transduction, metabolic control, and regulation of innate immunity. Under excessive stress/damage or loss of its homeostasis (right), the MIM becomes depolarized and releases mitochondrial components (e.g., mtDNA, cardiolipin, *N*-formyl peptide, and mROS) into the cytosol by a mechanism not yet completely elucidated. In addition to PAMPs derived from microorganisms, mDAMPs are recognized as alarmins that trigger inflammatory responses within the host.

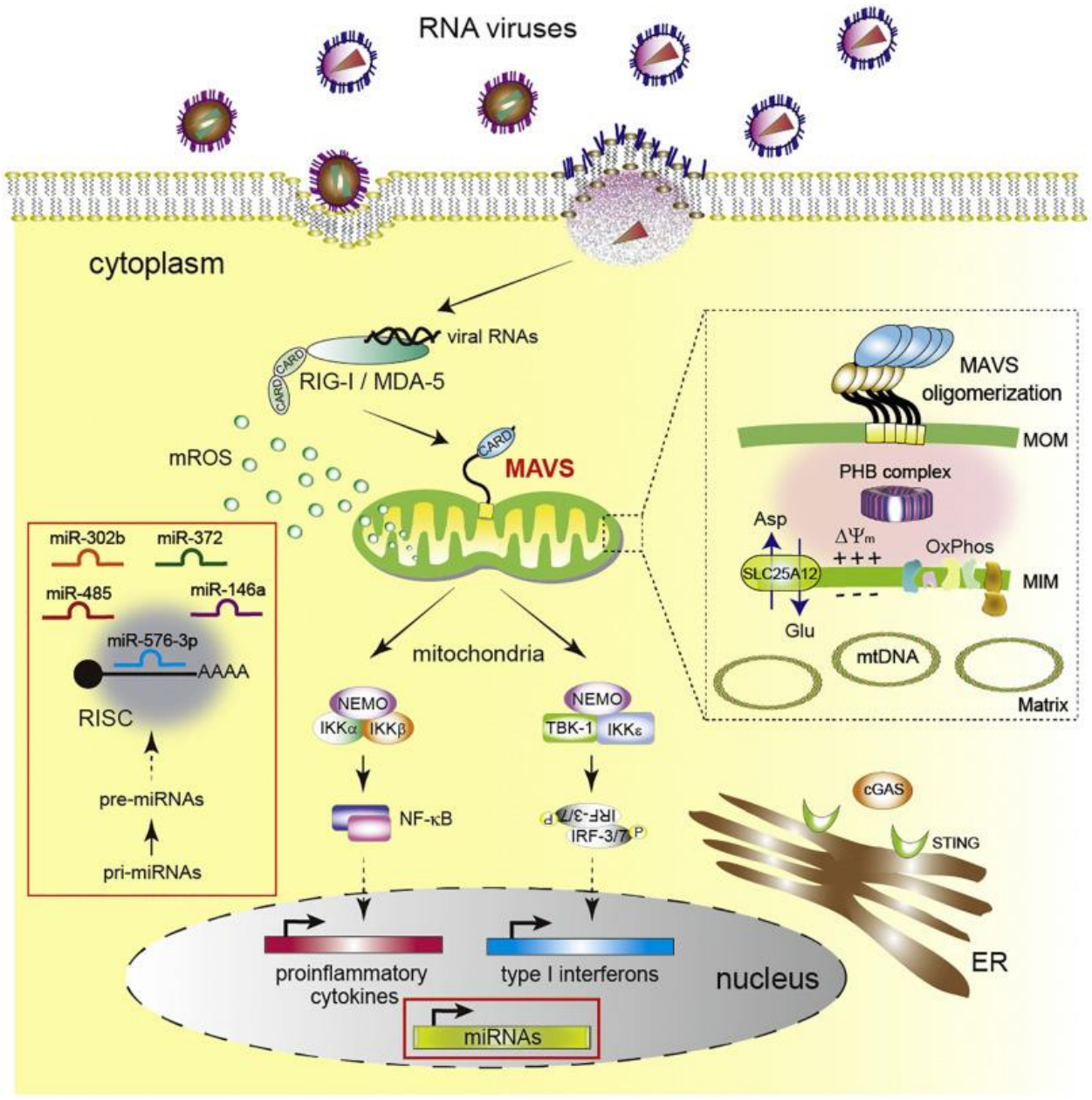

Figure 5. Overview of innate immunity against RNA viruses in mammals (RLR pathway) *[20]*. Viral infections (cytosolic virus-derived RNAs) of mammalian cells are initially detected by the host PRRs (RIG-I and MDA-5) and initiate the RLR-mediated signaling pathway. MAVS acts as adaptors of the PRRs, which activate NF-κB or IRF-3/7, resulting in the rapid production of proinflammatory cytokines and type I interferons (early phase). In this pathway, mitochondria serve as a signaling platform at the MOM, which activates/regulates various kinds of downstream

molecules. In addition, dynamic mitochondrial properties (i.e., $\Delta\psi_m$, OxPhos activity, mitochondrial-related metabolites, etc.) under the MOM also contribute to fine-tune signaling events (right dashed box). A topologic gap between MAVS and the mitochondrial properties is filled by PHB complexes that construct a bridge between the MOM and MIM upon viral infection [74]. At longer times post-infection (~24 h: late phase), some miRNAs are upregulated in cells (bottom red box), and many modulate the immune response. miR-146a, miR-302b, miR-372, miR-485, and miR-576-3p undergo sequential negative regulation of antiviral responses following viral infection, a process that is critical for terminating excess RLR signaling (left red box). Mitochondria are also involved in activating the cGAS/STING signaling pathway. MDA-5, melanoma differentiation-associated gene 5. NEMO, NF-κB essential modulator. RISC, RNA-induced silencing complex. $\Delta\psi_m$, mitochondrial membrane potential.

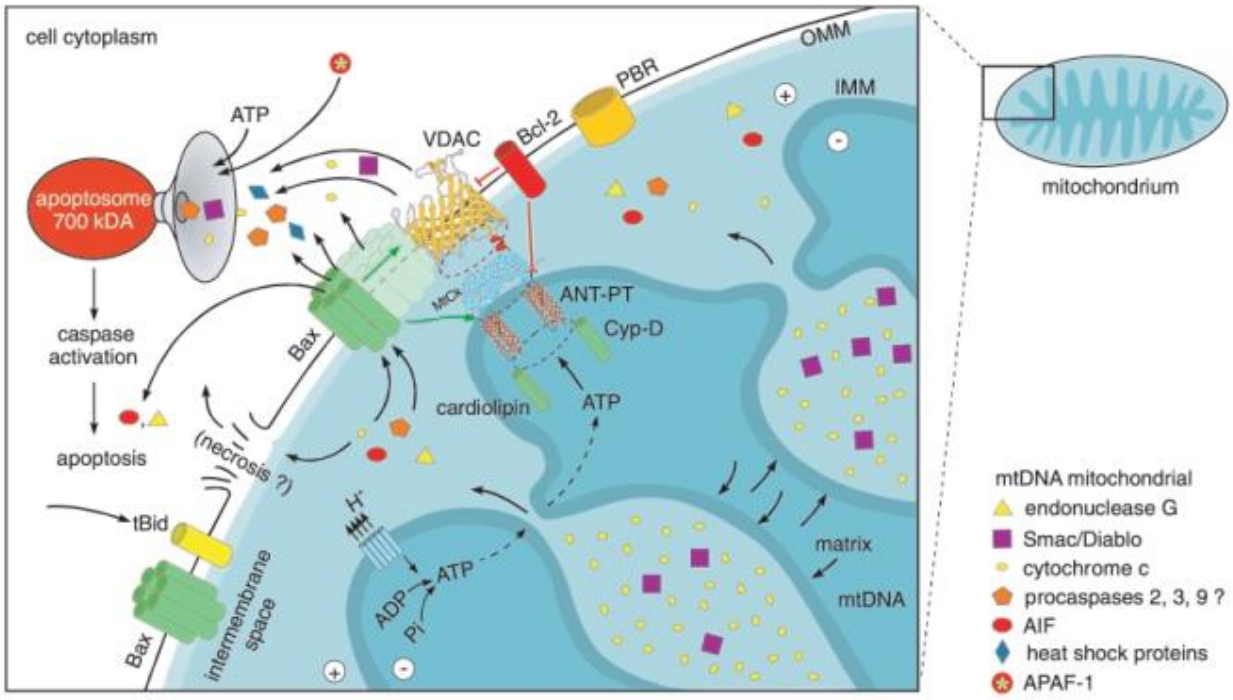

Figure 6. Mitochondrial regulation of apoptotic cell death [6]. During apoptosis induction, the ANT conductance and permeability increase to 700 pS and 1.5 kDa, respectively. This leads to osmotic swelling of the mitochondrial matrix by water influx followed by compression of the intercristal space. The apoptogenic proteins are released into the intermembrane space. Some authors, however, reported cytochrome c release in the absence of IMM depolarization. The expelling of cytochrome c into the cytoplasm may be accomplished either by rupture of the OMM, which, however, is more likely in necrosis, or by escape through channels formed by Bax multimers with or without VDAC. Bax monomers do not exhibit apoptotic activity, and the antiapoptotic Bcl-2 itself inhibits VDAC channel formation. It is not yet clear whether caspases (2, 3, and 9) are really located inside mitochondria. The ejected proteins cytochrome c, caspases, ATP, and the cytoplasmic apoptosis protease activating factor-1 (APAF-1) associate in the cytosol to huge apoptosome complexes (700 kDa), which cleave downstream caspases.

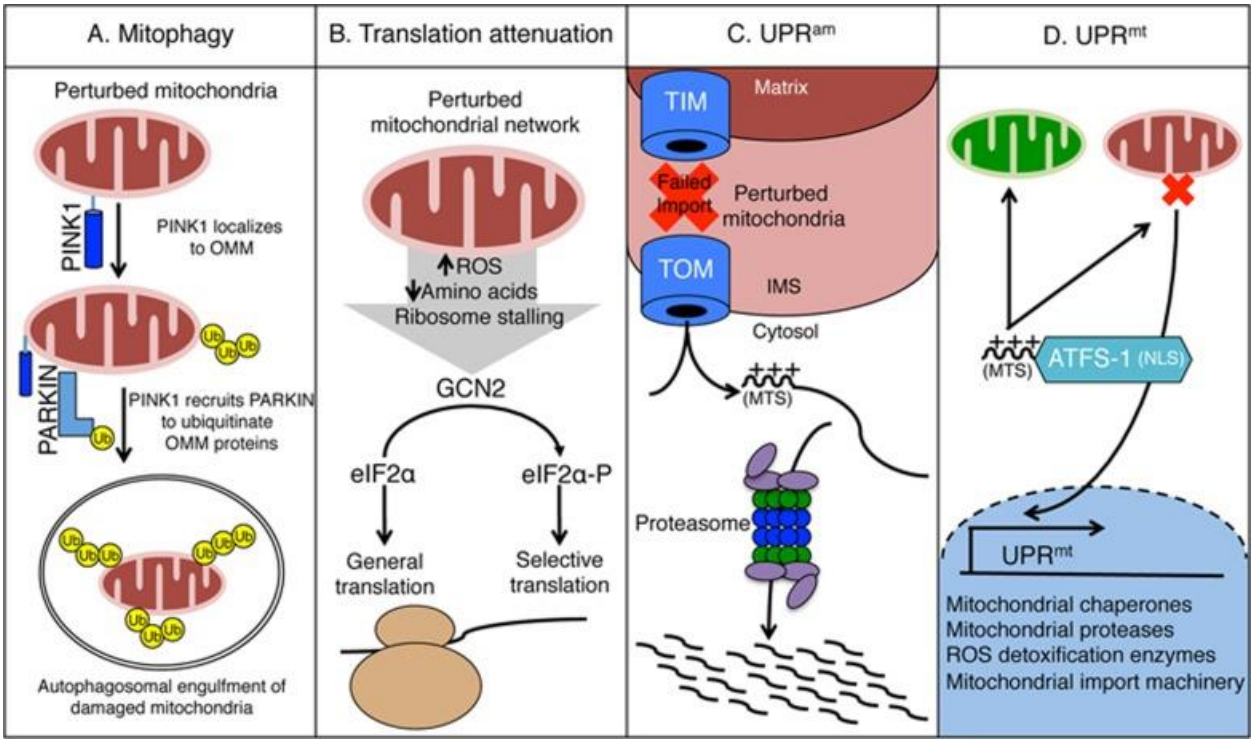

Figure 7. Mitochondrial stress response pathways *[26]*. **(A)** Recognition and selective degradation of damaged mitochondria are mediated by mitophagy. The kinase PINK1 is stabilized specifically on damaged mitochondria where it recruits the ubiquitin ligase Parkin, which ubiquitinates multiple mitochondrial outer membrane proteins. Ubiquitinated mitochondria are then engulfed by autophagosomes and trafficked to lysosomes, where they are degraded. **(B)** The kinase GCN2, which is activated during mitochondrial dysfunction, mediates translation attenuation during mitochondrial dysfunction by phosphorylating the translation initiation factor eIF2α, which serves to reduce the influx of proteins into mitochondria. **(C)** Accumulation of mislocalized mitochondrial proteins in the cytosol stimulates proteasome activity to limit the accumulation of the toxic proteins in a pathway dubbed UPR^{am} (unfolded protein response activated by mistargeted proteins). **(D)** The UPR^{mt} is regulated by the competing organelle targeting sequences in the transcription factor ATFS-1. If ATFS-1 is imported into the mitochondrial matrix via the MTS,

the transcription factor is degraded. However, if ATFS-1 cannot be imported due to mitochondrial dysfunction, it is trafficked to the nucleus, via the NLS, to activate transcription.

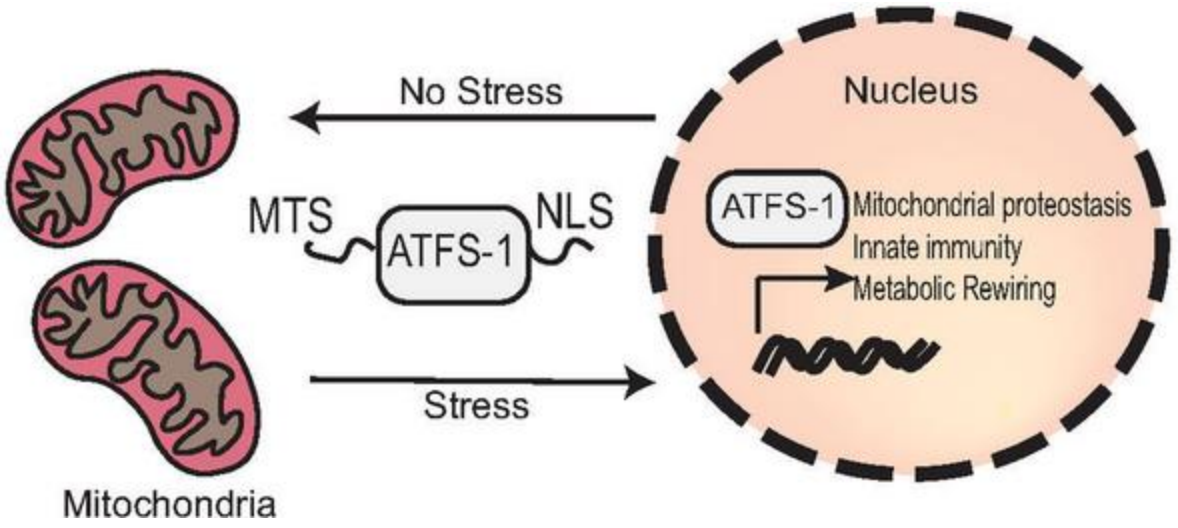

Figure 8. Schematic of the UPR^{mt} response *[69]*. ATFS-1 localizes to mitochondria via its mitochondria targeting signal (MTS), where it is degraded in the absence of stress. However, mitochondrial protein import is attenuated during mitochondrial stress, leading to ATFS-1 accumulation in the cytosol. ATFS-1 is then translocated to the nucleus via its nuclear localization signal (NLS). In the nucleus, ATFS-1 induces mitochondrial protective gene expression described in panel A, which promote survival and recovery from mitochondrial stress.

Chapter 2

Complementary approaches of chemical screening and classical genetics reveal protective roles of actin dynamics and the UPR^{mt} promoting mitochondrial recovery during stress

Mustafi Raisa Amin, Mohammed Adnan Qureshi[¶], Siraje A. Mahmud[¶], Jonathan L. Dowgielewicz, Karen Juanez, Piya Ghose, Mark W. Pellegrino[*]

Department of Biology, University of Texas Arlington, Arlington, TX, 76019

[¶]These authors contributed equally

*Corresponding author. E-mail: mark.pellegrino@uta.edu

**(in review; *Genetics*)

Abstract

The decline in mitochondrial function is associated with organismal aging as well as human diseases. Cells use various means to mitigate the ill effects of mitochondrial dysfunction, including the activation of the mitochondrial unfolded protein (UPR^{mt}) that modulates gene expression related to organelle recovery. Due to the importance of recovery mechanisms during mitochondrial stress, the UPR^{mt} has relevant implications for various diseases, including cancer. As some cancers can experience varying degrees of mitochondrial dysfunction, so too are their reliance on the UPR^{mt} for survival. Consequently, inhibition of the UPR^{mt} reduces cancer cell viability while having little effect on healthy cells. Therefore, the identification of small molecules and pathways that can inhibit the UPR^{mt} may have therapeutic properties in the treatment of certain cancers. Here, we employed a *C. elegans*-based chemical screening approach to identify small molecule inhibitors of the UPR^{mt}. Of the small molecules discovered was the selective serotonin reuptake transporter inhibitor Paroxetine. Accordingly, UPR^{mt}-associated phenotypes were found to be suppressed with Paroxetine treatment. In addition, during the course of investigating the mechanism of Paroxetine action, we serendipitously discovered that actin remodeling is also involved in mediating mitochondrial recovery through the regulation of the UPR^{mt}. Interestingly, actin remodeling regulates the UPR^{mt} in part through a cell non-autonomous mechanism from neurons. Thus, we identify new means of controlling UPR^{mt} activity using a combination of chemical and genetic approaches.

Introduction

Mitochondria are double-membrane organelles with an essential role in producing cellular energy in the form of ATP through the actions of the electron transport chain via oxidative phosphorylation (OXPHOS). Beyond its critical role in generating ATP, mitochondria are also required for ion balance (e.g., calcium homeostasis), fatty acid b-oxidation, and orchestrating a number of signaling pathways, including programmed cell death (1-3). Loss of mitochondrial integrity is associated with organismal aging and the development of disease (4,5). Cancer is one of the many diseases linked to mitochondrial dysfunction, which was first proposed by Otto Warburg in the 1920s following a seminal discovery that cancer cells rely on glycolysis as opposed to aerobic respiration for energy production (6). However, more recent findings indicate a reliance on mitochondrial function in certain cancers, suggesting that mitochondria are likely metabolically reprogrammed in some cancer types rather than being defective (7-9).

Cells use multiple mechanisms to mitigate mitochondrial stress and reestablish homeostasis including the modulation of gene transcription via retrograde signaling pathways such as the mitochondrial unfolded protein response (UPR^{mt}) (10-12). First discovered in mammalian cells, the activation of the UPR^{mt} was associated with the upregulation of genes such as mitochondrial chaperones and quality control proteases that help relieve proteotoxicity during stress (13-15). The mechanics of the UPR^{mt} have been more thoroughly dissected using the model organism *Caenorhabditis elegans*. Notably, the bZIP transcription factor ATFS-1 was identified as the critical regulator of the UPR^{mt} (16-18). The regulation of ATFS-1 is largely dependent on its mitochondrial targeting sequence and mitochondrial import efficiency (17). ATFS-1 is imported into healthy mitochondria that are protein import-competent and turned over proteolytically by the matrix protease Lon. However, import efficiency into mitochondria is reduced during

mitochondrial stress resulting in the localization of ATFS-1 into the nucleus. ATFS-1 transcriptionally regulates a plethora of genes involved in mitochondrial recovery, including those with functions in proteostasis, reactive oxygen species detoxification, and metabolic rewiring (17,18). ATFS-1 also regulates genes with functions in innate immunity as a pathogen defense strategy (19-21). Notably, the transcriptional response mediated by ATFS-1 is required to maintain organismal viability in the presence of mitochondrial stress. Multiple genetic approaches have successfully identified other regulators of the UPR^{mt} with a variety of molecular roles (21-25).

The UPR^{mt} may have clinical potential due to its role in mitochondrial recovery. This is particularly true in cancer due to the mitochondrial dysfunction that is sometimes observed with these diseased cell types (26,27). Accordingly, cancer cells activate and require a UPR^{mt} to mitigate their underlying mitochondrial stress. Indeed, increases in mitochondrial chaperone expression have been observed in certain cancer types (28,29), suggesting an activation of this pathway. Also, the presumptive mammalian ATFS-1 homolog ATF5 that regulates a similar UPR^{mt} (30) is known to be upregulated in certain cancers (31). And consistent with a role in promoting mitochondrial recovery, inhibition of ATF5 reduces the growth of thyroid oncocytoma cells bearing mitochondrial stress (30). In addition, loss of ATF5 function can specifically kill tumor cells while having negligible effects on healthy cells (32). Therefore, identifying strategies or reagents that can block the UPR^{mt} may have clinical relevance with regards to cancer-targeted therapies.

Chemical-based screens are an attractive alternative to genetic approaches to identify modulators of a given pathway. *C. elegans* is a particularly amenable system to pursue whole animal small molecule screens owing to its rapid life cycle, conserved molecular pathways, and transparent nature that allows the application of fluorescent protein-based reporters for rapid screening (33-36). For example, *C. elegans*-based chemical screening has been used to identify novel compounds

that can inhibit the SKN-1 oxidative stress pathway (37). In the current study, we employed a similar strategy to identify small molecule inhibitors of the UPR^{mt}. Of the 1280 compounds tested, 33 were found to attenuate the UPR^{mt}. Here we describe our findings for one of the identified small molecules, the selective serotonin reuptake transporter inhibitor Paroxetine. In addition, while exploring how Paroxetine repressed the UPR^{mt}, we discovered that actin dynamics also play a role in maintaining mitochondrial homeostasis during stress via regulation of the UPR^{mt}.

Materials and Methods

C. elegans strains and maintenance

General maintenance of *C. elegans* and genetic procedures were performed as previously described using Nematode Growth Medium (NGM) (38) and *Escherichia coli* OP50 as a food source. Ethidium bromide (30 µg/ml) or paraquat (0.5 mM) were spread over NMG plates that were previously seeded with *E. coli* OP50. For *wsp-1(gm324)* experiments, 20 µg/ml ethidium bromide was used in order to allow *wsp-1(gm324)* mutant animals to grown to at least the L4 stage for quantification of *hsp-6p*::GFP expression levels. For heat shock conditions, L1 stage animals were raised at 30^{o}C for 3 hrs and then shifted to 25^{o}C until the adult stage was reached. For Paroxetine and Fluoxetine experiments, 15 µM and 30 µM of each drug (Sigma Aldrich), respectively, were spread over *E. coli* OP50 plates. For supplementation with serotonin, serotonin creatine sulfate (Sigma Aldrich) was added to NGM media before pouring at a final concentration of 5 mM (39). *C. elegans* were maintained at 20^{o}C unless otherwise noted. *C. elegans* strains used in this study were obtained from the Caenorhabditis Genetics Center and include: N2 Bristol, *zcIs13*(*hsp-6*::GFP) (strain SJ4100), *zcIs4(hsp-4::GFP*), *dvIs70(hsp-16.2p::GFP + rol-6(su1006)), agIs17(myo-2p::mCherry, irg-1p::GFP), clk-1(qm30), zcIs14(myo-3::GFP(mit)), mod-5(n3314), nrf-1(sa524), nrf-2/vhp-1(sa366), nrf-4(sa528), nrf-5(sa531), nrf-6(sa525), wsp-1(sa363), wsp-1(gm324), unc-73(e936), unc-34(e315), and mig-10(ct41)*. For generation of *nrf-1(sa524); zcIs13(hsp-6::GFP)* and *nrf-4(sa528); zcIs13(hsp-6::GFP),* we selected transgenic progeny that were resistant to the nose contraction caused by Fluoxetine. RNAi experiments were performed as previously described (40).

Prestwick chemical screen

We used the Prestwick Library to screen for small molecules that could inhibit the UPR^{mt}. The Prestwick Library is a collection of 1280 small molecules composed predominantly of drugs that have been approved by the FDA and other agencies. 24-well cell culture plates containing solid Nematode Growth Medium (38) were seeded with *E. coli* OP50. After four days of bacterial growth, individual Prestwick compounds were added to each well at a final concentration of 100 µM in combination with either ethidium bromide (final concentration 30 µg/ml) for the primary screen or paraquat (final concentration 0.5 mM) for the secondary screen. DMSO in combination with ethidium bromide or paraquat was used as the vehicle control. Eggs from gravid *C. elegans* strain *hsp-6p*::GFP were harvested by bleaching and dispensed into each well. GFP expression was qualitatively examined after four days.

Microscopy

Fluorescent images were acquired using a Zeiss AxioCam mounted on a Zeiss M2 Bio stereo microscope or Zeiss Imager.Z2 microscope (Carl Zeiss Imaging). *myo-3p*::GFP^{mt} images were acquired using a Nikon Eclipse Ti2-E inverted spinning disk confocal microscope (Nikon Instruments Inc.).

Oxygen consumption assay

The oxygen consumption assay was performed as previously described using the MitoXpress Xtra oxygen consumption assay kit (Agilent, USA) (41). Briefly, 100-150 animals synchronized to the

L4 stage were washed extensively with S-basal solution before transferring to a 96-well plate using a volume of 90 µl plus 10 µl of oxygen probe. Wells were covered with mineral oil and readings performed using a Synergy Neo 2 plate reader and Gen5 software (Biotek).

Body thrashing assay

Animals synchronized to the L4 stage were placed in a 10 µl drop of S-Basal solution and allowed to acclimate for 1 min before measuring the total number of body bends performed in 10 sec. One body bend was characterized as a complete right to left motion.

Lifespan analysis

Lifespan assays were performed at 20^{o}C using one hundred *C. elegans* at the L4 stage per replicate. Animals were transferred every 1-2 days until all progeny had been laid and scored as dead when they became unresponsive to touch. Animals were censored if they had escaped or ruptured. Statistical analysis was performed using GraphPad Prism software whereby the log-rank (Mantel-Cox) test was performed to generate a *p* value. All statistical analysis are summarized in Supplementary Table S4.

Pathogen infection survival analysis

Analysis of host survival during pathogen infection was performed as previously described (42). Briefly, survival assay plates were prepared from overnight cultures of *P. aeruginosa* PA14 which were used to seed standard NGM plates, allowed to incubate overnight at room temperature,

followed by overnight incubation at 37°C. Animals were age-synchronized on *E. coli* OP50 plates until the L4 stage prior to transferring to *P. aeruginosa* survival assay plates. Statistical analysis was performed using GraphPad Prism software and the log-rank (Mantel-Cox) test. All statistical analyses are summarized in Supplementary Table S4.

Whole-genome sequencing

Whole-genome sequencing was performed as previously described (41).

Plasmid construction

The following tissue-specific promoters were cloned into the plasmid pPD49.26 using the designated restriction sites: for neuronal expression, 3594 kb *rgef-1* promoter using PstI and BamHI sites; for hypodermal expression 3810 kb *lin-26* promoter using HindIII and PstI sites, for intestinal expression 897 kb *vha-6* promoter using HindIII and BamHI sites. RNA and cDNA synthesis were prepared from mixed-staged *C. elegans* using standard procedures. The *wsp-1a* cDNA was then amplified and cloned into XmaI and MscI sites of each tissue-specific plasmid.

Germline transformation

Rescue experiments were performed via microinjection using standard techniques (43). For *wsp-1(sa363)* rescue, 10 ng/µl of fosmid WRM0617cE07 was used for injection. For tissue-specific rescue experiments, the following concentrations were used: 25 ng/µl P_{rgef-1}::*wsp-1a*, 25 ng/µl P_{lin-}

$_{26}$::*wsp-1a*, 10 ng/µl P$_{vha-6}$::*wsp-1a*. For rescue experiments, P$_{myo-2}$::mCherry was used as a co-injection marker at a concentration of 5 ng/µl.

Strains and plasmids are available upon request. The authors affirm that all data necessary for confirming the conclusions of the article are present within the article, figures, and tables.

Results

A whole animal chemical screen identifies small molecule inhibitors of the UPR^{mt}

We screened the Prestwick Chemical Library for inhibitors of the UPR^{mt} using a *C. elegans* whole animal screening approach (Figure 1A). The Prestwick Chemical Library is a collection of 1280 small molecules that are predominantly (approximately 95%) approved for clinical use. We used the *C. elegans* strain SJ4100 that contains a transcriptional green fluorescent reporter (GFP) for the *C. elegans* mitochondrial *hsp70* chaperone homolog *hsp-6* to screen the chemical library. Under healthy conditions, this transgenic strain shows negligible fluorescence, whereas, in the presence of mitochondrial stress, a robust increase in expression and fluorescence is observed (44). We first conducted the screen of all 1280 compounds in the presence of ethidium bromide (EtBr), which depletes mitochondria of its own DNA, resulting in imbalances to mitochondrial homeostasis that activates the UPR^{mt} (17,44). Our primary screen using ethidium bromide as a stress reagent identified 297 compounds (Figure 1B and Supplementary Table S1). We then performed a secondary screen using the hits obtained in the primary screen for further validation. The secondary screen employed the oxidizing reagent paraquat which increases mitochondrial

reactive oxygen species causing activation of the UPR^{mt} (45). Our secondary screen using paraquat as a stress reagent yielded 33 compounds that could attenuate UPR^{mt} signaling (Figure 1B, Supplementary Table S2). Each of the identified compounds possessed different potencies in their ability to attenuate UPR^{mt} activity (Supplementary Table S3).

We further refined our list by assessing the effect of each small molecule on the development of animals in the presence or absence of mitochondrial stress. We predicted that if the identified compounds inhibited the UPR^{mt} that this would impair animal development during stress due to a lack of mitochondrial recovery, similar to what is observed with loss of ATFS-1 (17). However, if the identified drug were to slow the development of animals irrespective of mitochondrial stress, then it may only be impairing general animal fitness. Only five of the identified drugs slowed animal development synergistically in the presence of mitochondrial stress. The five identified compounds included the monoamine oxidase inhibitor Clorgyline hydrochloride, the corticosteroid Clobetasol propionate, the anticholinergic drug Chlorprothixene hydrochloride, the calcium channel blocker Felodipine, and finally, the selective serotonin reuptake transporter inhibitor Paroxetine (Supplementary Figure S1A). We noticed that Fluoxetine, a selective serotonin reuptake transporter inhibitor that is analogous to Paroxetine, also suppressed the UPR^{mt} during stress (Supplementary Figure S1B), similar to Paroxetine (Figure 1C). However, Fluoxetine had less severe effects on the development of animals during stress compared to Paroxetine (Supplementary Figure S1A). We chose the selective serotonin reuptake transporter inhibitor class for further investigation due to their shared mechanism of action, using Paroxetine as a representative drug.

We next examined whether the inhibitory effects of Paroxetine were specific to the UPR^{mt} or whether other cellular stress response pathways were similarly suppressed by this drug. We

examined three cellular stress response pathways: the endoplasmic reticulum unfolded protein response (UPR^{er}) using the *hsp-4p*::GFP reporter, the heat shock response using the *hsp-16.2p*::GFP reporter, and finally, the protein translation stress response using the *irg-1p*::GFP reporter (8,46,47). Paroxetine did not inhibit the UPR^{er} in the presence of the ER stress reagent tunicamycin (Figure 1D). Paroxetine also did not attenuate the *hsp-16.2p*::GFP reporter in the presence of heat stress (Figure 1E). Lastly, Paroxetine treatment did not prevent induction of *irg-1p*::GFP under conditions of impaired protein translation using *eft-2* RNAi (Figure 1F). Consistently, we found no difference in the development of animals exposed to ER, heat, or translation stress in the presence or absence of Paroxetine (Supplementary Figure S2). These data suggest that Paroxetine downregulates the UPR^{mt} stress response specifically.

Next, we wished to explore at what level of the UPR^{mt} pathway Paroxetine may be acting upon. Here, we employed the *atfs-1* gain-of-function mutant, *atfs-1(et18)*, which contains a point mutation in the mitochondrial targeting sequence of ATFS-1 impairing its entry into mitochondria, resulting in constitutive nuclear import and activation of the UPR^{mt} (48). Paroxetine failed to inhibit the UPR^{mt} resulting from the *atfs-1(et18)* gain of function mutant and did not impair its development (Supplementary Figure S3), suggesting that it does not act directly on ATFS-1 itself.

Paroxetine impairs mitochondrial homeostasis during stress

We next assayed the effects of Paroxetine on mitochondrial function in the presence or absence of mitochondrial stress. For these assays, we used the *clk-1(qm30)* mutant, which possesses defective oxidative phosphorylation that activates the UPR^{mt} (49,50). We confirmed that Paroxetine could suppress the UPR^{mt} in *clk-1(qm30)* animals (Supplementary Figure S4). Consistent with reducing

UPR^{mt} activation, Paroxetine further delayed the development of *clk-1(qm30)* animals (Figure 2A). We first monitored oxygen consumption rates which were unaffected in wild-type animals exposed to Paroxetine (Figure 2B). In accordance with previous reports (49,51,52), oxygen consumption rates were reduced in *clk-1(qm30)* animals relative to wild-type animals (Figure 2C). Oxygen consumption rates were further reduced in the presence of Paroxetine (Figure 2D), consistent with its ability to impair the UPR^{mt} and mitochondrial recovery.

Next, we examined the effects of Paroxetine on mitochondrial morphology using a mitochondrial-targeted GFP (GFP^{mt}) expressed in the muscle under the myosin promoter *myo-3*. We observed that in contrast to the tubular mitochondrial appearance of wild-type control animals, Paroxetine treatment increased the proportion of animals with fragmented mitochondria, suggesting enhanced dysfunction (Figure 2E). The expression of GFP^{mt} from the *myo-3* promoter is relatively high, which can challenge mitochondrial protein folding and homeostasis (53). This is thought to create a sensitized background to conditions that disrupt mitochondrial proteostasis (49,53). Consistent with reduced mitochondrial homeostasis, muscle function deteriorated to a greater degree in *myo-3p*::GFP^{mt} animals treated with Paroxetine, as reflected by their reduced thrashing rates (Figure 2F).

Together, these results indicate that Paroxetine perturbs mitochondrial recovery during stress by impairing the activation of the UPR^{mt}.

Paroxetine suppresses UPR^{mt}-associated phenotypes

We next examined the effects of Paroxetine on traits mediated by the UPR^{mt} by first assessing its impact on animal lifespan. A close association exists between mitochondrial function and

organismal aging (5). Related to this paradigm, reduction of function mutations in select electron transport chain genes (e.g., *clk-1*) extend organismal lifespan (49,54-56), and some in a UPR^{mt}-dependent manner (56,57). We, therefore, examined if Paroxetine could suppress mitochondrial stress-induced increases in longevity by inhibiting the UPR^{mt}. Consistently, Paroxetine suppressed the extended lifespan of *clk-1(qm30)* animals without reducing the lifespan of wild-type animals (Figure 3A, B).

We next examined the effects of Paroxetine on host survival during bacterial pathogen infection. ATFS-1 was previously shown to promote host survival during infection with *Pseudomonas aeruginosa*, an opportunistic bacterial pathogen that targets mitochondrial function (19,20,42). In addition, priming animals for the UPR^{mt} could extend host survival when subsequently challenged with *P. aeruginosa* (19,21). We, therefore, asked whether Paroxetine treatment could render animals hypersusceptible to infection, as well as suppress the increased host survival of UPR^{mt}-primed animals. Interestingly, Paroxetine decreased the survival of wild-type animals challenged with *P. aeruginosa* (Figure 3C). In addition, Paroxetine reduced the extended host survival of *clk-1(qm30)* when infected with *P. aeruginosa* (Figure 3D), consistent with its ability to inhibit the UPR^{mt}. Therefore, Paroxetine suppresses UPR^{mt}-associated increases in host resistance. Together, our assays of animal lifespan and host survival during infection support an anti-UPR^{mt} action exhibited by Paroxetine.

Inhibition of Paroxetine or Fluoxetine's clinical target ortholog does not suppress the UPR^{mt}

Paroxetine is a neuromodulator used in the treatment of psychiatric disorders, including depression. Paroxetine increases levels of serotonin in the synapse by inhibiting serotonin reuptake

transporters. We wished to test whether the serotonin reuptake transporter was the molecular target of Paroxetine responsible for suppressing the UPR^{mt}. If so, we predicted that genetically disabling serotonin reuptake transporter function in *C. elegans* would repress UPR^{mt} activation in the presence of mitochondrial stress. *C. elegans* possesses one serotonin reuptake transporter ortholog, MOD-5, which similarly regulates serotonin levels at the synapse (58). We used the *mod-5(n3314)* mutant, which represents a null allele of this gene (58). In contrast to Paroxetine treatment, however, *mod-5(n3314)* surprisingly did not suppress the UPR^{mt} during mitochondrial stress (Figure 4A). Consistently, *mod-5(n3314)* mutant animals did not exhibit obvious differences in developmental rates in the presence of mitochondrial stress (Figure 4B). Furthermore, loss of MOD-5 had negligible effects on the lifespans of wild-type or *clk-1(qm30)* animals (Figures 4C, D). As further validation, we asked whether supplementation of serotonin could inhibit the UPR^{mt}, knowing that the serotonin reuptake transporter functions in limiting this neurotransmitter. Consistently, serotonin supplementation was unable to suppress the UPR^{mt} under stress (Supplementary Figure S5). Therefore, our results suggest that Paroxetine impairs UPR^{mt} signaling through an unconventional molecular target independent of the serotonin reuptake transporter.

"nrf" pathway genes do not mediate the repression of the UPR^{mt} by Paroxetine

Since the clinical target of Paroxetine did not appear to mediate its inhibitory effects on the UPR^{mt}, we next wished to explore other possible mechanisms of action. It was previously shown that Paroxetine or Fluoxetine treatment results in serotonin-independent phenotypes in *C. elegans,* including a hypercontracted nose phenotype (59). Choy and Thomas (1999) (59) conducted a forward genetics screen to isolate suppressors of this hypercontracted nose phenotype, of which seven suppressors were discovered and annotated as "*nrf"* genes (*n*ose *r*esistant to *F*luoxetine)

(59). We wished to explore whether these "*nrf*" mutants could restore the activity of the UPR^{mt} in the presence of Paroxetine. Only four of the seven *nrf* genes were genetically mapped to a single gene in the original screen: *nrf-2* (currently known as *vhp-1*) encodes a protein phosphatase, *nrf-5* encodes a cholesterol esther transfer protein involved in lipid transport, *nrf-6* encodes a lipid binding protein, and *ndg-4* encodes an O-acyltransferase-like protein (59). Subsequent studies have shown that *ndg-4, nrf-5*, and *nrf-6* likely function in the same pathway (59-61). However, none of the "*nrf*" pathway mutants tested restored the activation of the UPR^{mt} during stress in the presence of Paroxetine (Figure 5A). We were unable to test whether loss of *nrf-5* could restore UPR^{mt} activity in the presence of Paroxetine during stress due to close proximity of the *nrf-5* gene and the *hsp-6p*::GFP transgene. However, *nrf-5* mutants continued to be developmentally arrested during stress in the presence of Paroxetine, suggesting it does not suppress the inhibition of the UPR^{mt} caused by this drug (Figure 5D). In fact, none of the *nrf* pathway mutants were resistant to the developmental arrest caused by Paroxetine during stress (Figure 5D). Therefore, this suggests that Paroxetine inhibits the UPR^{mt} using a mechanism that is independent of the *nrf* pathways.

Actin cytoskeleton regulation acts in concert with the UPR^{mt} during mitochondrial stress

While we were unable to determine the anti-UPR^{mt} mechanism of Paroxetine, we were nonetheless intrigued that one of the *nrf* alleles examined, *sa363*, of the originally named gene *nrf-3*, displayed substantial developmental arrest in the presence of mitochondrial stress (Figure 5C). Little difference in development was observed for the *sa363* mutant in the absence of stress (Figure 5B). We wished to identify the gene associated with the *sa363* allele since it was only mapped at the chromosomal level in the original screen (59). Using whole-genome sequencing, we determined that the gene responsible for the hypersusceptibility to mitochondrial stress in *sa363* animals is

wsp-1, the *C. elegans* homolog of N-WASP (Wiskott Aldrich syndrome protein (Figure 6A). Proteins of the WASP family are involved in actin nucleation through activation of actin-related protein 2 and 3 (Arp2/3), and are regulated by Cdc42, a member of the Rho family of GTPases (62). The *wsp-1* gene encodes for two isoforms: WSP-1A and WSP-1B (63). The *sa363* mutation is located in the splice acceptor site of the first intron of *wsp-1,* which specifically disables the WSP-1A isoform (Figure 6A). We carried out a transformation rescue experiment to confirm that the developmental arrest of *sa363* animals during mitochondrial stress was due to impaired WSP-1 function. Indeed, introduction of the wild-type *wsp-1* locus into the *sa363* mutant background restored wild-type developmental rates in the presence of mitochondrial stress (Supplementary Figure S6). We next tested a second mutant allele of *wsp-1*, *gm324*, which specifically removes the second and third exon of the *wsp-1A* isoform (Figure 6A and (63)). Developmental arrest was also observed with *wsp-1(gm324)* animals under stress, whereas little change in development occurred in the absence of stress (Supplementary Figure S6).

We also tested whether WSP-1 mediated the hypercontracted nose phenotype observed with *sa363* animals during Fluoxetine exposure. We found that introduction of the wild-type *wsp-1* locus into *sa363* animals rendered them susceptible to the hypercontracted nose phenotype caused by Fluoxetine (Supplementary Figure S7). Furthermore, *wsp-1(gm324)* animals were resistant to the hypercontracted nose phenotype similar to *nrf-3(sa363)* animals (Supplementary Figure S7). Therefore, *nrf-3(sa363)* is indeed a loss of function allele of *wsp-1*.

We next tested the involvement of other regulators of the actin network through an examination of UNC-73/Trio, UNC-34/Ena/VASP, and MIG-10/Lamellipodin (64-66). Similar to *wsp-1* mutants, all three regulators of actin polymerization significantly slowed animal development in

the presence of mitochondrial stress (Supplementary Figure S8). Therefore, actin remodeling is necessary for recovery during periods of mitochondrial dysfunction.

Loss of WSP-1 perturbed animal development during mitochondrial stress, suggesting that actin remodeling may affect the UPR^{mt} during mitochondrial recovery. We therefore examined the activity of the UPR^{mt} in the presence or absence of WSP-1. Interestingly, UPR^{mt} activity was reduced in *wsp-1(gm324)* mutant animals in the presence of mitochondrial stress (Figures 6B, C), suggesting that actin dynamics play some role in the regulation of this stress response. To explore this further, we examined animal development during mitochondrial stress (using *clk-1(qm30)* animals) in the presence or absence of WSP-1 and/or ATFS-1. As expected (17), loss of ATFS-1 via RNAi resulted in a further impairment of *clk-1(qm30)* development (Figure 6D). Similarly, loss of WSP-1 also further slowed *clk-1(qm30)* development (Figure 6D). However, simultaneous loss of WSP-1 and ATFS-1 did not result in a more pronounced developmental impairment during stress (Figure 6D), suggesting that actin dynamics and ATFS-1/UPR^{mt} are acting in the same pathway to promote mitochondrial homeostasis.

We next explored the role of actin remodeling during mitochondrial recovery by examining the extended lifespan of *clk-1(qm30)* animals. Consistently, while we observed no difference in the lifespan of *wsp-1* mutants compared to wild-type (Figure 6E), loss of WSP-1 reduced the lifespan of long-lived *clk-1(qm30)* animals (Figure 6F). Thus, actin remodeling supports mitochondrial recovery during stress, presumably through regulation of the UPR^{mt}.

WSP-1 regulates UPR^{mt} activity both cell-autonomously and non-autonomously

WSP-1 was previously found to act at the active zone in neurons to control synaptic vesicle release (63). This prompted us to examine a possible cell non-autonomous role of WSP-1 in mediating mitochondrial recovery. To explore this further, we expressed the *wsp-1a* cDNA under the control of tissue-specific promoters in the neurons, intestine, or hypodermis. Interestingly, all tissue-specific expression constructs of *wsp-1a* activated the UPR^{mt} in the absence of stress to varying degrees, notably with expression of *wsp-1a* in the neurons or intestine (Figure 7A). During stress, expression of *wsp-1a* in neurons or intestine restored UPR^{mt} activity in *wsp-1(gm324)* animals, whereas expression in hypodermis had a modest effect (Figure 7B). We also found that expression of *wsp-1a* in neurons or hypodermis could partially restore the development of *wsp-1(gm324)* animals during stress (Figure 7C). Surprisingly, expression of *wsp-1a* in the intestine did not rescue the development of stressed *wsp-1(gm324)* animals as well in comparison (Figure 7C), despite a restoration of UPR^{mt} activity. Possibly, overexpression of *wsp-1a* in the intestine imparts other deleterious effects that prohibit growth during stress.

Discussion

Together, we used a chemical-based screen to identify small molecule inhibitors of the UPR^{mt}. We were successful in isolating a number of UPR^{mt} inhibitors from this chemical screening approach including the antidepressant Paroxetine. Paroxetine treatment had negligible effects on mitochondrial function in healthy animals but further reduced mitochondrial homeostasis in those animals experiencing stress. In our pursuit of Paroxetine's anti-UPR^{mt} mechanism of action, we also unexpectedly discovered that actin dynamics plays a role in mitochondrial recovery using

classical genetics. Our data suggests that actin dynamics positively regulates, at least partially, the activation of the UPR^{mt} cell non-autonomously from neuronal tissues (Figure 7D).

Paroxetine treatment perturbed mitochondrial homeostasis during stress through a repressive action on the UPR^{mt} via an unidentified mechanism. We provide evidence that the suppressive effect of Paroxetine on UPR^{mt} activity is independent of its clinical target, the serotonin reuptake transporter. Interestingly, Paroxetine was previously shown to induce mitochondrial-associated apoptosis in the human breast cancer cell line MCF-7 (67). Here, Paroxetine treatment led to increases in reactive oxygen species and reduced mitochondrial membrane potential. Paroxetine-mediated mitochondrial-associated apoptosis was reduced in the presence of antioxidants, suggesting a link between increased oxidative stress and cell death in this cancer cell line following treatment with this drug. A similar association between Paroxetine treatment, increased reactive oxygen species and mitochondrial-associated apoptosis was also discovered with astrocytes (68). These outcomes are consistent with our findings of increased mitochondrial dysfunction in stressed *C. elegans* treated with Paroxetine. The anti-UPR^{mt} mechanism of Paroxetine was unfortunately not discovered in this study. Other unconventional molecular targets of Paroxetine have been previously discovered in other organisms including the norepinephrine transporter, muscarinic receptor, and cytochrome P450 2D6 (69), but whether these targets have any relevance to UPR^{mt} activity is not known. Therefore, a further exploration into Paroxetine's mechanism of action may unveil new regulatory aspects of the UPR$^{mt.}$

In pursuit of Paroxetine's mechanism, we unexpectedly discovered that the WASP homolog WSP-1 and other regulators of actin cytoskeleton dynamics are important for mitochondrial recovery, in part through the regulation of the UPR^{mt}. Interestingly, actin cytoskeleton integrity was previously found to mediate recovery during heat stress. Here, the main regulator of the heat shock response,

the transcription factor HSF-1, maintains actin cytoskeletal networks through transcriptional upregulation of *pat-10,* encoding a calcium binding protein of the troponin complex (70). PAT-10 was required for resistance to heat stress independent of the troponin complex. In addition, regulation of actin cytoskeleton remodeling via Rho GTPase signaling facilitated resistance to heat and oxidative stress (71). Our data showing a requirement for WSP-1 and other regulators of actin polymerization during mitochondrial recovery via the UPR^{mt} further supports the critical need of cytoskeletal remodeling during cellular stress.

The mechanism of how actin remodeling regulates the UPR^{mt} is not known. However, our findings suggest that WSP-1 acts at least partially from the nervous system to drive UPR^{mt} activation in the intestine in a cell non-autonomous manner (57). Cell non-autonomous UPR^{mt} signaling from the neurons to intestine involves multiple signals (22,25,72). Among these signals is the Wnt secretion factor MIG-14 which mediates the induction of UPR^{mt} in peripheral tissues resulting from stress in neurons (22). It is possible that tight regulation of actin remodeling might be necessary for the secretion of this Wnt signal to drive cell non-autonomous regulation of the UPR^{mt}. Consistently, actin cytoskeleton regulation has been implicated in Wnt secretion from cholinergic motor neurons (73). Here, the tetraspan protein HIC-1 regulates Wnt secretion through association with the actin-binding protein NAB-1. Therefore, further exploration of the role of WSP-1 and actin dynamics in the regulation of the UPR^{mt}, in both cell-autonomous and non-autonomous contexts, is warranted.

Acknowledgements

We thank the *Caenorhabditis* Genetic Center which is funded by the NIH Office of Research Infrastructure (P40 OD010440) for providing some of the worm strains used in this study. Research support was provided by the National Institutes of Health (5R35GM128885), and Cancer Prevention & Research Institute of Texas (RR160053; M.W.P. and RR100091; P.G.), CPRIT Scholars in Cancer Research.

References

1. Baughman, J. M., Perocchi, F., Girgis, H. S., Plovanich, M., Belcher-Timme, C. A., Sancak, Y., Bao, X. R., Strittmatter, L., Goldberger, O., Bogorad, R. L., Koteliansky, V., and Mootha, V. K. (2011) Integrative genomics identifies MCU as an essential component of the mitochondrial calcium uniporter. *Nature* **476**, 341-345
2. De Stefani, D., Raffaello, A., Teardo, E., Szabo, I., and Rizzuto, R. (2011) A forty-kilodalton protein of the inner membrane is the mitochondrial calcium uniporter. *Nature* **476**, 336-340
3. Wang, C., and Youle, R. J. (2009) The role of mitochondria in apoptosis*. *Annu Rev Genet* **43**, 95-118
4. Schulz, A. M., and Haynes, C. M. (2015) UPR(mt)-mediated cytoprotection and organismal aging. *Biochim Biophys Acta* **1847**, 1448-1456
5. Sun, N., Youle, R. J., and Finkel, T. (2016) The Mitochondrial Basis of Aging. *Mol Cell* **61**, 654-666
6. Warburg, O., Wind, F., and Negelein, E. (1927) The Metabolism of Tumors in the Body. *J Gen Physiol* **8**, 519-530
7. Zong, W. X., Rabinowitz, J. D., and White, E. (2016) Mitochondria and Cancer. *Mol Cell* **61**, 667-676
8. Dickinson, A., Yeung, K. Y., Donoghue, J., Baker, M. J., Kelly, R. D., McKenzie, M., Johns, T. G., and St John, J. C. (2013) The regulation of mitochondrial DNA copy number in glioblastoma cells. *Cell Death Differ* **20**, 1644-1653
9. Weinberg, F., Hamanaka, R., Wheaton, W. W., Weinberg, S., Joseph, J., Lopez, M., Kalyanaraman, B., Mutlu, G. M., Budinger, G. R., and Chandel, N. S. (2010)

Mitochondrial metabolism and ROS generation are essential for Kras-mediated tumorigenicity. *Proc Natl Acad Sci U S A* **107**, 8788-8793

10. Qureshi, M. A., Haynes, C. M., and Pellegrino, M. W. (2017) The mitochondrial unfolded protein response: Signaling from the powerhouse. *J Biol Chem* **292**, 13500-13506
11. Melber, A., and Haynes, C. M. (2018) UPR(mt) regulation and output: a stress response mediated by mitochondrial-nuclear communication. *Cell Res* **28**, 281-295
12. Shpilka, T., and Haynes, C. M. (2018) The mitochondrial UPR: mechanisms, physiological functions and implications in ageing. *Nat Rev Mol Cell Biol* **19**, 109-120
13. Zhao, Q., Wang, J., Levichkin, I. V., Stasinopoulos, S., Ryan, M. T., and Hoogenraad, N. J. (2002) A mitochondrial specific stress response in mammalian cells. *EMBO J* **21**, 4411-4419
14. Horibe, T., and Hoogenraad, N. J. (2007) The chop gene contains an element for the positive regulation of the mitochondrial unfolded protein response. *PLoS One* **2**, e835
15. Aldridge, J. E., Horibe, T., and Hoogenraad, N. J. (2007) Discovery of genes activated by the mitochondrial unfolded protein response (mtUPR) and cognate promoter elements. *PLoS One* **2**, e874
16. Haynes, C. M., Yang, Y., Blais, S. P., Neubert, T. A., and Ron, D. (2010) The matrix peptide exporter HAF-1 signals a mitochondrial UPR by activating the transcription factor ZC376.7 in C. elegans. *Mol Cell* **37**, 529-540
17. Nargund, A. M., Pellegrino, M. W., Fiorese, C. J., Baker, B. M., and Haynes, C. M. (2012) Mitochondrial import efficiency of ATFS-1 regulates mitochondrial UPR activation. *Science* **337**, 587-590

18. Nargund, A. M., Fiorese, C. J., Pellegrino, M. W., Deng, P., and Haynes, C. M. (2015) Mitochondrial and nuclear accumulation of the transcription factor ATFS-1 promotes OXPHOS recovery during the UPR(mt). *Mol Cell* **58**, 123-133

19. Pellegrino, M. W., Nargund, A. M., Kirienko, N. V., Gillis, R., Fiorese, C. J., and Haynes, C. M. (2014) Mitochondrial UPR-regulated innate immunity provides resistance to pathogen infection. *Nature* **516**, 414-417

20. Jeong, D. E., Lee, D., Hwang, S. Y., Lee, Y., Lee, J. E., Seo, M., Hwang, W., Seo, K., Hwang, A. B., Artan, M., Son, H. G., Jo, J. H., Baek, H., Oh, Y. M., Ryu, Y., Kim, H. J., Ha, C. M., Yoo, J. Y., and Lee, S. V. (2017) Mitochondrial chaperone HSP-60 regulates anti-bacterial immunity via p38 MAP kinase signaling. *EMBO J* **36**, 1046-1065

21. Liu, Y., Samuel, B. S., Breen, P. C., and Ruvkun, G. (2014) Caenorhabditis elegans pathways that surveil and defend mitochondria. *Nature* **508**, 406-410

22. Berendzen, K. M., Durieux, J., Shao, L. W., Tian, Y., Kim, H. E., Wolff, S., Liu, Y., and Dillin, A. (2016) Neuroendocrine Coordination of Mitochondrial Stress Signaling and Proteostasis. *Cell* **166**, 1553-1563 e1510

23. Merkwirth, C., Jovaisaite, V., Durieux, J., Matilainen, O., Jordan, S. D., Quiros, P. M., Steffen, K. K., Williams, E. G., Mouchiroud, L., Tronnes, S. U., Murillo, V., Wolff, S. C., Shaw, R. J., Auwerx, J., and Dillin, A. (2016) Two Conserved Histone Demethylases Regulate Mitochondrial Stress-Induced Longevity. *Cell* **165**, 1209-1223

24. Tian, Y., Garcia, G., Bian, Q., Steffen, K. K., Joe, L., Wolff, S., Meyer, B. J., and Dillin, A. (2016) Mitochondrial Stress Induces Chromatin Reorganization to Promote Longevity and UPR(mt). *Cell* **165**, 1197-1208

25. Shao, L. W., Niu, R., and Liu, Y. (2016) Neuropeptide signals cell non-autonomous mitochondrial unfolded protein response. *Cell Res* **26**, 1182-1196

26. Bonora, E., Porcelli, A. M., Gasparre, G., Biondi, A., Ghelli, A., Carelli, V., Baracca, A., Tallini, G., Martinuzzi, A., Lenaz, G., Rugolo, M., and Romeo, G. (2006) Defective oxidative phosphorylation in thyroid oncocytic carcinoma is associated with pathogenic mitochondrial DNA mutations affecting complexes I and III. *Cancer Res* **66**, 6087-6096

27. Petros, J. A., Baumann, A. K., Ruiz-Pesini, E., Amin, M. B., Sun, C. Q., Hall, J., Lim, S., Issa, M. M., Flanders, W. D., Hosseini, S. H., Marshall, F. F., and Wallace, D. C. (2005) mtDNA mutations increase tumorigenicity in prostate cancer. *Proc Natl Acad Sci U S A* **102**, 719-724

28. Ghosh, J. C., Dohi, T., Kang, B. H., and Altieri, D. C. (2008) Hsp60 regulation of tumor cell apoptosis. *J Biol Chem* **283**, 5188-5194

29. Wadhwa, R., Takano, S., Kaur, K., Deocaris, C. C., Pereira-Smith, O. M., Reddel, R. R., and Kaul, S. C. (2006) Upregulation of mortalin/mthsp70/Grp75 contributes to human carcinogenesis. *Int J Cancer* **118**, 2973-2980

30. Fiorese, C. J., Schulz, A. M., Lin, Y. F., Rosin, N., Pellegrino, M. W., and Haynes, C. M. (2016) The Transcription Factor ATF5 Mediates a Mammalian Mitochondrial UPR. *Curr Biol* **26**, 2037-2043

31. Sears, T. K., and Angelastro, J. M. (2017) The transcription factor ATF5: role in cellular differentiation, stress responses, and cancer. *Oncotarget* **8**, 84595-84609

32. Angelastro, J. M., Canoll, P. D., Kuo, J., Weicker, M., Costa, A., Bruce, J. N., and Greene, L. A. (2006) Selective destruction of glioblastoma cells by interference with the activity or expression of ATF5. *Oncogene* **25**, 907-916

33. O'Reilly, L. P., Luke, C. J., Perlmutter, D. H., Silverman, G. A., and Pak, S. C. (2014) C. elegans in high-throughput drug discovery. *Adv Drug Deliv Rev* **69-70**, 247-253

34. Jones, A. K., Buckingham, S. D., and Sattelle, D. B. (2005) Chemistry-to-gene screens in Caenorhabditis elegans. *Nat Rev Drug Discov* **4**, 321-330

35. Schwendeman, A. R., and Shaham, S. (2016) A High-Throughput Small Molecule Screen for C. elegans Linker Cell Death Inhibitors. *PLoS One* **11**, e0164595

36. Cai, Y., Cao, X., and Aballay, A. (2014) Whole-animal chemical screen identifies colistin as a new immunomodulator that targets conserved pathways. *mBio* **5**

37. Leung, C. K., Wang, Y., Malany, S., Deonarine, A., Nguyen, K., Vasile, S., and Choe, K. P. (2013) An ultra high-throughput, whole-animal screen for small molecule modulators of a specific genetic pathway in Caenorhabditis elegans. *PLoS One* **8**, e62166

38. Brenner, S. (1974) The genetics of Caenorhabditis elegans. *Genetics* **77**, 71-94

39. Chao, M. Y., Komatsu, H., Fukuto, H. S., Dionne, H. M., and Hart, A. C. (2004) Feeding status and serotonin rapidly and reversibly modulate a Caenorhabditis elegans chemosensory circuit. *Proc Natl Acad Sci U S A* **101**, 15512-15517

40. Kamath, R. S., Fraser, A. G., Dong, Y., Poulin, G., Durbin, R., Gotta, M., Kanapin, A., Le Bot, N., Moreno, S., Sohrmann, M., Welchman, D. P., Zipperlen, P., and Ahringer, J. (2003) Systematic functional analysis of the Caenorhabditis elegans genome using RNAi. *Nature* **421**, 231-237

41. Amin, M. R., Mahmud, S. A., Dowgielewicz, J. L., Sapkota, M., and Pellegrino, M. W. (2020) A novel gene-diet interaction promotes organismal lifespan and host protection during infection via the mitochondrial UPR. *PLoS Genet* **16**, e1009234

42. Mahmud, S. A., Qureshi, M. A., Sapkota, M., and Pellegrino, M. W. (2020) A pathogen branched-chain amino acid catabolic pathway subverts host survival by impairing energy metabolism and the mitochondrial UPR. *PLoS Pathog* **16**, e1008918

43. Kadandale, P., Chatterjee, I., and Singson, A. (2009) Germline transformation of Caenorhabditis elegans by injection. *Methods Mol Biol* **518**, 123-133

44. Yoneda, T., Benedetti, C., Urano, F., Clark, S. G., Harding, H. P., and Ron, D. (2004) Compartment-specific perturbation of protein handling activates genes encoding mitochondrial chaperones. *J Cell Sci* **117**, 4055-4066

45. Runkel, E. D., Liu, S., Baumeister, R., and Schulze, E. (2013) Surveillance-activated defenses block the ROS-induced mitochondrial unfolded protein response. *PLoS Genet* **9**, e1003346

46. Dunbar, T. L., Yan, Z., Balla, K. M., Smelkinson, M. G., and Troemel, E. R. (2012) C. elegans detects pathogen-induced translational inhibition to activate immune signaling. *Cell Host Microbe* **11**, 375-386

47. Estes, K. A., Dunbar, T. L., Powell, J. R., Ausubel, F. M., and Troemel, E. R. (2010) bZIP transcription factor zip-2 mediates an early response to Pseudomonas aeruginosa infection in Caenorhabditis elegans. *Proc Natl Acad Sci U S A* **107**, 2153-2158

48. Rauthan, M., Ranji, P., Aguilera Pradenas, N., Pitot, C., and Pilon, M. (2013) The mitochondrial unfolded protein response activator ATFS-1 protects cells from inhibition of the mevalonate pathway. *Proc Natl Acad Sci U S A* **110**, 5981-5986

49. Baker, B. M., Nargund, A. M., Sun, T., and Haynes, C. M. (2012) Protective coupling of mitochondrial function and protein synthesis via the eIF2alpha kinase GCN-2. *PLoS Genet* **8**, e1002760

50. Kayser, E. B., Sedensky, M. M., Morgan, P. G., and Hoppel, C. L. (2004) Mitochondrial oxidative phosphorylation is defective in the long-lived mutant clk-1. *J Biol Chem* **279**, 54479-54486

51. Felkai, S., Ewbank, J. J., Lemieux, J., Labbe, J. C., Brown, G. G., and Hekimi, S. (1999) CLK-1 controls respiration, behavior and aging in the nematode Caenorhabditis elegans. *EMBO J* **18**, 1783-1792

52. Braeckman, B. P., Houthoofd, K., De Vreese, A., and Vanfleteren, J. R. (1999) Apparent uncoupling of energy production and consumption in long-lived Clk mutants of Caenorhabditis elegans. *Curr Biol* **9**, 493-496

53. Benedetti, C., Haynes, C. M., Yang, Y., Harding, H. P., and Ron, D. (2006) Ubiquitin-like protein 5 positively regulates chaperone gene expression in the mitochondrial unfolded protein response. *Genetics* **174**, 229-239

54. Yang, W., and Hekimi, S. (2010) Two modes of mitochondrial dysfunction lead independently to lifespan extension in Caenorhabditis elegans. *Aging Cell* **9**, 433-447

55. Wong, A., Boutis, P., and Hekimi, S. (1995) Mutations in the clk-1 gene of Caenorhabditis elegans affect developmental and behavioral timing. *Genetics* **139**, 1247-1259

56. Wu, Z., Senchuk, M. M., Dues, D. J., Johnson, B. K., Cooper, J. F., Lew, L., Machiela, E., Schaar, C. E., DeJonge, H., Blackwell, T. K., and Van Raamsdonk, J. M. (2018) Mitochondrial unfolded protein response transcription factor ATFS-1 promotes longevity in a long-lived mitochondrial mutant through activation of stress response pathways. *BMC Biol* **16**, 147

57. Durieux, J., Wolff, S., and Dillin, A. (2011) The cell-non-autonomous nature of electron transport chain-mediated longevity. *Cell* **144**, 79-91

58. Ranganathan, R., Sawin, E. R., Trent, C., and Horvitz, H. R. (2001) Mutations in the Caenorhabditis elegans serotonin reuptake transporter MOD-5 reveal serotonin-dependent and -independent activities of fluoxetine. *J Neurosci* **21**, 5871-5884

59. Choy, R. K., and Thomas, J. H. (1999) Fluoxetine-resistant mutants in C. elegans define a novel family of transmembrane proteins. *Mol Cell* **4**, 143-152

60. Watts, J. L., and Browse, J. (2006) Dietary manipulation implicates lipid signaling in the regulation of germ cell maintenance in C. elegans. *Dev Biol* **292**, 381-392

61. Brejning, J., Norgaard, S., Scholer, L., Morthorst, T. H., Jakobsen, H., Lithgow, G. J., Jensen, L. T., and Olsen, A. (2014) Loss of NDG-4 extends lifespan and stress resistance in Caenorhabditis elegans. *Aging Cell* **13**, 156-164

62. Sawa, M., Suetsugu, S., Sugimoto, A., Miki, H., Yamamoto, M., and Takenawa, T. (2003) Essential role of the C. elegans Arp2/3 complex in cell migration during ventral enclosure. *J Cell Sci* **116**, 1505-1518

63. Zhang, Y., and Kubiseski, T. J. (2010) Caenorhabditis elegans wsp-1 regulation of synaptic function at the neuromuscular junction. *J Biol Chem* **285**, 23040-23046

64. Steven, R., Kubiseski, T. J., Zheng, H., Kulkarni, S., Mancillas, J., Ruiz Morales, A., Hogue, C. W., Pawson, T., and Culotti, J. (1998) UNC-73 activates the Rac GTPase and is required for cell and growth cone migrations in C. elegans. *Cell* **92**, 785-795

65. Krause, M., Leslie, J. D., Stewart, M., Lafuente, E. M., Valderrama, F., Jagannathan, R., Strasser, G. A., Rubinson, D. A., Liu, H., Way, M., Yaffe, M. B., Boussiotis, V. A., and Gertler, F. B. (2004) Lamellipodin, an Ena/VASP ligand, is implicated in the regulation of lamellipodial dynamics. *Dev Cell* **7**, 571-583

66. Withee, J., Galligan, B., Hawkins, N., and Garriga, G. (2004) Caenorhabditis elegans WASP and Ena/VASP proteins play compensatory roles in morphogenesis and neuronal cell migration. *Genetics* **167**, 1165-1176

67. Cho, Y. W., Kim, E. J., Nyiramana, M. M., Shin, E. J., Jin, H., Ryu, J. H., Kang, K. R., Lee, G. W., Kim, H. J., Han, J., and Kang, D. (2019) Paroxetine Induces Apoptosis of Human Breast Cancer MCF-7 Cells through Ca(2+)-and p38 MAP Kinase-Dependent ROS Generation. *Cancers (Basel)* **11**

68. Then, C. K., Liu, K. H., Liao, M. H., Chung, K. H., Wang, J. Y., and Shen, S. C. (2017) Antidepressants, sertraline and paroxetine, increase calcium influx and induce mitochondrial damage-mediated apoptosis of astrocytes. *Oncotarget* **8**, 115490-115502

69. Bourin, M., Chue, P., and Guillon, Y. (2001) Paroxetine: a review. *CNS Drug Rev* **7**, 25-47

70. Baird, N. A., Douglas, P. M., Simic, M. S., Grant, A. R., Moresco, J. J., Wolff, S. C., Yates, J. R., 3rd, Manning, G., and Dillin, A. (2014) HSF-1-mediated cytoskeletal integrity determines thermotolerance and life span. *Science* **346**, 360-363

71. Patel, R., Sriramoji, S., Marucci, M., Aziz, I., Shah, S., and Sesti, F. (2017) Cytoskeletal remodeling via Rho GTPases during oxidative and thermal stress in Caenorhabditis elegans. *Biochem Biophys Res Commun* **492**, 338-342

72. Zhang, Q., Wu, X., Chen, P., Liu, L., Xin, N., Tian, Y., and Dillin, A. (2018) The Mitochondrial Unfolded Protein Response Is Mediated Cell-Non-autonomously by Retromer-Dependent Wnt Signaling. *Cell* **174**, 870-883 e817

73. Tikiyani, V., Li, L., Sharma, P., Liu, H., Hu, Z., and Babu, K. (2018) Wnt Secretion Is Regulated by the Tetraspan Protein HIC-1 through Its Interaction with Neurabin/NAB-1. *Cell Rep* **25**, 1856-1871 e1856

74. Lee, K. S., Iwanir, S., Kopito, R. B., Scholz, M., Calarco, J. A., Biron, D., and Levine, E. (2017) Serotonin-dependent kinetics of feeding bursts underlie a graded response to food availability in C. elegans. *Nat Commun* **8**, 14221

Figures

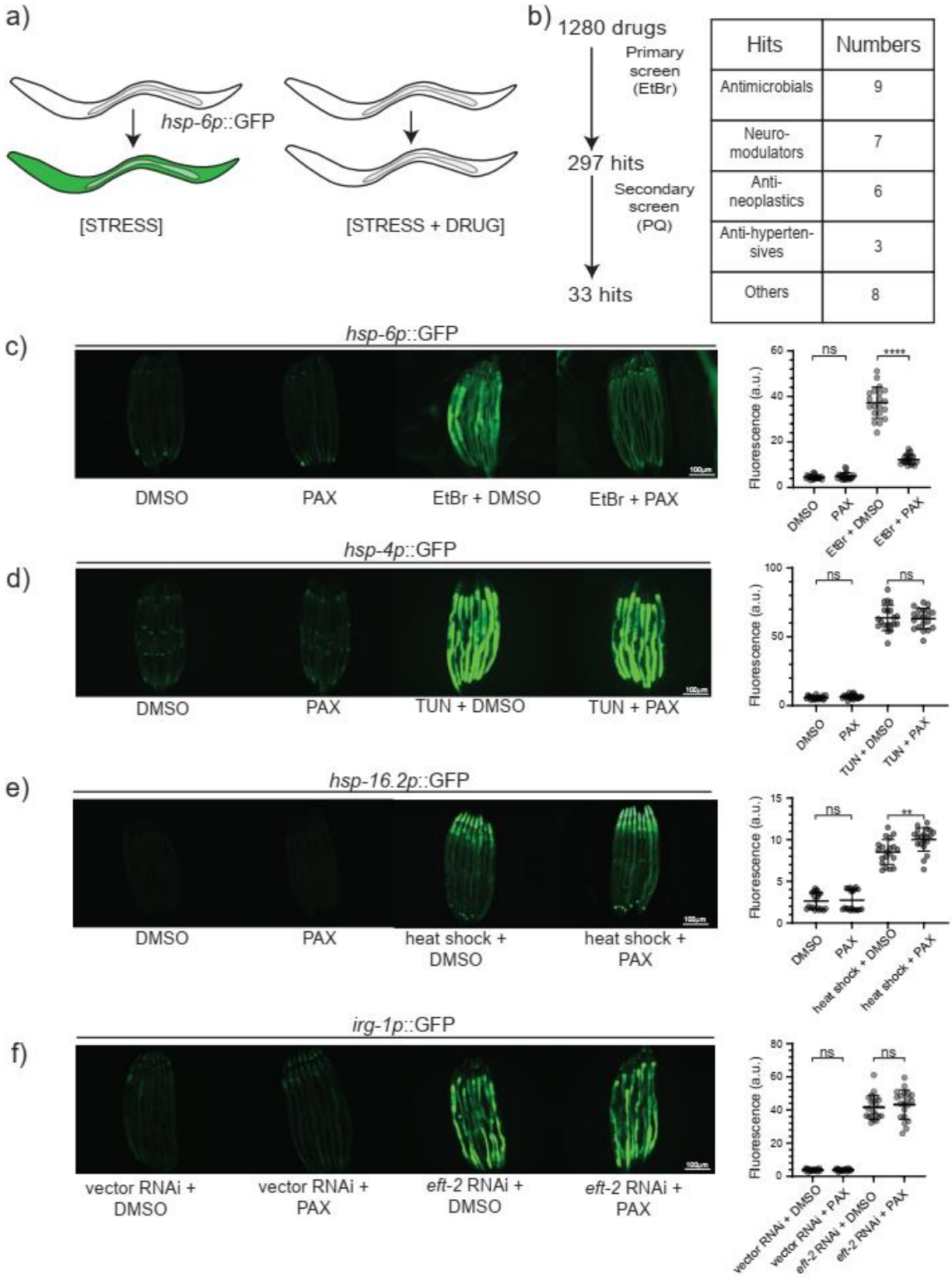

Hits	Numbers
Antimicrobials	9
Neuro-modulators	7
Anti-neoplastics	6
Anti-hyperten-sives	3
Others	8

Figure 1. Whole animal chemical screen identification of Paroxetine as a small molecule inhibitor of the UPR^{mt} in *C. elegans.*

A) Schematic of chemical screening strategy. EtBr; Ethidium bromide; PQ; Paraquat.

B) Categories of positive small molecules from the secondary screen that inhibit the UPR^{mt}.

C-F) Photomicrographs and quantifications of wild-type C) *hsp-6p*::GFP animals in the presence or absence of 30 µg/ml ethidium bromide, D) *hsp-4p*::GFP animals in the presence or absence of 3 µg/ml tunicamycin, E) *hsp-16.2p*::GFP animals in the presence or absence of heat shock (30^{o}C for 3 hrs), and F) *irg-1p*::GFP animals in the presence or absence of *eft-2* RNAi. All animals in C-F) were grown in the presence or absence of 15 µM Paroxetine (PAX), where indicated. Quantification of fluorescence intensities expressed as arbitrary units (A.U.); (mean $\pm$SD; $n \geq 20$ worms); *ns*, non-significant, ** $p<0.01$, **** $p<0.0001$ (Student's *t* test).

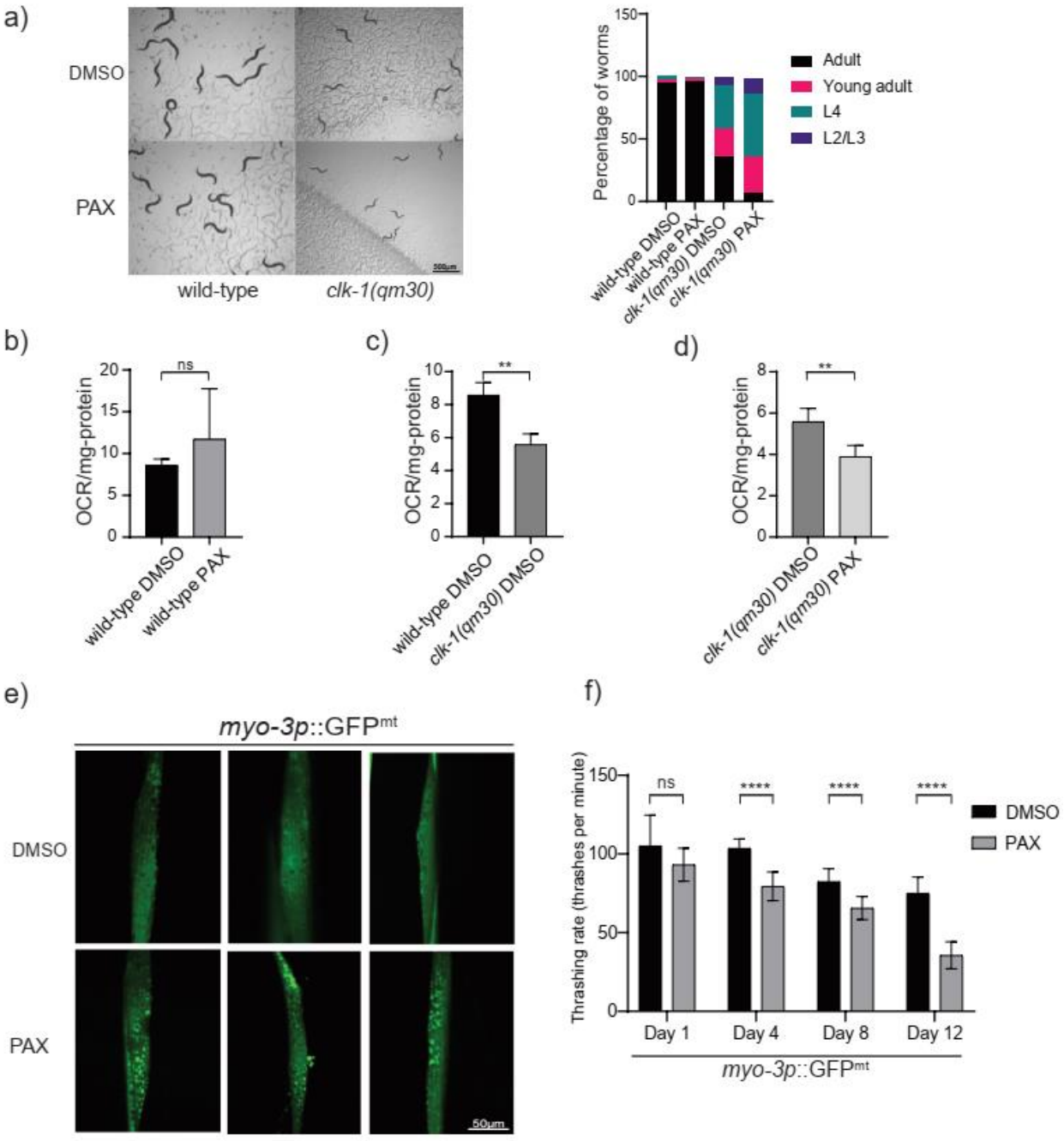

Figure 2. Paroxetine enhances mitochondrial impairment during stress.

A) Photomicrographs and quantification of wild-type and *clk-1(qm30)* animal development in the presence or absence of 15 µM Paroxetine (PAX) ($n \geq 100$worms).

B-D) Quantification of oxygen consumption rates (OCR) for B) wild-type animals in the presence or absence of 15 µM Paroxetine (PAX), C) wild-type and *clk-(qm30)* animals, and D) *clk-1(qm30)* animals in the presence or absence of 15 µM Paroxetine (PAX). (mean ±SD; n=3); *ns*, non-significant, ** $p<0.01$, (Student's *t* test).

E) Representative photomicrographs of mitochondrial morphology in wild-type animals in the presence or absence of 15 µM Paroxetine (PAX) as visualized using the *myo-3p*::GFP^{mt} reporter.

F) Quantification of body trashing rate of wild-type *myo-3p*::GFP^{mt} animals in the presence or absence of 15 µM Paroxetine (PAX). (mean ±SD; *n*=10 worms); *ns*, non-significant, **** $p<0.0001$ (Student's *t* test).

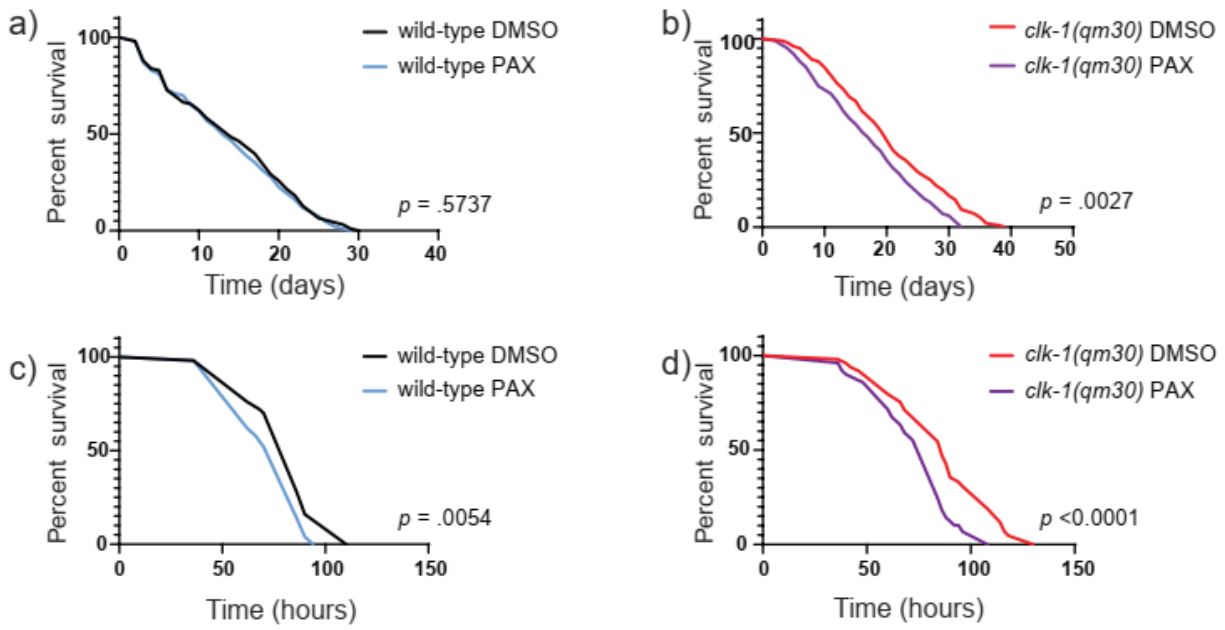

Figure 3. Paroxetine suppresses UPR^{mt}-associated extensions in lifespan and survival during pathogen infection.

Lifespans of A) wild-type and B) *clk-1(qm30)* animals in the presence or absence or 15 µM Paroxetine (PAX). See Supplementary Table 4 for all statistics pertaining to lifespan assays.

Survival of C) wild-type and D) *clk-1(qm30)* animals during infection with *P. aeruginosa* PA14 which were previously treated with 15 µM Paroxetine (PAX). See Supplementary Table 4 for all statistics pertaining to survival assays.

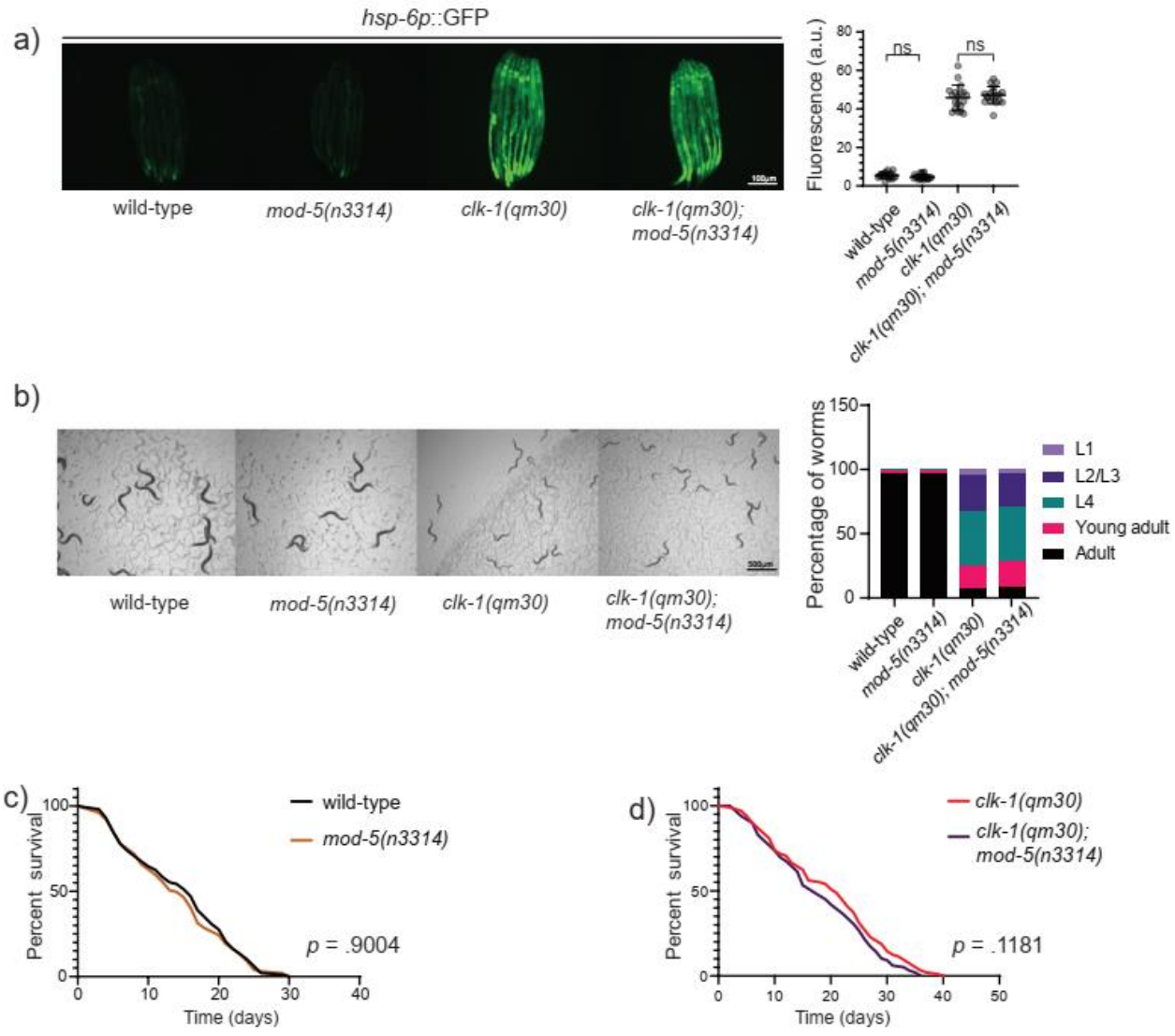

Figure 4. Paroxetine inhibits the UPR^{mt} independently of the serotonin reuptake transporter.

A) Photomicrographs and quantification of *hsp-6p*::GFP expression in wild-type and *mod-5(n3314)*, *clk-1(qm30)*, *clk-1(qm30); mod-5(n3314)* animals. Quantification of fluorescence intensities expressed as arbitrary units (A.U.); (mean ±SD; $n \geq 20$ worms); *ns*, non-significant, (Student's *t* test).

B) Photomicrographs and quantification of development for wild-type, *mod-5(n3314)*, *clk-1(qm30)*, and *clk-1(qm30); mod-5(n3314)* animals ($n \geq 100$worms).

C) Lifespans of wild-type and *mod-5(n3314)* animals.

D) Lifespans of *clk-1(qm30)* and *clk-1(qm30); mod-5(n3314)* animals.

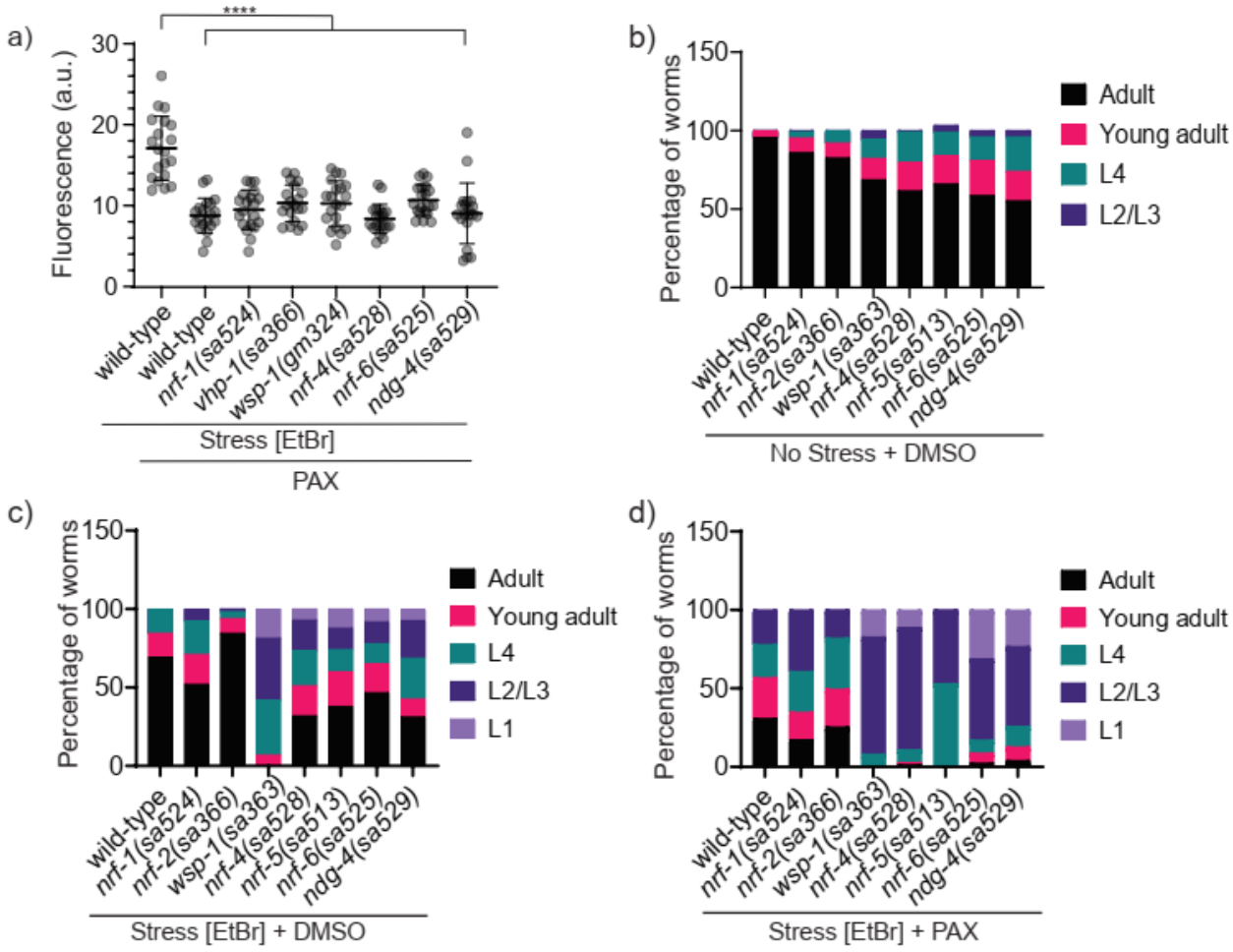

Figure 5. "*nrf*" mutants are not resistant to the anti-UPR^{mt} activity of Paroxetine.

A) Quantification of *hsp-6p*::GFP expression in wild-type, *nrf-1(sa524)*, *vhp-1(sa366)*, *wsp-1(gm324)*, *nrf-4(sa528)*, *nrf-6(sa525)*, and *ndg-4(sa529)* exposed to 20 µg/ml ethidium bromide in the presence or absence of 15 µM Paroxetine (PAX). Note that *vhp-1* was previously known as *nrf-2*. Quantification of fluorescence intensities expressed as arbitrary units (A.U.); (mean ±SD; $n \geq 20$ worms); **** $p<0.0001$ (Student's *t* test).

B-D) Quantification of development for wild-type, *nrf-1(sa524)*, *vhp-1(sa366)*, *wsp-1(sa363)*, *nrf-4(sa528)*, *nrf-5(sa513)*, *nrf-6(sa525)*, and *ndg-4(sa529)* animals in the absence of stress (B), in the

presence of stress (30 µg/ml ethidium bromide) (C), or in the presence stress (30 µg/ml ethidium bromide) and 15 µM Paroxetine (PAX) (D); ($n \geq 100$ worms).

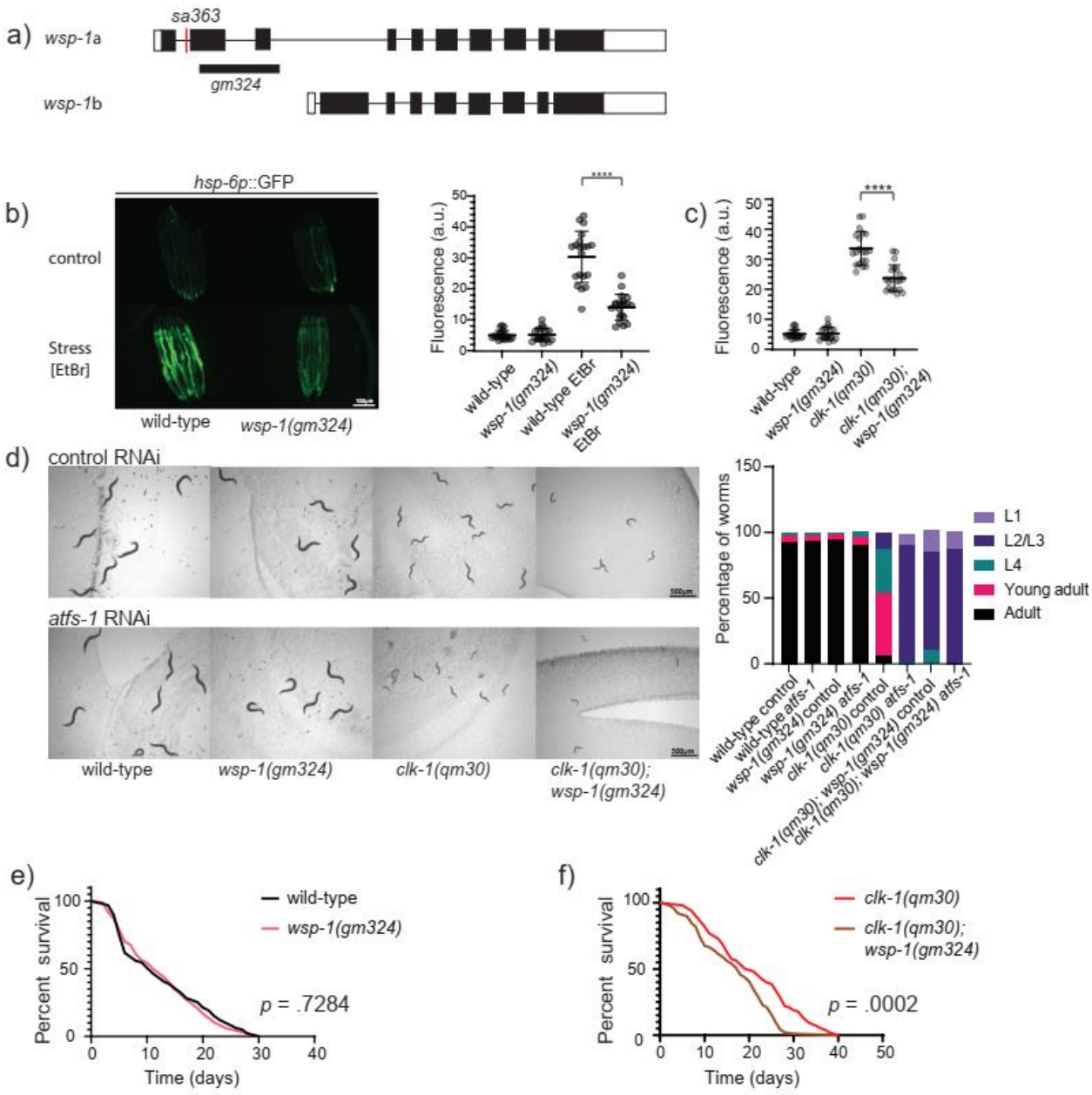

Figure 6. Actin cytoskeleton remodeling regulates the UPR^{mt} to promote mitochondrial recovery.

A) Schematic of *wsp-1* gene structure showing the two encoded transcripts, *wsp-1a* and *wsp-1b*, as well as the locations of the *sa363* and *gm324* mutations.

B, C) Photomicrographs and/or quantification of *hsp-6p*::GFP expression in B) wild-type and *wsp-1(gm324)* animals in the presence or absence of 30 µg/ml ethidium bromide or C) *clk-1(qm30), clk-1(qm30)*; *wsp-1(gm324)* animals. Quantification of fluorescence intensities expressed as arbitrary units (A.U.); (mean $\pm$SD; $n \geq 20$ worms); ****$p<0.0001$(Student's *t* test).

D) Quantification of animal development in wild-type, *clk-1(qm30)*, *wsp-1(gm324)*, or *clk-1(qm30); wsp-1(gm324)* fed control or *atfs-1* RNAi ($n \geq 100$ worms).

E) Lifespans of wild-type and *wsp-1(gm324)* animals.

F) Lifespans of *clk-1(qm30)* and *clk-1(qm230); wsp-1(gm324)* animals.

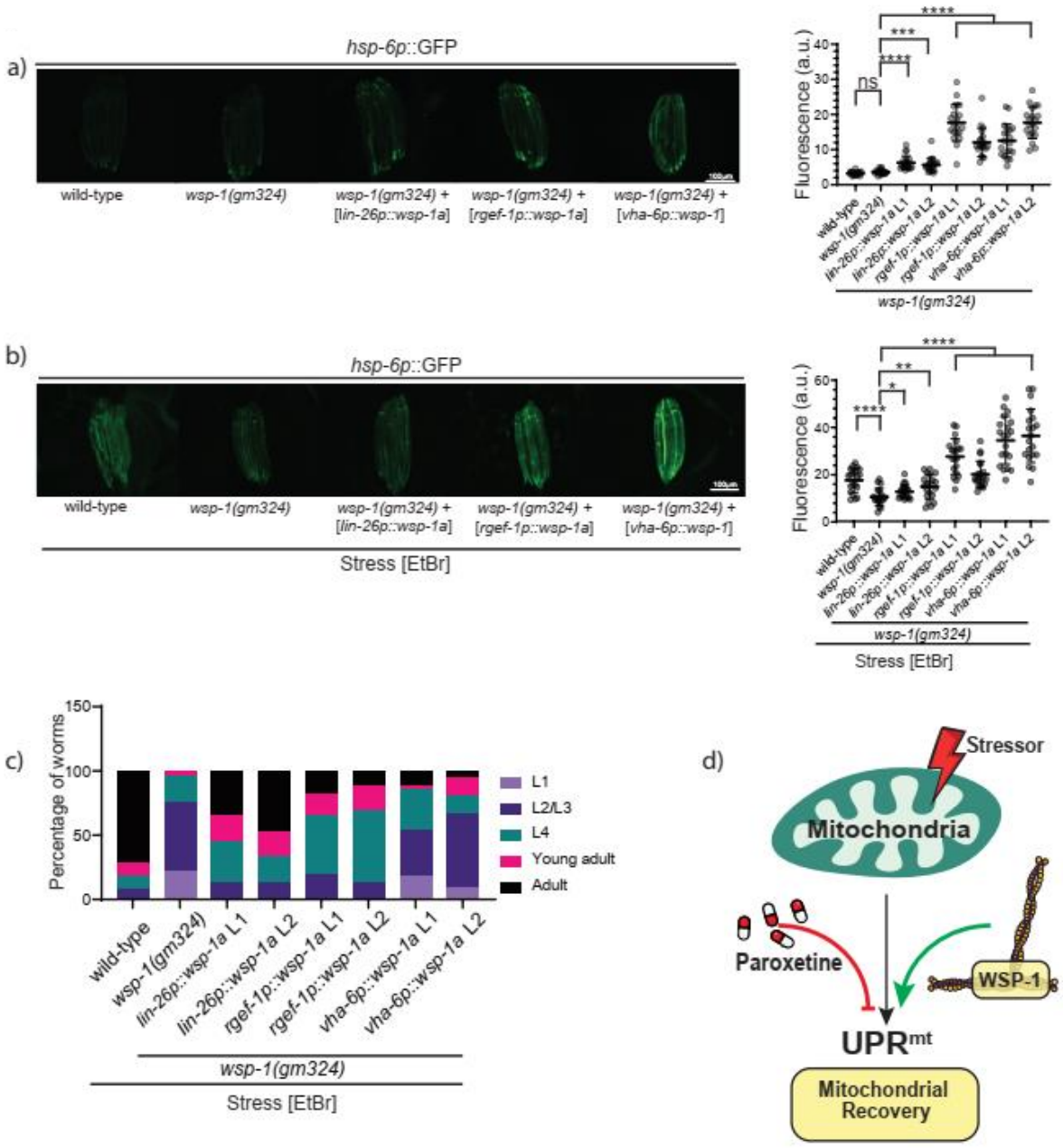

Figure 7. Actin remodeling supports mitochondrial recovery during stress partly through a cell-non-autonomous mechanism.

A, B) Photomicrographs and quantification of *hsp-6p*::GFP expression in wild-type, *wsp-1(gm324)*, *wsp-1(gm324)*[P$_{rgef-1}$::*wsp-1a*], *wsp-1(gm324)*[P$_{vha-6}$::*wsp-1a*], or *wsp-1(gm324)*[P$_{lin-26}$::*wsp-1a*] animals in the presence or absence of 20 µg/ml ethidium bromide. Two independent

transgenic lines (L1 and L2) were examined (mean ±SD; $n \geq 20$ worms); *ns*, non-significant, *$p<0.05$, **$p<0.01$, ***$p<0.001$, ****$p<0.0001$ (Student's *t* test).

C) Quantification of developmental stage in wild-type, *wsp-1(gm324)*, *wsp-1(gm324)*[P_{rgef-1}::*wsp-1a*], *wsp-1(gm324)*[P_{vha-6}::*wsp-1a*], or *wsp-1(gm324)*[P_{lin-26}::*wsp-1a*] animals in the presence or absence of 20 µg/ml ethidium bromide ($n \geq 100$ worms).

D) Model. The UPR^{mt} pathway promotes mitochondrial recovery during stress. Using chemical screening, we discovered that the anti-depressant drug Paroxetine suppresses the activity of the UPR^{mt}, exacerbating mitochondrial dysfunction during stress. We also provide genetic evidence that actin remodeling regulators such as *wsp-1*/WASP positively regulate the UPR^{mt}, promoting mitochondrial homeostasis during stress.

SUPPLEMENTARY FIGURES

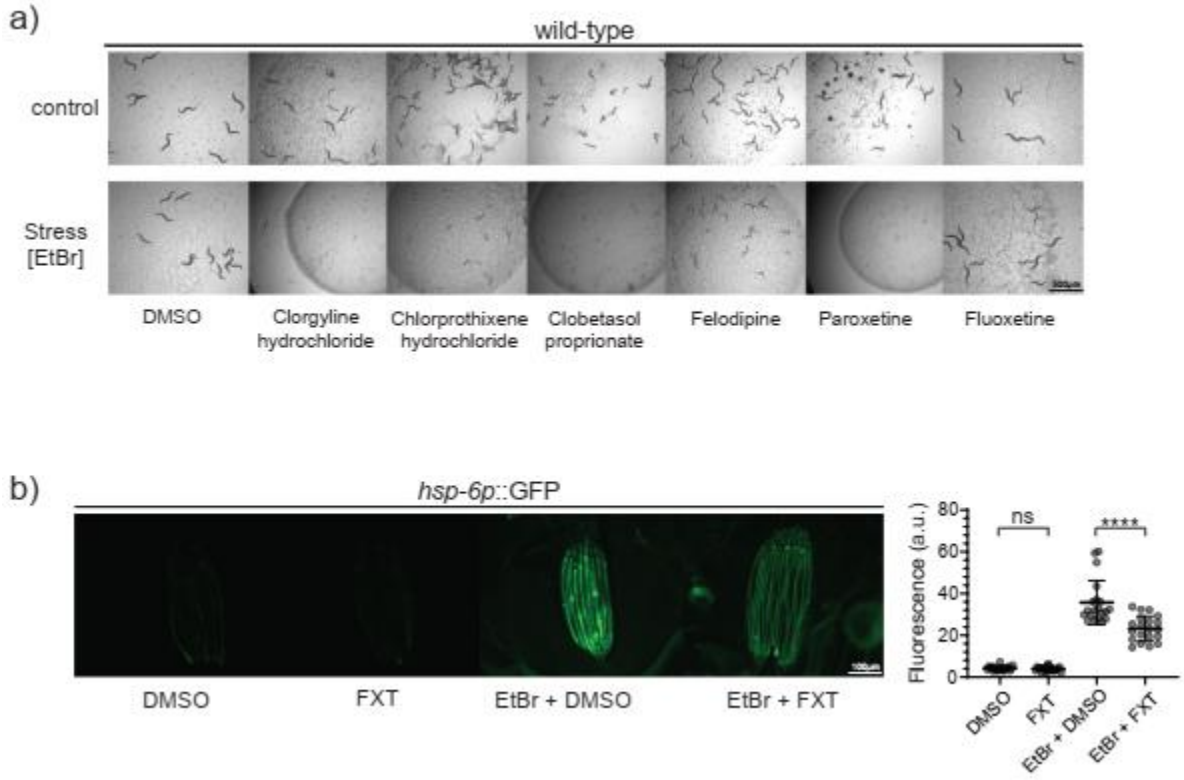

Supplementary Figure S1. Clorgyline hydrochloride, Chlorprothixene hydrochloride, Clobetasol proprionate, Felodipine, and Paroxetine impair development of wild-type animals during mitochondrial stress.

a) Photomicrographs of animal development in the presence or absence of 30 µg/ml ethidium bromide and in the presence or absence of 70 µM Clobetasol proprionate, 40 µM Clorgyline hydrochloride, 80 µM Chlorprothixene hydrochloride, 20 µM Felodipine, 15 µM Paroxetine, 30 µM Fluoxetine (FXT).

b) Photomicrographs and quantification of *hsp-6p*::GFP expression in wild-type animals grown in the presence or absence of 30 µg/ml ethidium bromide and/or 30 µM Fluoxetine. Quantification

of fluorescence intensities expressed as arbitrary units (A.U.); (mean ±SD; $n \geq 20$ worms); *ns*, non-significant, ****$p<0.0001$ (Student's *t* test).

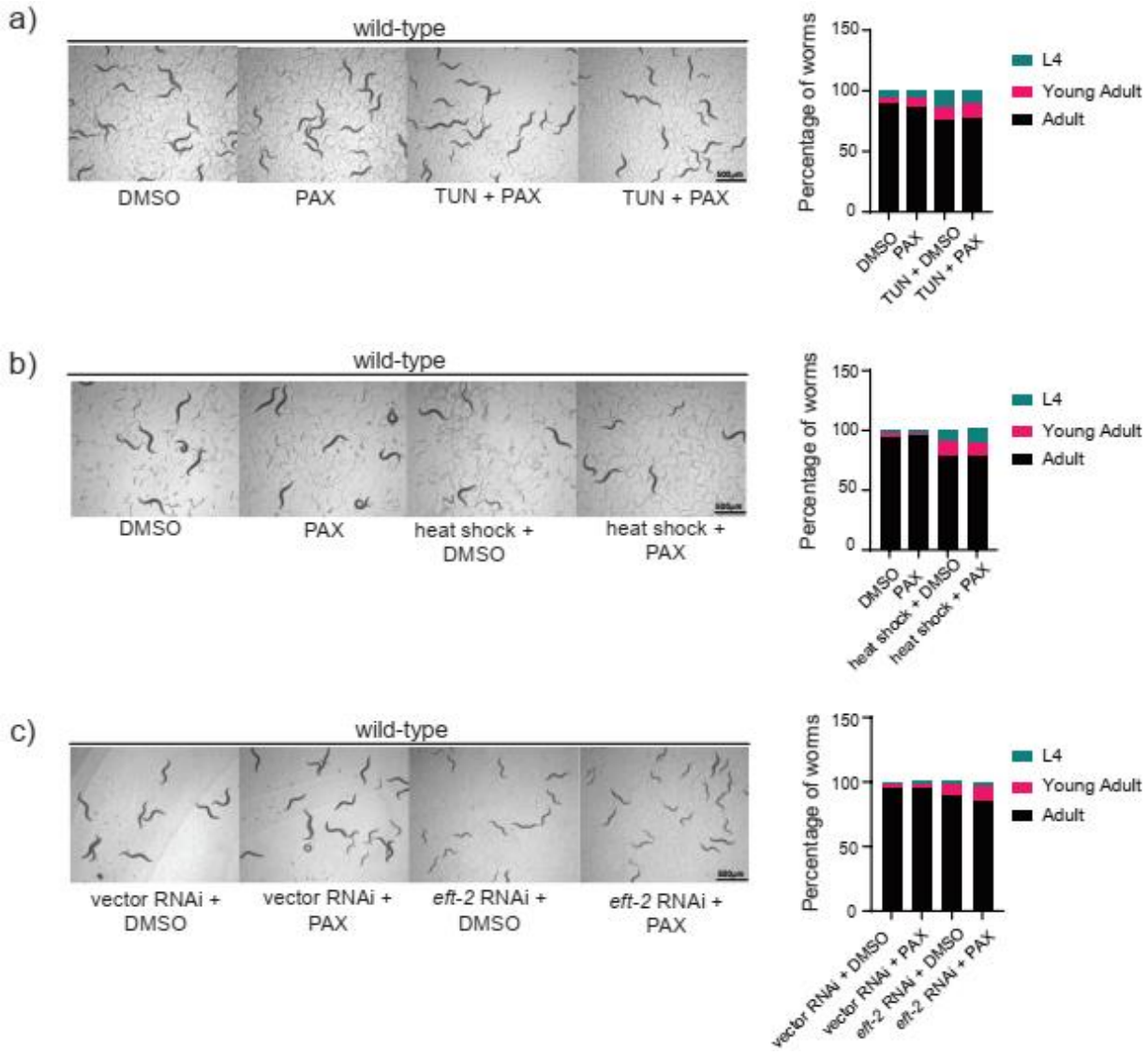

Supplementary Figure S2. Paroxetine does not impair animal development during ER, heat, or translation stress.

Photomicrographs and quantifications of wild-type animal development exposed to A) 3 µg/ml tunicamycin, B) heat shock, C) *eft-2*(RNAi), in the presence or absence of 15 µM Paroxetine (PAX). ($n \geq 100$ worms).

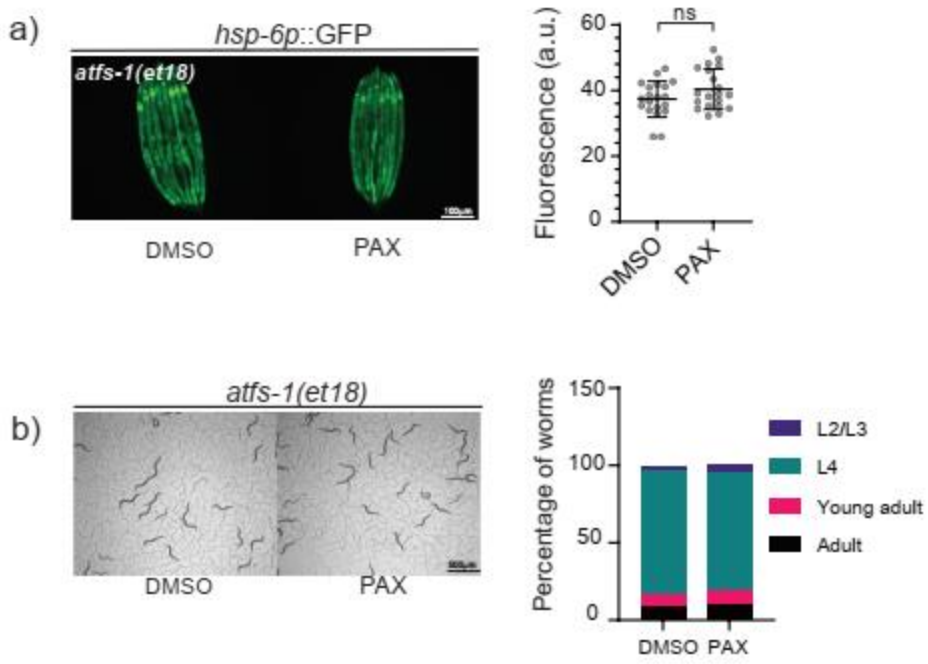

Supplementary Figure S3. Paroxetine does not suppress the UPR^{mt} at the level of ATFS-1.

A) Photomicrographs and quantification of *hsp-6p*::GFP expression in *atfs-1(et18)* animals grown in the presence or absence of 15 µM Paroxetine (PAX). Quantification of fluorescence intensities expressed as arbitrary units (A.U.); (mean ±SD; $n \geq 20$ worms); *ns*, non-significant, (Student's *t* test).

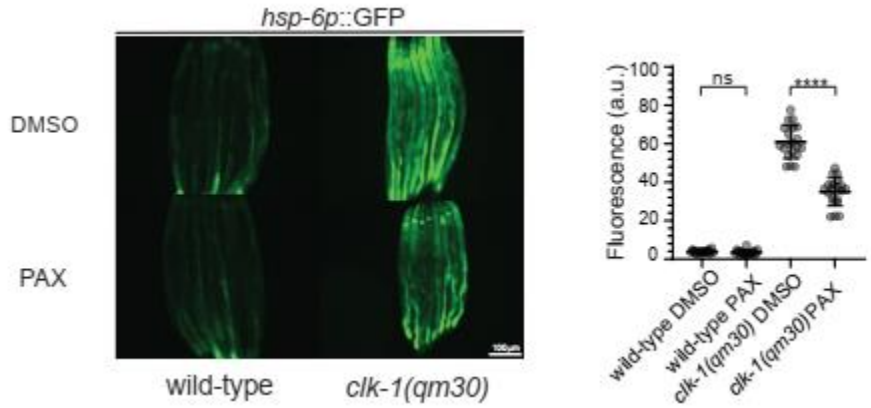

Supplementary Figure S4. Paroxetine suppresses the UPR^{mt} in *clk-1(qm30)* animals.

Photomicrographs and quantification of *hsp-6p*::GFP expression in wild-type or *clk-1(qm30)* in the presence or absence of 15 µM Paroxetine (PAX). Quantification of fluorescence intensities expressed as arbitrary units (A.U.); (mean ±SD; $n \geq 20$ worms); *ns*, non-significant, ****$p<0.0001$ (Student's *t* test).

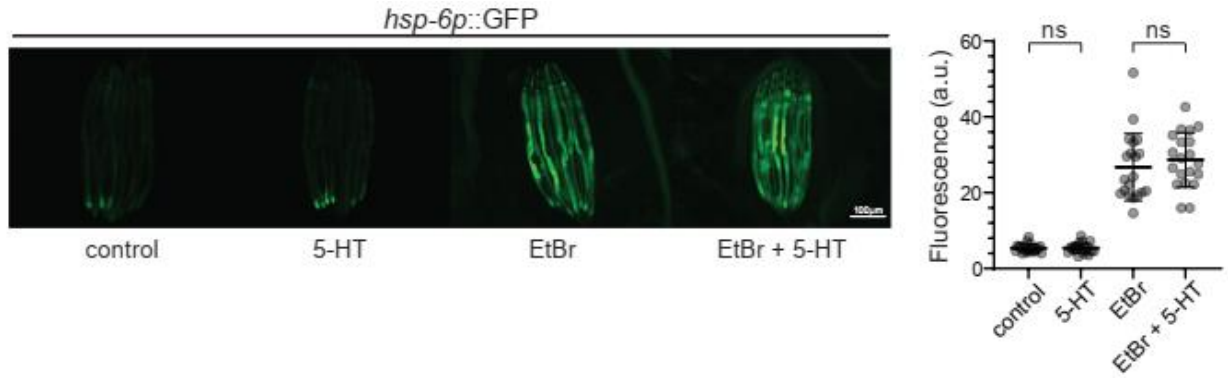

Supplementary Figure S5. Serotonin supplementation does not suppress the UPR^{mt}.

Photomicrographs and quantification of *hsp-6p*::GFP expression in wild-type animals in the presence or absence of 5 mM serotonin (5-HT) (74) (mean ±SD; $n \geq 20$ worms); *ns*, non-significant (Student's *t* test).

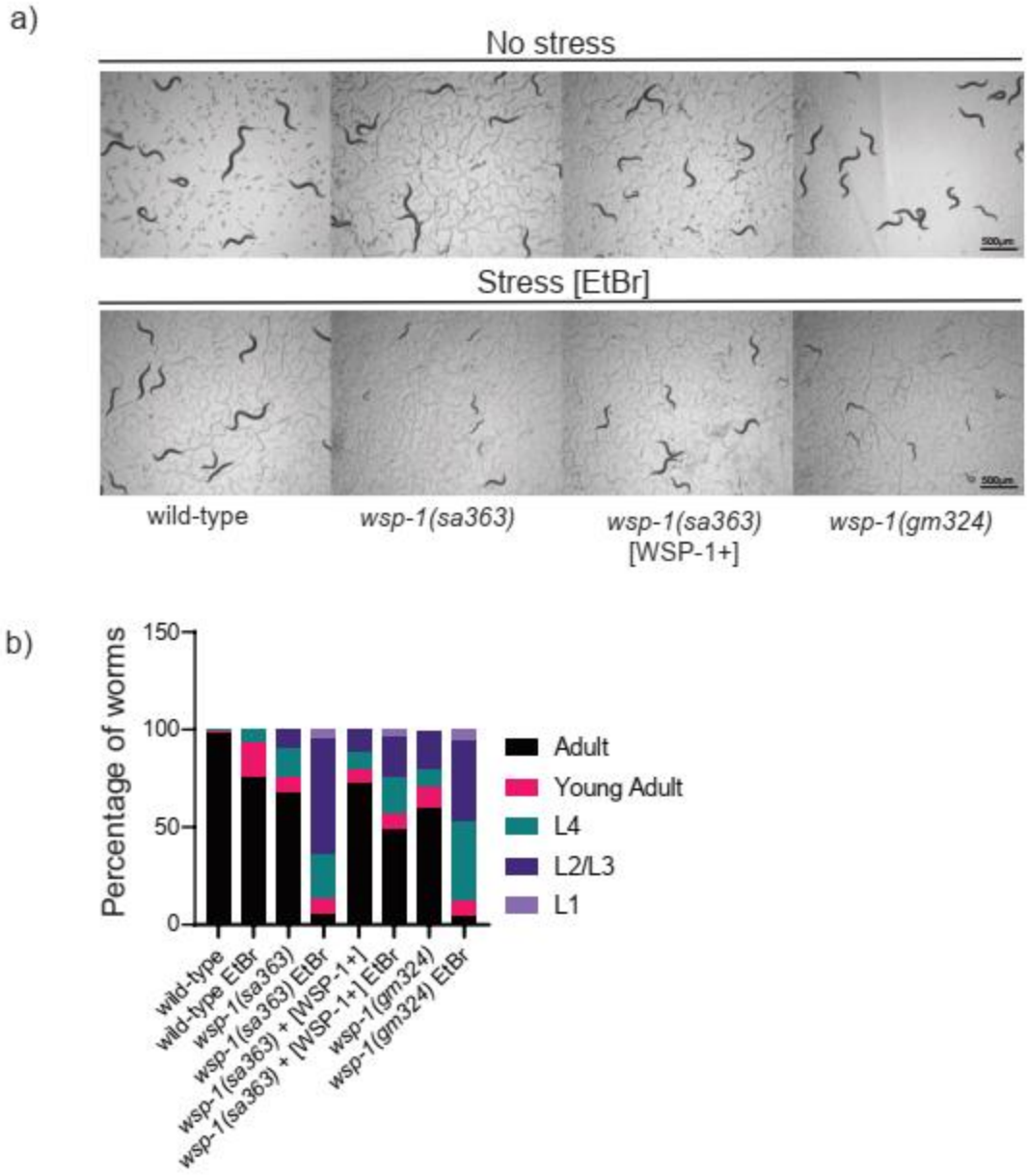

Supplementary Figure S6. Introduction of wild-type WSP-1 rescues the slowed development of *nrf-3(sa363)* animals during stress.

A) Photomicrographs and quantification of wild-type, *wsp-1(sa363)*, and *wsp-1(sa363)* [WSP-1+], and *wsp-1(gm324)* development exposed to 30µg/ml ethidium bromide ($n \geq 100$ worms).

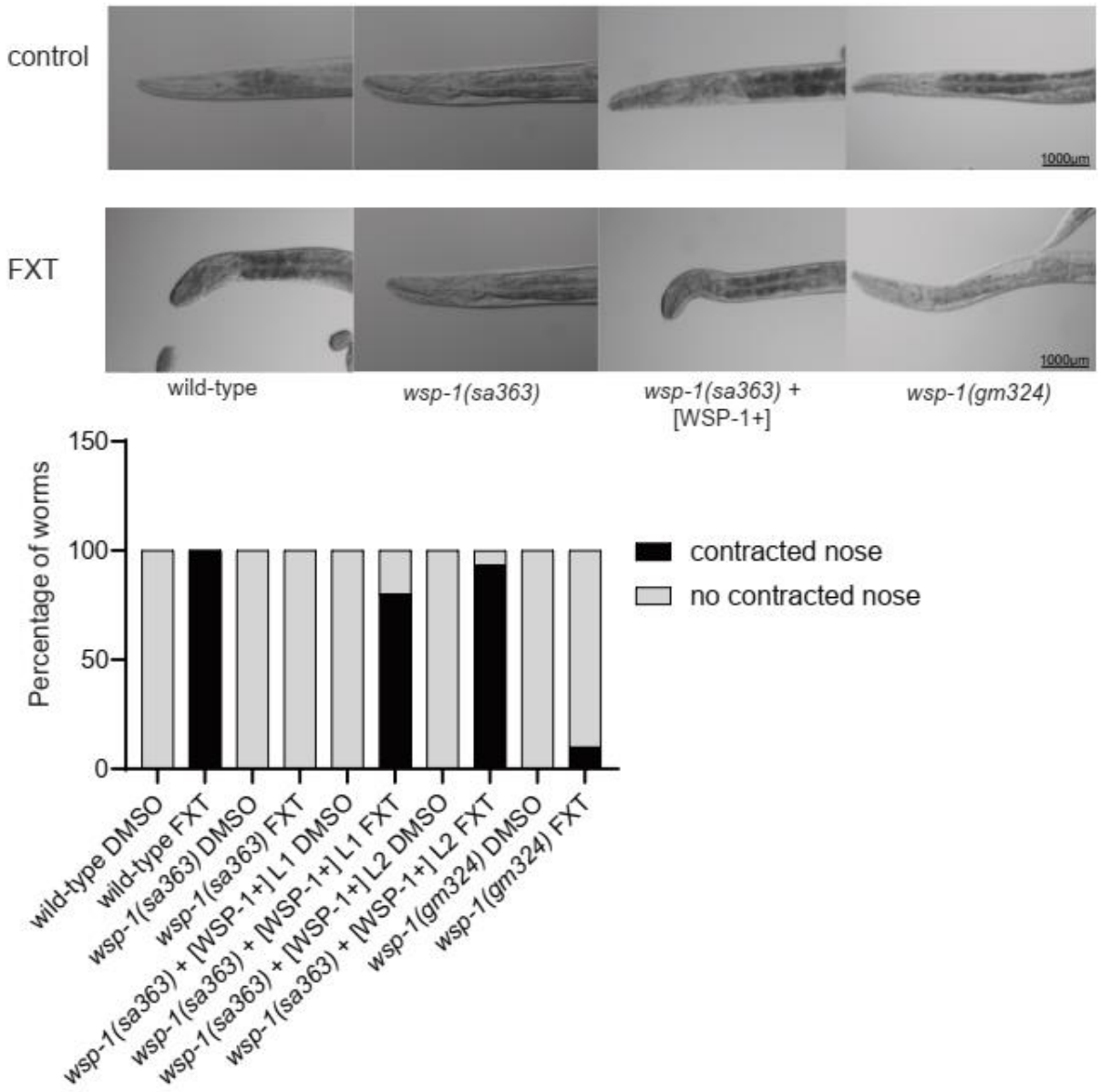

Supplementary Figure S7. *nrf-3(sa363)* represents a reduction of function mutation in *wsp-1*, encoding a homolog of WASP.

Photomicrographs and quantification of wild-type, *wsp-1(sa363)*, *wsp-1(sa363)* [WSP-1+], and *wsp-1(gm324)* nose morphology in the presence or absence of 1 mg/ml Fluoxetine (FXT) for 30 min ($n \geq 20$ worms).

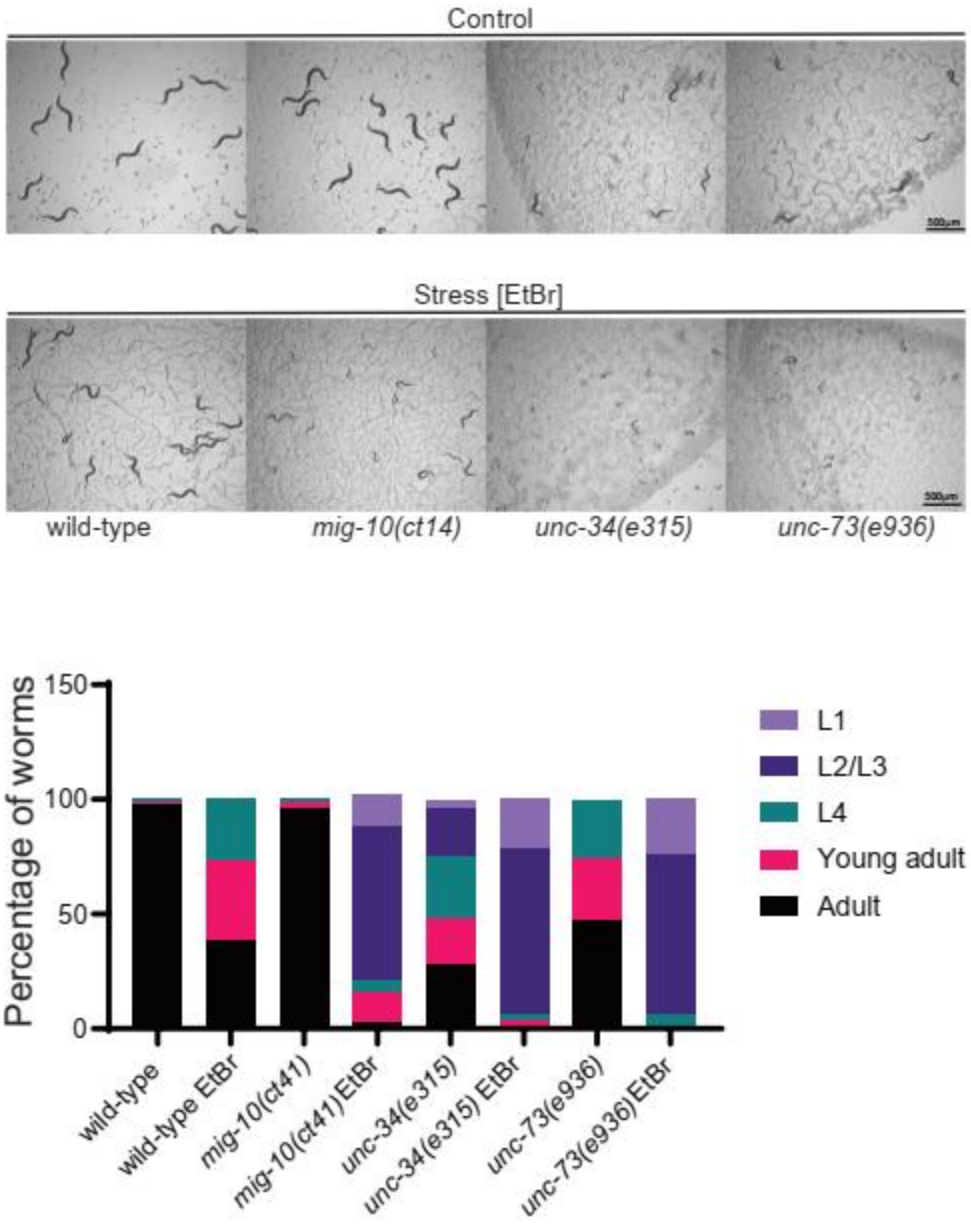

Supplementary Figure S8. Actin polymerization regulators are required for animal development during mitochondrial stress.

A, B) Quantification of animal development in the absence of mitochondrial stress for A) wild-type, *unc-73(e936), unc-34(e315), and mig-10(ct41)* or B) in the presence of 30 µg/ml ethidium bromide ($n \geq 100$ worms).

SUPPLEMENTARY TABLES

Suppl. Table 1_Genetics

PlateNumber PositionNumber	Prestw number	chemical name	mol weight	CAS number	FDA approved	blood brain barrier
01D05	Prestw-34	Triamterene	253.26837	396-01-0	Yes	
01G05	Prestw-64	Chlorpromazine hydrochloride	355.33235	69-09-0	Yes	Yes
02E05	Prestw-1184	Tioconazole	387.71781	65899-73-2	Yes	
02G04	Prestw-143	Chlorhexidine	505.4574	55-56-1	Yes	
02B02	Prestw-91	Khellin	260.24874	82-02-0		
02G06	Prestw-145	Chlortetracycline hydrochloride	515.35118	64-72-2	Yes	
03B05	Prestw-174	Alverine citrate salt	473.57135	5560-59-8		
03D06	Prestw-1231	Asenapine maleate	401.85025	85650-56-2	Yes	
03H06	Prestw-1771	Carmofur	257.26687	61422-45-5		
04A03	Prestw-242	Flavoxate hydrochloride	427.93212	3717-88-2	Yes	
04D06	Prestw-275	Fenofibrate	360.84097	49562-28-9	Yes	
04E02	Prestw-281	Fludrocortisone acetate	422.49832	514-36-3	Yes	
04E03	Prestw-282	Fenoterol hydrobromide	384.27319	1944-12-3		
04G05	Prestw-304	Econazole nitrate	444.70492	24169-02-6	Yes	
04H03	Prestw-312	Flunarizine dihydrochloride	477.42926	30484-77-6		Yes
04H04	Prestw-313	Trifluoperazine dihydrochloride	480.42667	440-17-5	Yes	
05C05	Prestw-344	Clorgyline hydrochloride	308.63757	17780-75-5		
05F04	Prestw-373	Amethopterin (R,S)	454.44894	60388-53-6		Yes
05G05	Prestw-384	Probucol	516.85501	23288-49-5	Yes	
05H05	Prestw-394	Kanamycin A sulfate	582.58536	25389-94-0	Yes	
06A05	Prestw-1288	Idebenone	338.44795	58186-27-9		Yes
06C02	Prestw-421	Suloctidil	337.57205	54063-56-8		
06C03	Prestw-1368	Zotepine	331.86726	26615-21-4		

06D06	Prestw-435	Cyclosporin A	1202.64247	59865-13-3	Yes	
06F04	Prestw-1257	Calcipotriene	412.61805	112965-21-6	Yes	
06H02	Prestw-1358	Vatalanib	346.82235	212141-54-3		
07B02	Prestw-491	Metixene hydrochloride	345.93798	1553-34-0		
07D02	Prestw-511	Fluoxetine hydrochloride	345.79528	59333-67-4	Yes	
07E05	Prestw-524	Tiabendazole	201.25139	148-79-8		
07G05	Prestw-544	Tobramycin	467.52369	32986-56-4	Yes	
07H02	Prestw-551	Hexetidine	339.6129	141-94-6		
07H04	Prestw-553	Pentamidine isethionate	592.69217	140-64-7	Yes	
08A02	Prestw-1188	Ziprasidone Hydrochloride	449.40569	138982-67-9	Yes	
08B02	Prestw-571	Tetracaïne hydrochloride	300.8317	136-47-0	Yes	
08B03	Prestw-572	Mometasone furoate	521.44255	83919-23-7	Yes	
08D03	Prestw-1407	Etofenamate	369.34366	30544-47-9		
08D06	Prestw-1410	Exemestane	296.41308	107868-30-4	Yes	
08E05	Prestw-1252	Butenafine Hydrochloride	353.93931	101828-21-1	Yes	
08F03	Prestw-1501	Fenipentol	164.24957	583-03-9		
08H02	Prestw-1210	Alendronate sodium	271.08014	121268-17-5	Yes	
09D04	Prestw-1456	Opipramol dihydrochloride	436.42902	909-39-7		
09E02	Prestw-1318	Pranoprofen	255.27576	52549-17-4		
09H05	Prestw-714	Isosorbide dinitrate	236.13926	87-33-2	Yes	
09C05	Prestw-1432	Loratadine	382.89381	79794-75-5	Yes	
10B02	Prestw-731	Sulfaquinoxaline sodium salt	322.32317	967-80-6		
10D04	Prestw-753	Demeclocycline hydrochloride	501.32409	64-73-3	Yes	
10G02	Prestw-781	Clobetasol propionate	466.98219	25122-46-7	Yes	
10H04	Prestw-793	Cloperastine hydrochloride	366.33435	14984-68-0		
10H05	Prestw-794	Eucatropine hydrochloride	327.85467	536-93-6		
11A02	Prestw-801	Carbinoxamine maleate salt	406.86971	3505-38-2	Yes	
11D05	Prestw-834	Novobiocin sodium salt	634.6212	1476-53-5	Yes	

11E02	Prestw-1455	Olanzapine	312.43975	132539-06-1	Yes	
11E04	Prestw-843	Nafcillin sodium salt monohydrate	454.48106	7177-50-6	Yes	
11F02	Prestw-851	Paroxetine Hydrochloride	365.83552	110429-35-1	Yes	
12B02	Prestw-1486	Cortisol acetate	404.50789	50-03-3	Yes	
12B03	Prestw-1416	Flubendazol	313.29074	31430-15-6		
12F02	Prestw-931	Propofol	178.27666	2078-54-8	Yes	
12F05	Prestw-934	Flucytosine	129.09438	2022-85-7	Yes	Yes
13A06	Prestw-1415	Floxuridine	246.19682	50-91-9	Yes	
13E05	Prestw-1004	Meptazinol hydrochloride	269.81763	59263-76-2		
13E06	Prestw-1005	Apramycin	539.58782	37321-09-8		
13G02	Prestw-1021	Isradipine	371.39632	75695-93-1	Yes	
13H02	Prestw-1031	Halofantrine hydrochloride	536.89727	36167-63-2	Yes	
13H04	Prestw-1033	Nomegestrol acetate	370.49315	58652-20-3		
14A06	Prestw-1045	Sertaconazole nitrate	500.79122	99592-39-9	Yes	
14B02	Prestw-1051	Moricizine hydrochloride	463.98722	31883-05-3	Yes	
14D05	Prestw-1074	Cyproterone acetate	416.94933	427-51-0		
14E02	Prestw-1081	(S)-propranolol hydrochloride	295.81224	4199-10-4	Yes	Yes
14F02	Prestw-1091	Spaglumic acid	304.25877	4910-46-7		
14H05	Prestw-1114	Saquinavir mesylate	766.96463	149845-06-7	Yes	
15A02	Prestw-1283	Buspirone hydrochloride	421.97449	33386-08-2	Yes	

15B02	Prestw-1206	Acetylcysteine	163.19638	616-91-1	Yes	
15B03	Prestw-1435	Melengestrol acetate	396.53139	2919-66-6		
15B04	Prestw-1246	Bromhexine hydrochloride	412.59787	611-75-6		
15C06	Prestw-1371	Celecoxib	381.37923	169590-42-5	Yes	
15D02	Prestw-1203	5-fluorouracil	130.07911	51-21-8	Yes	Yes
15D04	Prestw-1444	Mitotane	320.0478	53-19-0	Yes	Yes
15D06	Prestw-1479	Triclosan	289.54739	3380-34-5	Yes	
15E02	Prestw-1383	Clofibrate	242.70455	637-07-0	Yes	

15E06	Prestw-1419	Fluocinolone acetonide	452.4999	67-73-2	Yes	
15F02	Prestw-1196	Topotecan	421.45686	123948-87-8	Yes	
15F03	Prestw-1232	Atorvastatin	558.6557	134523-00-5	Yes	
15G03	Prestw-1244	Bosentan	551.62608	147536-97-8	Yes	
15H04	Prestw-1421	Formoterol fumarate	804.90234	43229-80-7	Yes	
15H06	Prestw-1319	Pravastatin	424.53917	81093-37-0	Yes	
16A02	Prestw-1764	Nelfinavir mesylate	663.90238	159989-65-8	Yes	
16B02	Prestw-1773	Ipriflavone	280.32642	35212-22-7		
16B03	Prestw-1762	Ezetimibe	409.43667	163222-33-1	Yes	
16B05	Prestw-1760	Tegaserod maleate	417.46869	189188-57-6	Yes	
16C02	Prestw-1708	(R)-Duloxetine hydrochloride	333.8832	116539-60-7	Yes	
16C03	Prestw-1706	Donepezil hydrochloride	415.9646	120011-70-3	Yes	
16C04	Prestw-1703	1,8-Dihydroxyanthraquinone	240.21746	117-10-2		
16D04	Prestw-1766	Benidipine hydrochloride	542.03674	91599-74-5		
16D05	Prestw-1770	Perospirone	426.58515	150915-41-6		
16E02	Prestw-1730	Cefuroxime axetil	510.48314	64544-07-6	Yes	
16E03	Prestw-1720	Anagrelide	256.09279	68475-42-3	Yes	
16E04	Prestw-1701	Clopidogrel	321.82842	113665-84-2	Yes	
16F02	Prestw-1736	Irbesartan	428.54151	138402-11-6	Yes	
16F04	Prestw-1750	Terbinafine	291.4401	91161-71-6	Yes	
16G02	Prestw-1752	Epirubicin hydrochloride	579.99325	56390-09-1	Yes	No
16G03	Prestw-1741	Loteprednol etabonate	466.96347	82034-46-6	Yes	
16G04	Prestw-1744	Tolterodine tartrate	475.58729	209747-05-7	Yes	
16G05	Prestw-1775	Lomerizine hydrochloride	505.00952	101477-54-7		
16H05	Prestw-1729	Ceftibuten	410.43003	97519-39-6	Yes	
17A07	Prestw-6	Isoflupredone acetate	420.48238	338-98-7		
17D10	Prestw-39	Diflunisal	250.20371	22494-42-4	Yes	
17E07	Prestw-46	Naphazoline hydrochloride	246.74205	550-99-2	Yes	
17E09	Prestw-48	Dicyclomine hydrochloride	345.95727	67-92-5	Yes	

17E10	Prestw-49	Amyleine hydrochloride	271.78994	532-59-2		
17F07	Prestw-56	Sulpiride	341.43226	15676-16-1		
17F08	Prestw-57	Benoxinate hydrochloride	344.88528	5987-82-6	Yes	
17G08	Prestw-67	Miconazole	416.13708	22916-47-8	Yes	
17H07	Prestw-76	Dibucaine	343.47303	85-79-0	Yes	
17H10	Prestw-79	Diphemanil methylsulfate	389.51764	62-97-5	Yes	
18A07	Prestw-86	Acyclovir	225.20857	59277-89-3	Yes	Yes
18A08	Prestw-87	Diazoxide	230.67419	364-98-7	Yes	Yes
18B07	Prestw-96	Guanabenz acetate	291.13874	23256-50-0	Yes	
18B08	Prestw-97	Disulfiram	296.5403	97-77-8	Yes	
18B10	Prestw-99	Mianserine hydrochloride	300.83447	21535-47-7		
18D10	Prestw-119	Picotamide monohydrate	394.43389	80530-63-8		
18D11	Prestw-120	Triamcinolone	394.44414	124-94-7	Yes	
18F10	Prestw-139	Cefotaxime sodium salt	477.45302	64485-93-4	Yes	
18F11	Prestw-140	Tetracycline hydrochloride	480.90615	64-75-5	Yes	
18H09	Prestw-158	Neomycin sulfate	712.73301	1405-10-3	Yes	
18H10	Prestw-159	Dihydrostreptomycin sulfate	1461.43386	5490-27-7	Yes	
18H11	Prestw-160	Gentamicine sulfate	1488.81475	1405-41-0	Yes	No
19A08	Prestw-167	Riluzole hydrochloride	270.66202	not available	Yes	Yes
19B07	Prestw-176	Iproniazide phosphate	277.21877	305-33-9		
19B11	Prestw-180	Flutamide	276.21712	13311-84-7	Yes	
19C08	Prestw-187	Catharanthine	336.43763	2468-21-5		
19D11	Prestw-200	Camptothecine (S,+)	348.36152	7689-03-4		
19E07	Prestw-206	Meclofenamic acid sodium salt	336.15244	6385-02-0	Yes	
19E11	Prestw-210	Fenbendazole	299.35376	43210-67-9		
19G10	Prestw-229	Nefopam hydrochloride	289.80805	23327-57-3		
19G11	Prestw-230	Phentolamine hydrochloride	317.82145	73-05-2	Yes	
19H07	Prestw-236	Dilazep dihydrochloride	677.62567	20153-98-4		

19H10	Prestw-239	Orphenadrine hydrochloride	305.85108	341-69-5	Yes	
19H11	Prestw-240	Proglumide	334.41892	6620-60-6		
20A07	Prestw-246	Pinacidil	245.32988	85371-64-8	Yes	
20A09	Prestw-248	Clonidine hydrochloride	266.55915	4205-91-8	Yes	Yes
20A10	Prestw-249	Bupropion hydrochloride	276.20848	31677-93-7	Yes	Yes
20A11	Prestw-250	Alprenolol hydrochloride	285.81703	13707-88-5		
20B07	Prestw-256	Isotretinoin	300.44496	4759-48-2	Yes	
20B08	Prestw-257	Retinoic acid	300.44496	302-79-4		
20B09	Prestw-258	Antazoline hydrochloride	301.82205	2508-72-7	Yes	

20C09	Prestw-268	Vinpocetine	350.46472	42971-09-5		
20D09	Prestw-278	Cinnarizine	368.52646	298-57-7		
20D10	Prestw-279	Methylprednisolone, 6-alpha	374.4814	83-43-2	Yes	
20E08	Prestw-287	Oxybutynin chloride	393.95824	1508-65-2	Yes	
20E10	Prestw-289	Pyrilamine maleate	401.46644	59-33-6	Yes	
20F07	Prestw-296	Acemetacin	415.83371	53164-05-9		
20F08	Prestw-297	Benzydamine hydrochloride	345.87563	132-69-4		
20F11	Prestw-300	Diperodon hydrochloride	433.93916	537-12-2		
20G08	Prestw-307	Oxytetracycline dihydrate	496.47526	6153-64-6	Yes	
20G10	Prestw-309	Amodiaquin dihydrochloride	464.82346	6398-98-7	Yes	
20G11	Prestw-310	Mebeverine hydrochloride	466.02237	2753-45-9		
20H10	Prestw-319	Clofilium tosylate	510.18478	92953-10-1		
21A07	Prestw-326	Methyldopa (L,-)	211.21941	555-30-6	Yes	
21A08	Prestw-327	Cefoperazone dihydrate	681.70812	not available	Yes	
21A09	Prestw-328	Zoxazolamine	168.5837	61-80-3		
21A10	Prestw-329	Tacrine hydrochloride	234.7309	1684-40-8	Yes	
21B07	Prestw-336	Chlormezanone	273.74019	80-77-3	Yes	
21C09	Prestw-348	Chlorprothixene hydrochloride	352.32883	6469-93-8	Yes	
21C11	Prestw-350	Clozapine	326.83193	5786-21-0	Yes	

21D10	Prestw-359	Dextromethorphan hydrobromide	370.33336	6700-34-1	Yes	
21E07	Prestw-366	Ambroxol hydrochloride	414.57018	23828-92-4		
21E09	Prestw-368	Bepridil hydrochloride	403.01235	74764-40-2	Yes	
21F08	Prestw-377	Nafronyl oxalate	473.57135	3200-06-4		Yes
21F11	Prestw-380	Clebopride maleate	489.96026	84370-95-6		
21G07	Prestw-386	GBR 12909 dihydrochloride	523.49878	67469-78-7		
21H08	Prestw-397	Clomiphene citrate (Z,E)	598.09862	50-41-9	Yes	
21H09	Prestw-398	Oxantel pamoate	820.95091	68813-55-8		
21H11	Prestw-400	Hesperidin	610.57418	520-26-3		
22A10	Prestw-409	Amiodarone hydrochloride	681.78455	19774-82-4	Yes	
22A11	Prestw-410	Amphotericin B	924.10236	1397-89-3	Yes	Yes
22B10	Prestw-419	Bisacodyl	361.40103	603-50-9	Yes	
22C07	Prestw-426	Buflomedil hydrochloride	343.85407	35543-24-9		
22D09	Prestw-438	Doxorubicin hydrochloride	579.99325	25316-40-9	Yes	
22E07	Prestw-446	Carteolol hydrochloride	328.84225	51781-21-6	Yes	
22F08	Prestw-457	Meclozine dihydrochloride	463.88228	1104-22-9	Yes	
22F09	Prestw-458	Melatonin	232.28467	73-31-4		
22H09	Prestw-478	Felodipine	384.26243	72509-76-3	Yes	

22H11	Prestw-1385	Closantel	663.08388	57808-65-8		
23A08	Prestw-487	Daunorubicin hydrochloride	563.99385	23541-50-6	Yes	
23A09	Prestw-488	Dosulepin hydrochloride	331.91089	897-15-4		
23B07	Prestw-496	Tiaprofenic acid	260.31394	33005-95-7		
23C08	Prestw-1159	Sibutramine hydrochloride	316.31744	125494-59-9	Yes	
23C10	Prestw-509	Bromperidol	420.32536	10457-90-6		
23C11	Prestw-510	Cyclizine hydrochloride	302.85041	303-25-3	Yes	
23D09	Prestw-518	Budesonide	430.54613	51333-22-3	Yes	
23E07	Prestw-526	Ethionamide	166.2463	536-33-4	Yes	Yes
23G09	Prestw-548	Chloroquine diphosphate	515.87164	50-63-5	Yes	

23H07	Prestw-1144	Mirtazapine	265.36108	61337-67-5	Yes	
23H09	Prestw-558	Gliclazide	323.41692	21187-98-4		
23H10	Prestw-559	DO 897/99	490.47781	not available		
24A07	Prestw-566	Eserine hemisulfate salt	648.78458	64-47-1		Yes
24A08	Prestw-1139	Itraconazole	705.65031	84625-61-6	Yes	Yes
24A11	Prestw-1449	Nicotinamide	122.12752	98-92-0		
24B10	Prestw-1297	Lacidipine	455.55601	103890-78-4		
24C09	Prestw-588	Galanthamine hydrobromide	368.27379	1953-04-4	Yes	
24C11	Prestw-1409	Etretinate	354.49375	54350-48-0	Yes	
24D09	Prestw-598	Xylazine	220.33872	7361-61-7		Yes
24E07	Prestw-1331	Rimantadine Hydrochloride	215.76884	13392-28-4	Yes	
24E09	Prestw-1460	Oxibendazol	249.27165	20559-55-1		
24H09	Prestw-1392	Dexfenfluramine hydrochloride	267.72419	3239-45-0		
24H10	Prestw-1408	Etoricoxib	358.84945	202409-33-4		
24H11	Prestw-1341	Sertindole	440.95242	106516-24-9		
25B07	Prestw-656	Lanatoside C	985.14007	17575-22-3		
25B08	Prestw-657	Benzamil hydrochloride	356.2168	2898-76-2		
25C09	Prestw-1165	Acitretin	326.43957	55079-83-9	Yes	
25C11	Prestw-1173	Irsogladine maleate	372.16972	84504-69-8		
25D07	Prestw-676	Beta-Escin	1131.28427	11072-93-8		
25D08	Prestw-631	Thiamine hydrochloride	337.27346	67-03-8	Yes	
25D11	Prestw-1363	Warfarin	308.33697	81-81-2	Yes	
25E07	Prestw-1799	Tigecycline	585.66288	220620-09-7	Yes	
25E08	Prestw-1465	Tramadol hydrochloride	299.84412	27203-92-5	Yes	
25F07	Prestw-696	Ethotoin	204.23049	86-35-1	Yes	
25F09	Prestw-698	Tetrahydrozoline hydrochloride	236.74684	522-48-5	Yes	
25G07	Prestw-706	Chlorcyclizine hydrochloride	337.29544	1620-21-9		
25G08	Prestw-707	Diphenylpyraline hydrochloride	317.86223	132-18-3		

25H07	Prestw-716	Pramoxine hydrochloride	329.87061	637-58-1	Yes	
25H11	Prestw-720	Cefuroxime sodium salt	446.37375	56238-63-2	Yes	
26A07	Prestw-726	Mephentermine hemisulfate	424.60722	1212-72-2	Yes	
26A08	Prestw-1140	Liranaftate	328.4363	88678-31-3		
26A10	Prestw-729	Sulfanilamide	172.20686	63-74-1	Yes	
26A11	Prestw-730	Balsalazide Sodium	401.28926	80573-04-2	Yes	
26B07	Prestw-736	Cefazolin sodium salt	476.49271	27164-46-1	Yes	
26D09	Prestw-758	Ribostamycin sulfate salt	552.55887	53797-35-6		
26D10	Prestw-759	Methacholine chloride	195.69116	62-51-1	Yes	
26E11	Prestw-770	Isopropamide iodide	480.43666	71-81-8	Yes	
26F07	Prestw-776	Guaifenesin	198.22068	93-14-1	Yes	
26G09	Prestw-788	Hexylcaine hydrochloride	297.82818	532-76-3	Yes	
26G10	Prestw-789	Drofenine hydrochloride	353.93654	548-66-3		
26G11	Prestw-790	Cycloheximide	281.35486	66-81-9		
26H07	Prestw-796	Lithocholic acid	376.5846	434-13-9		
26H09	Prestw-798	Dienestrol	266.34296	84-17-3	Yes	
26H11	Prestw-800	Amrinone	187.20273	60719-84-8	Yes	
27A07	Prestw-806	Trimipramine maleate salt	410.5177	521-78-8	Yes	Yes
27C08	Prestw-827	Propantheline bromide	448.40445	50-34-0	Yes	
27C11	Prestw-830	Ethaverine hydrochloride	431.964	985-13-7		
27D10	Prestw-839	Ganciclovir	255.23506	82410-32-0	Yes	
27D11	Prestw-840	Ethopropazine hydrochloride	348.9415	1094-08-2	Yes	
27E07	Prestw-846	Ethynylestradiol 3-methyl ether	310.44017	72-33-3	Yes	
27F07	Prestw-856	Tolmetin sodium salt dihydrate	315.30421	64490-92-2	Yes	
27G07	Prestw-866	Azacytidine-5	244.20864	320-67-2		
27G08	Prestw-867	Paromomycin sulfate	713.71774	1263-89-4	Yes	
27H09	Prestw-878	Ioversol	807.11988	87771-40-2	Yes	
27H11	Prestw-880	Carbachol	182.65165	51-83-2	Yes	
28A07	Prestw-886	Clioquinol	305.5037	130-26-7	Yes	
28A08	Prestw-887	Oxybenzone	228.24994	131-57-7	Yes	

28A09	Prestw-888	Promethazine hydrochloride	320.88732	58-33-3	Yes	
28A11	Prestw-1137	Esmolol hydrochloride	331.84292	81161-17-3	Yes	
28C07	Prestw-906	Fluspirilen	475.58672	1841-19-6		
28C09	Prestw-908	Ethynodiol diacetate	384.52024	297-76-7	Yes	
28D08	Prestw-917	Flurbiprofen	244.26806	5104-49-4	Yes	
28D09	Prestw-918	Nimodipine	418.45057	66085-59-4	Yes	

28D11	Prestw-920	L(-)-vesamicol hydrochloride	295.85587	112709-59-8		
28E07	Prestw-926	Idazoxan hydrochloride	240.69146	79944-56-2		
28F07	Prestw-936	Bephenium hydroxynaphthoate	443.54763	3818-50-6		
28G09	Prestw-948	Timolol maleate salt	432.49931	26921-17-5	Yes	
28H10	Prestw-959	Proparacaine hydrochloride	330.85819	5875-06-9	Yes	
28H11	Prestw-960	Aminocaproic acid	131.17601	60-32-2	Yes	
29B07	Prestw-976	Tracazolate hydrochloride	340.85625	41094-88-6		
29C09	Prestw-1452	Norgestimate	369.50842	35189-28-7	Yes	
29D09	Prestw-998	Zuclopenthixol dihydrochloride	473.89629	633-59-0		Yes
29D11	Prestw-1000	Lymecycline	602.64701	992-21-2		
29E07	Prestw-1802	Darunavir	547.67584	635728-49-3	Yes	
29F07	Prestw-1016	Moxonidine	241.68189	75438-57-2		
29G08	Prestw-1027	Tocainide hydrochloride	228.72394	71395-14-7	Yes	Yes
29H09	Prestw-1038	Methyldopate hydrochloride	275.73456	2508-79-4	Yes	
30A07	Prestw-1046	Repaglinide	452.59897	135062-02-1	Yes	
30A11	Prestw-1050	Quinethazone	289.74244	73-49-4	Yes	
30B07	Prestw-1056	Trifluridine	296.20477	70-00-8	Yes	
30C09	Prestw-1068	Thiethylperazine dimalate	667.80337	52239-63-1	Yes	
30D10	Prestw-1803	Methicillin sodium	402.40458	7246-14-2	Yes	
30D11	Prestw-1080	Methiazole	265.33625	108579-67-5		
30E07	Prestw-1086	D-cycloserine	102.09347	68-41-7	Yes	Yes
30E11	Prestw-1090	Homosalate	262.35194	118-56-9		

30F07	Prestw-1096	Estriol	288.39018	50-27-1		
30F08	Prestw-1097	(-)-Isoproterenol hydrochloride	247.72401	5984-95-2	Yes	
30G08	Prestw-1107	Ramipril	416.52189	87333-19-5	Yes	
30H08	Prestw-1117	Azaperone	327.40509	1649-18-9		Yes
30H09	Prestw-1118	Cefepime hydrochloride	517.0293	123171-59-5	Yes	
31A08	Prestw-1482	Valproic acid	144.21552	99-66-1	Yes	Yes
31A09	Prestw-1280	Mepivacaine hydrochloride	282.81636	1722-62-9	Yes	
31C08	Prestw-1483	Fludarabine	285.23664	21679-14-1	Yes	
31C09	Prestw-1484	Cladribine	285.69184	4291-63-8	Yes	Yes
31D09	Prestw-1187	Granisetron	312.41818	109889-09-0	Yes	
31D10	Prestw-1224	Anthralin	226.234	1143-38-0		
31D11	Prestw-1492	Lamotrigine	256.09564	84057-84-1	Yes	
31E11	Prestw-1352	Tulobuterol	227.73636	41570-61-0		
31F07	Prestw-1236	Benztropine mesylate	403.54473	132-17-2	Yes	Yes
31F08	Prestw-1359	Vecuronium bromide	637.74839	50700-72-6	Yes	
31G09	Prestw-1376	Cilnidipine	492.53341	132203-70-4		
31H08	Prestw-1334	Rivastigmine	250.34364	123441-03-2	Yes	Yes
31H09	Prestw-1342	Sildenafil	474.5862	139755-83-2	Yes	
31H10	Prestw-1207	Acetylsalicylic acid	180.16171	50-78-2	Yes	

Supplementary Table S1. Chemical names and properties of the small molecules that were identified in the primary screen that inhibited the UPR^{mt}.

Suppl. Table 2_Genetics

PlateNumber PositionNumber	Prestw number	chemical name	mol weight	CAS number	FDA approved	blood brain barrier
02G04	Prestw-143	Chlorhexidine	505.4574	55-56-1	Yes	
02G06	Prestw-145	Chlortetracycline	515.35118	64-72-2	Yes	
03H06	Prestw-1771	Carmofur	257.26687	61422-45-5		
04H03	Prestw-312	Flunarizine dihydrochloride	477.42926	30484-77-6		Yes
04H04	Prestw-313	Trifluoperazine	480.42667	440-17-5	Yes	
05C05	Prestw-344	Clorgyline hydrochloride	308.63757	17780-75-5		
06C02	Prestw-421	Suloctidil	337.57205	54063-56-8		
06H02	Prestw-1358	Vatalanib	346.82235	212141-54-3		
07D02	Prestw-511	Fluoxetine hydrochloride	345.79528	59333-67-4	Yes	
07H04	Prestw-553	Pentamidine isethionate	592.69217	140-64-7	Yes	
10D04	Prestw-753	Demeclocycline	501.32409	64-73-3	Yes	
10G02	Prestw-781	Clobetasol propionate	466.98219	25122-46-7	Yes	
11F02	Prestw-851	Paroxetine Hydrochloride	365.83552	110429-35-1	Yes	
12F05	Prestw-934	Flucytosine	129.09438	2022-85-7	Yes	Yes
13G02	Prestw-1021	Isradipine	371.39632	75695-93-1	Yes	
15D02	Prestw-1203	5-fluorouracil	130.07911	51-21-8	Yes	Yes
17G08	Prestw-67	Miconazole	416.13708	22916-47-8	Yes	
18H11	Prestw-160	Gentamicine sulfate	1488.81475	1405-41-0	Yes	No
19D11	Prestw-200	Camptothecine (S,+)	348.36152	7689-03-4		
20B09	Prestw-258	Antazoline hydrochloride	301.82205	2508-72-7	Yes	
21C09	Prestw-348	Chlorprothixene	352.32883	6469-93-8	Yes	
21H08	Prestw-397	Clomiphene citrate (Z,E)	598.09862	50-41-9	Yes	
22A10	Prestw-409	Amiodarone hydrochloride	681.78455	19774-82-4	Yes	
22H09	Prestw-478	Felodipine	384.26243	72509-76-3	Yes	

23C10	Prestw-509	Bromperidol	420.32536	10457-90-6		
24A08	Prestw-1139	Itraconazole	705.65031	84625-61-6	Yes	Yes
24B10	Prestw-1297	Lacidipine	455.55601	103890-78-4		
24E09	Prestw-1460	Oxibendazol	249.27165	20559-55-1		
30D11	Prestw-1080	Methiazole	265.33625	108579-67-5		
30E11	Prestw-1090	Homosalate	262.35194	118-56-9		
31C08	Prestw-1483	Fludarabine	285.23664	21679-14-1	Yes	
32A08	Prestw-1719	Amorolfine hydrochloride	353.98017	78613-38-4	Yes	
32B07	Prestw-1753	Tegafur	200.17093	17902-23-7		Yes

Supplementary Table S2. Chemical names and properties of the small molecules that were identified in the secondary screen that inhibited the UPR^{mt}.

Prestw number	Chemical name	10 uM	20 uM	30 uM	40 uM	50 uM	60 uM	70 uM	80 uM
Prestw-143	Chlorhexidine								
Prestw-145	Chlortetracycline hydrochloride								
Prestw-1771	Carmofur								
Prestw-312	Flunarizine dihydrochloride								
Prestw-313	Trifluoperazine dihydrochloride								
Prestw-344	Clorgyline hydrochloride								
Prestw-421	Suloctidil								
Prestw-1358	Vatalanib								
Prestw-511	Fluoxetine hydrochloride								
Prestw-553	Pentamidine isethionate								
Prestw-753	Demeclocycline hydrochloride								
Prestw-781	Clobetasol propionate								
Prestw-851	Paroxetine Hydrochloride								
Prestw-934	Flucytosine								
Prestw-1021	Isradipine								
Prestw-1203	5-fluorouracil								
Prestw-67	Miconazole								
Prestw-160	Gentamicine sulfate								
Prestw-200	Camptothecine (S,+)								
Prestw-258	Antazoline hydrochloride								
Prestw-348	Chlorprothixene hydrochloride								
Prestw-397	Clomiphene citrate (Z,E)								
Prestw-409	Amiodarone hydrochloride								
Prestw-478	Felodipine								
Prestw-509	Bromperidol								
Prestw-1139	Itraconazole								
Prestw-1297	Lacidipine								
Prestw-1460	Oxibendazol								
Prestw-1080	Methiazole								
Prestw-1090	Homosalate								
Prestw-1483	Fludarabine								

Prestw-1719	Amorolfine hydrochloride								
Prestw-1753	Tegafur								

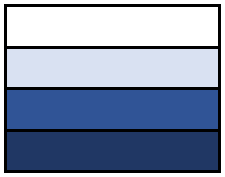

0% UPR^{mt} repression
5-50% UPR^{mt} repression
50%-90% UPR^{mt} repression
> 90% UPR^{mt} repression

Supplementary Table S3. Dose response of small molecules identified in the secondary screen and their effects on the UPR^{mt}.

Figure	*Trial*	*Strain 1*	*Mean Survival 1*	*Strain 2*	*Mean Survival 2*	*Percentage change*	*p-value*	*p-value summary*
3A	1	wild-type DMSO	13.51	wild-type PAX	13.43	0.59568131	0.5737	ns
	2	wild-type DMSO	13.43	wild-type PAX	13.39	0.298730396	0.8424	ns
	3	wild-type DMSO	12.85	wild-type PAX	13.55	-5.166051661	0.632	ns
3B	1	*clk-1(qm30)* DMSO	19.64	*clk-1(qm30)* PAX	16.82	16.76575505	0.0027	***
	2	*clk-1(qm30)* DMSO	20.69	*clk-1(qm30)* PAX	17.25	19.94202899	0.0073	**
	3	*clk-1(qm30)* DMSO	18.95	*clk-1(qm30)* PAX	16.45	15.19756839	0.0463	*
3C	1	wild-type DMSO	83	wild-type PAX	75.32	10.19649495	0.0054	**
	2	wild-type DMSO	82.2	wild-type PAX	69.08	18.9924725	0.0003	***
	3	wild-type DMSO	81.76	wild-type PAX	75.16	8.781266631	0.0072	**
3D	1	*clk-1(qm30)* DMSO	83.88	*clk-1(qm30)* PAX	72.274	16.05833356	<0.0001	****
	2	*clk-1(qm30)* DMSO	83.04	*clk-1(qm30)* PAX	70.53	17.73713313	0.0027	**
	3	*clk-1(qm30)* DMSO	77.04	*clk-1(qm30)* PAX	72.56	6.174200662	0.0465	*
4C	1	wild-type	14.26	*mod-5(n3314)*	14.46	-1.383125864	0.9004	ns
	2	wild-type	14.43	*mod-5(n3314)*	14.02	2.924393723	0.6623	ns
	3	wild-type	14.05	*mod-5(n3314)*	13.91	1.006470165	0.8719	ns
4D	1	*clk-1(qm30)*	19.29	*clk-1(qm30); mod-5(n3314)*	17.57	9.789413773	0.1181	ns

	2	*clk-1(qm30)*	19.46	*clk-1(qm30); mod-5(n3314)*	18.08	7.632743363	0.0542	ns
	3	*clk-1(qm30)*	18.89	*clk-1(qm30); mod-5(n3314)*	18.35	2.942779292	0.2672	ns
6E	1	wild-type	12.53	*wsp-1(gm324)*	12.27	2.118989405	0.7284	ns
	2	wild-type	12.33	*wsp-1(gm324)*	12.78	-3.521126761	0.7811	ns
	3	wild-type	13.08	*wsp-1(gm324)*	12.34	5.996758509	0.4376	ns
6F	1	*clk-1(qm30)*	20.2475	*clk-1(qm30); wsp-1(gm324)*	16.0909	25.831992	0.0002	****
	2	*clk-1(qm30)*	19.723	*clk-1(qm30); wsp-1(gm324)*	16.01	23.19175515	0.0003	****
	3	*clk-1(qm30)*	19.05	*clk-1(qm30); wsp-1(gm324)*	15.33	24.26614481	0.0004	****

Supplementary Table S4. Statistics relating to lifespan and survival assays.

Chapter 3

A novel gene-diet interaction promotes organismal lifespan and host protection during infection via the mitochondrial UPR

Mustafi Raisa Amin[1], Siraje Arif Mahmud[1], Jonathan L. Dowgielewicz, Madhab Sapkota, and Mark W. Pellegrino.[*]

[1]equal contribution

[*]correspondence: mark.pellegrino@uta.edu

(Published in Amin MR, Mahmud SA, Dowgielewicz JL, Sapkota M, Pellegrino MW (2020) A novel gene-diet interaction promotes organismal lifespan and host protection during infection via the mitochondrial UPR. PLOS Genetics 16(12): e1009234. https://doi.org/10.1371/journal.pgen.1009234)

Abstract

Cells use a variety of mechanisms to maintain optimal mitochondrial function including the mitochondrial unfolded protein response (UPR^{mt}). The UPR^{mt} mitigates mitochondrial dysfunction by differentially regulating mitoprotective gene expression through the transcription factor ATFS-1. Since UPR^{mt} activation is commensurate with organismal benefits such as extended lifespan and host protection during infection, we sought to identify pathways that promote its stimulation. Using unbiased forward genetics screening, we isolated novel mutant alleles that could activate the UPR^{mt}. Interestingly, we identified one reduction of function mutant allele (*osa3*) in the mitochondrial ribosomal gene *mrpl-2* that activated the UPR^{mt} in a diet-dependent manner. We find that *mrpl-2(osa3)* mutants lived longer and survived better during pathogen infection depending on the diet they were fed. A diet containing low levels of vitamin B12 could activate the UPR^{mt} in *mrpl-2(osa3)* animals. Also, we find that the vitamin B12-dependent enzyme methionine synthase intersects with *mrpl-2(osa3)* to activate the UPR^{mt} and confer animal lifespan extension at the level of ATFS-1. Thus, we present a novel gene-diet pairing that promotes animal longevity that is mediated by the UPR^{mt}.

Keywords: UPR^{mt}, diet, mitochondria, mitonuclear imbalance, methionine restriction, *C. elegans*, stress response, lifespan, *atfs-1*, *mrpl-2*, *metr-1*.

Introduction

Because of their endosymbiotic origin, mitochondria possess their own genome and ribosomes that are used to express and translate a minor portion of the mitochondrial proteome [1]. The mitochondrial genome encodes 13 (12 in *C. elegans*) subunits of the multimeric electron transport chain (ETC) complexes while the remaining components are expressed from the nuclear genome, translated on cytosolic ribosomes and imported into mitochondria using a sophisticated import pathway [2]. This requires a great deal of coordination between both the mitochondrial and nuclear genomes in order to efficiently assemble these multimeric ETC structures. Imbalances in mitonuclear coordination causes mitochondrial dysfunction that is sensed by cellular defense programs to help restore normal organelle function [3-5]. Retrograde signaling such as the mitochondrial unfolded protein response (UPR^{mt}) is one type of defense mechanism that is used to mitigate mitochondrial dysfunction [6, 7]. Here, decreased mitochondrial function is coupled to changes in gene expression that helps restore mitochondrial homeostasis. At the center of the UPR^{mt} is the bZIP transcription factor ATFS-1 that coordinates the changes in gene expression associated with this mitochondrial stress response [8, 9]. A defining characteristic of ATFS-1 is the presence of a mitochondrial targeting sequence that mediates its import into healthy mitochondria where it subsequently undergoes proteolytic degradation. Import efficiency is reduced in dysfunctional mitochondria allowing ATFS-1 to accumulate in the cytosol and be imported into the nucleus. ATFS-1 regulates a broad change in gene expression that in turn mediates mitochondrial recovery with roles in proteostasis, detoxification, and metabolic reprogramming [9].

Paradoxically, while a decline in mitochondrial function is associated with organismal aging and disease, there is considerable support that mild impairment can extend lifespan [10]. Conditions

that reduce mitochondrial function and extend lifespan are also associated with the activation of the UPR^{mt}. Evidence also exists demonstrating a requirement of the UPR^{mt} for mitochondrial stress-induced longevity. For example, the UPR^{mt} is required for the increase in lifespan that is observed in mitochondrial stressed animals with impaired ETC function [11, 12]. Also, disruptions to mitochondrial ribosome function results in mitonuclear imbalances that extend lifespan in a UPR^{mt}-dependent manner [3]. It is important to note that although UPR^{mt} activation is correlated with conditions that promote lifespan extension, it is not an absolute predictor of this phenomenon nor is it always required [5].

In addition to promoting lifespan extension, UPR^{mt} activation is also associated with protecting host survival during infection. Here, ATFS-1 regulates the expression of genes related to innate immunity, including anti-microbial peptides, lysozymes and C-type lectins [9, 13]. Consistently, ATFS-1 is required for protection during infection with pathogens that target mitochondrial function [13-15]. Also, priming the host for the UPR^{mt} prior to infection significantly improves host resistance to infection [13, 16].

Here, we have identified a reduction of function allele in the *C. elegans* mitochondrial ribosome gene *mrpl-2* using a forward genetics approach. We find that the *mrpl-2* mutant exhibits extended lifespan and increased survival during pathogen infection. However, the benefits conferred by *mrpl-2(osa3)* were diet-dependent. We find that a diet low in vitamin B12 acts synergistically with the *mrpl-2* mutant genetic background. Mechanistically, loss of the vitamin B12-dependent enzyme methionine synthase interacts with the *mrpl-2* mutant to drive the activation of the UPR^{mt}, thus promoting lifespan extension. Our data support a model in which genetically-induced mitonuclear imbalance and diet-mediated methionine restriction use a common mechanism to promote lifespan extension, including the activation of the UPR^{mt}.

Results

Forward genetic mutagenesis screen identifies novel alleles that activate the UPR^{mt} in diet-dependent and independent manners

Because activation of the UPR^{mt} is correlated with extended lifespan and increased survival during pathogen infection, we sought to perform a forward genetic screen to uncover novel alleles capable of activating the UPR^{mt} using the strain SJ4100 *hsp-6p*::GFP (Fig 1A and 1B). *C. elegans hsp-6* encodes the ortholog of the mitochondrial chaperone mtHSP70 and its expression is induced during the UPR^{mt} [17]. We obtained four independent viable mutants from this screen that could activate the *hsp-6p*::GFP reporter (mutant alleles *osa2-osa5*) (Fig 1C and 1D).

ATFS-1 is required for the development and/or fertility of mitochondrial stressed animals [9, 18], prompting us to investigate the effect of its knockdown by RNAi in all our identified mutants. Interestingly, while loss of ATFS-1 slowed the development and reduced the fertility of *osa2* and *osa5* animals, it had negligible effects for *osa3* and *osa4* (S1A Fig). We therefore examined UPR^{mt} activity in *osa2-osa5* animals in the presence or absence of ATFS-1. Consistent with causing a delay in animal development, loss of ATFS-1 suppressed the induction of *hsp-6p*::GFP in *osa2* and *osa5* animals (S1B Fig). Surprisingly, *hsp-6p*::GFP expression was not induced in *osa3* and *osa4* animals even when grown with empty RNAi plasmid control bacteria (S1B Fig). RNAi by feeding in *C. elegans* uses the RNase III-deficient *E. coli* strain HT115 (*E. coli* K12-type strain) as opposed to the standard *E. coli* uracil auxotroph strain OP50 (*E. coli* B-type strain). Since we had performed the forward genetics mutagenesis using *E. coli* OP50, we hypothesized that the type of diet may be influencing the activation of the UPR^{mt} in *osa3* and *osa4* animals. Indeed, we could recapitulate the absence of UPR^{mt} activation in *osa3* and *osa4* animals using *E. coli* HT115 bacteria that lacked the empty RNAi plasmid (Fig 1C and 1D). We also tested another *E. coli* K12 strain

BW25113 and the K12/B-type hybrid strain HB101 which similarly did not induce *hsp-6p*::GFP expression in *osa3* and *osa4* animals (Fig 1C and 1D). In contrast, the type of *E. coli* diet had no discernible effect on the activation of the UPR^{mt} in the *osa2* or *osa5* mutant backgrounds (Fig 1C and 1D). Thus, the type of diet influences the activation of the UPR^{mt} in the *osa3* and *osa4* genetic backgrounds.

We used whole genome sequencing to identify the genes responsible for the UPR^{mt} induction observed in *osa2-osa5*. The allele osa2 contained a mutation (GGT➔AGT[359 Gly➔Ser] in sucg-1, the C. elegans homolog of SUCLG2 succinyl-CoA ligase subunit beta (Fig 1E). The allele osa3 contained a mutation GGA➔GAA[125Gly➔Glu] in mrpl-2, the C. elegans homolog of MRPL2 mitochondrial ribosomal protein L2 subunit (Fig 1E). Consistently, knockdown of MRPL-2 and other mitochondrial ribosome subunits was previously found to activate the UPRmt [3,5]. For the osa5 allele we identified a GAT➔AAT[329Asp➔Asn] mutation in pdr-1, the C. elegans homolog of Parkin (Fig 1E). Reintroducing the wild-type *sucg-1* or *mrpl-2* gene locus by germline transformation could rescue UPR^{mt} activity back to wild-type levels for *osa2* and *osa3,* respectively (S2A and S2B Fig). However, re-introduction of the wild-type *pdr-1* locus into *osa5* animals did not rescue UPR^{mt} activity to wild-type levels (S2C Fig). Instead, germline transformation of wild-type animals with the *pdr-1* gene locus containing the *osa5* mutation was sufficient to induce the UPR^{mt} (S2C Fig). In contrast, germline transformation of wild-type animals with the wild-type *pdr-1* gene locus did not induce the UPR^{mt} (S2C Fig). Together, this suggests that *osa5* is a novel dominant allele of *pdr-1*. We were unable to map the gene responsible for the activation of the UPR^{mt} in *osa4* animals and therefore examined the connection between diet, genetic background, and UPR^{mt} activation using *mrpl-2(osa3)* animals.

Diet influences mitochondrial function in mrpl-2(osa3) animals

We next examined various parameters of mitochondrial function in wild-type and *mrpl-2(osa3)* animals fed the various *E. coli* diets. We first measured oxygen consumption levels which were surprisingly increased in *mrpl-2(osa3)* animals fed *E. coli* OP50 and BW25113, but not HT115, and HB101 (Fig 2A). We observed a similar trend when measuring ATP levels which were increased in *mrpl-2(osa3)* animals fed *E. coli* OP50 and BW25113, whereas no change occurred with HT115 and HB101 (Fig 2B). Increased mitochondrial activity or dysfunction can generate toxic reactive oxygen species (ROS) that perturbs protein homeostasis through the formation of carbonyl modifications. We therefore used the OxyBlot system which assesses protein carbonylation as a measure of oxidative damage. Interestingly, *mrpl-2(osa3)* animals fed a diet of *E. coli* OP50 showed reduced oxidative damage compared to wild-type (Fig 2C; S3 Fig). No change in oxidative damage was observed when *mrpl-2(osa3)* animals were fed diets of *E. coli* HT115, HB101, or BW25113 (Fig 2C and S3 Fig). Lastly, mitochondrial function was also examined through an assessment of mitochondrial membrane potential. Consistent with an activation of the UPR^{mt}, *mrpl-2(osa3)* animals displayed reduced mitochondrial membrane potential when fed a diet of *E. coli* OP50 (Fig 2D and S4A Fig). Mild increases in mitochondrial membrane potential were observed when *mrpl-2(osa3)* animals were fed diets of *E. coli* HT115 and HB101 (Fig 2D and S4A Fig). Surprisingly, mitochondrial membrane potential was also reduced when *mrpl-2(osa3)* animals were fed a diet of *E. coli* BW25113 despite no observable activation of the UPR^{mt} (Fig 2D and S4A Fig).

Slowed developmental rates are often a consequence of mitochondrial stress. However, we did not observe any significant change in developmental rates between wild-type and *mrpl-2(osa3)* fed on

the various diets (S4B Fig). While the development of *mrpl-2(osa3)* animals was not significantly different, we did notice that *mrpl-2(osa3)* animals appeared thinner and overall slightly smaller when fed *E. coli* OP50 whereas no difference was observed when these animals were fed *E. coli* HT115, HB101, or BW25113 (Fig 2E).

mrpl-2(osa3) extends lifespan and increases pathogen resistance in a diet-dependent manner

We next examined lifespans of wild-type and *mrpl-2(osa3)* animals fed the various diets. As expected with the activation of the UPR^{mt}, *mrpl-2(osa3)* animals lived longer than wild-type when fed *E. coli* OP50 (Fig 3A). No differences in lifespan between wild-type and *mrpl-2(osa3)* were observed when fed *E. coli* HT115, HB101, and BW25113 which is consistent with a lack of UPR^{mt} activation on these diets (Fig 3B-D). Importantly, an extrachromosomal array consisting of the wild-type *mrpl-2* gene locus suppressed the increased longevity of *mrpl-2(osa3)* animals in two independent transgenic lines resulting in normal (wild-type) lifespan levels (S5 Fig), indicating that mutation in *mrpl-2* is the cause of the observed lifespan extension.

We then measured various physiological markers of aging between wild-type and *mrpl-2(osa3)* under the different diets. We first measured thrashing rates which reflects body wall muscle integrity. We find that muscle function decline was less in *mrpl-2(osa3)* animals compared to wild-type when fed *E. coli* OP50 whereas no differences in thrashing rate was observed when *mrpl-2(osa3)* animals were fed other diets (Fig 3E). We then quantified pharyngeal pumping which is a reflection of the rate of food intake and found it to be higher in aged *mrpl-2(osa3)* animals compared to wild-type when fed *E. coli* OP50 whereas no difference was detected when fed *E. coli* HT115, HB101, and BW25113 (Fig 3F). Lastly, accumulation of lipofuscin is a hallmark of

aging in *C. elegans* that is reflected as intestinal autofluorescence [19]. The greatest reduction in autofluorescence was observed when *mrpl-2(osa3)* animals were fed *E. coli* OP50 but only a mild difference was observed when fed *E. coli* HT115, HB101, and no difference for BW25113 (Fig 3G). Therefore, *mrpl-2(osa3)* slows physiological markers of aging when fed a diet of *E. coli* OP50.

Next, we examined the effect of diet on the ability of *mrpl-2(osa3)* animals to survive infection with the opportunistic pathogen *Pseudomonas aeruginosa* [13]. Consistent with increased host resistance, pathogen colonization was lower in *mrpl-2(osa3)* animals that were previously fed *E. coli* OP50 whereas similar pathogen colonization levels were observed in *mrpl-2(osa3)* animals previously fed *E. coli* HT115, HB101, and BW25113 (Fig 4A and 4B). Accordingly, *mrpl-2(osa3)* animals survived significantly longer than wild-type animals during infection with *P. aeruginosa* if they were previously fed a diet of *E. coli* OP50 (Fig 4C). No difference in host survival was observed between wild-type and *mrpl-2(osa3)* animals when each were previously fed diets of *E. coli* HT115, HB101, or BW25113 (Fig 4D-F).

We next wished to confirm that mild dysfunction to mitochondrial translation was synergizing specifically with a diet of *E. coli* OP50 to induce the UPR^{mt}. Here, we treated wild-type animals with doxycycline, which was previously found to inhibit mitochondrial translation, activate the UPR^{mt} and increase *C. elegans* lifespan [3]. We find that exposure of wild-type animals to a mild dose of doxycycline activated the UPR^{mt} when fed a diet of *E. coli* OP50 but not HT115, HB101, or BW25113 (S6A Fig). In addition, exposure to a mild dose of doxycycline increased the lifespan of wild-type animals only when they were fed a diet of *E. coli* OP50, whereas no difference was observed when fed *E. coli* HT115, HB101, or BW25113 (S6B-E Fig). Thus, mild disruption to

mitochondrial translation either through genetic (*mrpl-2(osa3)*) or chemical (doxycycline) means activates the UPR^{mt} and extends lifespan in a diet-dependent manner.

Together, our data suggests an interplay exists between diet and the *mrpl-2(osa3)* genetic background that drives activation of the UPR^{mt}. Hereafter, we focus on the diets of *E. coli* OP50 and HT115 to dissect the mechanisms behind this interaction.

Vitamin B12 availability synergizes with mrpl-2(osa3) to activate the UPR^{mt}

We next explored the mechanism behind the relationship of diet and the activation of the UPR^{mt} in *mrpl-2(osa3)* animals. A recent study found that *E. coli* OP50 is deficient in the nutrient vitamin B12 compared to *E. coli* HT115 [20]. We hypothesized that lower levels of vitamin B12 in the *E. coli* OP50 diet might interact with *mrpl-2(osa3)* to drive the activation of the UPR^{mt}. Indeed, wild-type animals fed a diet of *E. coli* OP50 had lower levels of vitamin B12 compared to those fed a diet of *E. coli* HT115 (S7 Fig). We therefore supplemented the *E. coli* OP50 diet with two biologically active forms of vitamin B12, methylcobalamin and adenosylcobalamin, which are used as cofactors in the activation of associated effectors. Interestingly, we found that an *E. coli* OP50 diet supplemented with methylcobalamin or adenosylcobalamin was able to suppress the activation of *hsp-6p*::GFP in *mrpl-2(osa3)* animals (Fig 5A and 5B). The finding that either methylcobalamin or adenosylcobalamin could suppress the activation of the UPR^{mt} is likely due to their ability to be interconverted [21]. We next measured lifespans of wild-type or *mrpl-2(osa3)* animals fed an *E. coli* OP50 diet supplemented with methylcobalamin. Consistent with attenuating the activation of the UPR^{mt}, methylcobalamin supplementation suppressed the extended lifespan of *mrpl-2(osa3)* fed a diet of *E. coli* OP50 (Fig 5C).

Next, we examined the consequences of restricting vitamin B12 levels from the diet of *E. coli* HT115 using a previously established technique [22]. Restricting vitamin B12 levels was able to activate the UPR^{mt} in *mrpl-2(osa3)* animals but not in the wild-type, similar to when they were fed *E. coli* OP50 (Fig 5D and 5E). Supplementing with methylcobalamin attenuated UPR^{mt} activity in vitamin B12-restricted *mrpl-2(osa3)* animals (Fig 5D and 5E). Consistent with an activation of the UPR^{mt}, reducing vitamin B12 levels from the HT115 diet also enhanced the lifespan of *mrpl-2(osa3)* animals, which could be suppressed with methylcobalamin supplementation (Fig 5F). Together, our data suggest that the effect of diet on the activation of the UPR^{mt} in the *mrpl-2(osa3)* background is due to differences in vitamin B12 content.

Mitonuclear imbalance and methionine restriction act in a common pathway to promote lifespan extension

Vitamin B12 is used as a cofactor for two separate enzymes: methionine synthase which mediates the conversion of homocysteine to methionine during the S-adenosylmethionine/methionine cycle, and methylmalonyl-CoA mutase which converts L-methylmalonyl-CoA to succinyl-CoA (Fig 6A) [21]. Therefore, we tested the effects of genetically disabling these pathways under a vitamin B12 replete diet of HT115 using mutants in methionine synthase, (*metr-1(ok521)*) and methylmalonyl-CoA mutase (*mmcm-1(ok1637)*). Interestingly, *metr-1(ok521)* or *mmcm-1(ok1637)* individual loss of function mutants activated the UPR^{mt} when they were fed a diet of HT115 (Fig 6B and 6C). However, no further enhancement of the UPR^{mt} was observed for each mutation in combination with the *mrpl-2(osa3)* background (Fig 6B and 6C).

We then examined the effects of *mmcm-1(ok1637)* or *metr-1(ok521)* on the lifespan of *mrpl-2(osa3)* fed a vitamin B12-replete diet of *E. coli* HT115 or when fed a diet of *E. coli* OP50. Neither *mmcm-1(ok1637)* or *mmcm-1(ok1637); mrpl-2(osa3)* animals exhibited any significant change in lifespan fed a diet of *E. coli* HT115 (Fig 6E). Unexpectedly, a modest but significant increase in lifespan was observed in *metr-1(ok521)* single mutants fed *E. coli* HT115 (Fig 6D), previously found to have normal rates of aging when fed *E. coli* OP50 [23]. However, there was no significant difference in lifespan between *metr-1(ok521)* and *metr-1(ok521); mrpl-2(osa3)* mutants fed a diet of *E. coli* HT115 (Fig 6D). In contrast, a greater lifespan extension was observed in *metr-1(ok521)* animals fed the *E. coli* OP50 diet to levels comparable with *E. coli* OP50-fed *mrpl-2(osa3)* (Fig 6F). However, and interestingly, no further extension was observed in *metr-1(ok521); mrpl-2(osa3)* double mutant animals fed *E. coli* OP50 (Fig 6F). Surprisingly, although the lifespan of *mmcm-1(ok1637)* was not significantly extended compared to wild-type when fed a diet of *E. coli* OP50, *mmcm-1(ok1637)* nonetheless reduced the lifespan extension of *mrpl-2(osa3)* (Fig 6G). This suggests that *mrpl-2(osa3)* extends lifespan when fed a diet of OP50 in a MMCM-1-dependent manner.

Because the lifespan extensions of *mrpl-2(osa3)* and *metr-1(ok521)* animals were not additive in the double mutant background suggests that mitonuclear imbalance and methionine restriction may use a common pathway(s) to regulate aging. Indeed, wild-type animals fed a diet of *E. coli* OP50 were found to have lower levels of methionine compared to those fed a diet of *E. coli* HT115 (S8 Fig). In addition, supplementation with methionine, but not other amino acids, resulted in a near complete suppression of the UPR^{mt} in *mrpl-2(osa3)* animals fed a diet of *E. coli* OP50 (Fig 6H-I and S9 Fig). Consistently, methionine supplementation also completely suppressed the increase in longevity observed with *mrpl-2(osa3)* animals fed *E. coli* OP50 (Fig 6J).

ATFS-1 mediates extended lifespan resulting from mitonuclear imbalance or methionine restriction

We next performed transcriptomics to evaluate the changes in gene expression occurring during mitonuclear imbalance and methionine restriction using *mrpl-2(osa3)* and *metr-1(ok521)* animals, respectively. We hypothesized that *mrpl-2(osa3)* and *metr-1(ok521)* extended lifespan using at least one common pathway since the lifespan of the double mutant was not additive. Using a cutoff *p*-value of <0.05 (after Benjamini-Hochberg correction), our transcriptomic analysis indicated that there were relatively fewer genes that were differentially expressed in *metr-1(ok521)* animals relative to wild-type animals compared to those differentially expressed in *mrpl-2(osa3)* (Fig 7A-C and S2 Table). However, there was considerable overlap between the genes that were differentially expressed in each genetic background. Of the 46 genes that were upregulated in *metr-1(ok521)*, 26 were shared with *mrpl-2(osa3)* (Fig 7C). Similarly, of the 88 genes that were downregulated in *metr-1(ok521)* animals, 47 were in common with *mrpl-2(osa3)* (Fig 7C).

Since both mitonuclear imbalance and methionine restriction were able to induce the UPR^{mt}, we suspected that this pathway may be required for their effects on lifespan. Therefore, we next examined whether the increased longevity of *mrpl-2(osa3)* or *metr-1(ok51)* animals required the UPR^{mt} by using the *atfs-1(tm4525)* reduction of function mutant. As expected, loss of ATFS-1 reduced the activation of the UPR^{mt} in OP50-fed *mrpl-2(osa3)* and *metr-1(ok521)* animals (Fig 7D and 7E). Also, loss of ATFS-1 suppressed the increase in animal lifespan observed with *mrpl-2(osa3)* fed a diet of *E. coli* OP50 while having no significant effect in an otherwise wild-type background (Fig 7F). This is consistent with previous reports illustrating the need for the UPR^{mt} for mitonuclear imbalance-induced lifespan extension [3]. Interestingly, *atfs-1* reduction of function also suppressed the increase in lifespan resulting from *metr-1(ok521)* methionine

restriction (Fig 7G). Thus, ATFS-1 and the UPR^{mt} are required for lifespan extension resulting from both mitonuclear imbalance and methionine restriction.

Discussion

Our data suggests that the *mrpl-2(osa3)* allele is a reduction of function allele that creates a sensitized background for UPR^{mt} activation and that the type of diet can tip the balance in its favor (Fig 7H). Vitamin B12 availability appears to be the metabolite that determines whether a diet will activate the UPR^{mt} in the *mrpl-2(osa3)* background via the methionine synthase pathway. Consistently, under vitamin B12 replete conditions, the level of methionine restriction is insufficient to activate the UPR^{mt} in the *mrpl-2(osa3)* sensitized background and to extend lifespan. Interestingly, we find that disruption to the vitamin B12-dependent methionine synthesis pathway via inactivation of METR-1 also activates the UPR^{mt} and can extend animal lifespan. While bacterial diet is the main source of methionine for *C. elegans*, this amino acid can also be synthesized to a small degree via METR-1 and thus, reduced function of METR-1 results in a sensitized condition of methionine restriction [23]. Importantly, we find that a reduction of function mutation in *mrpl-2* and mild methionine restriction use a common mechanism of longevity regulation, including the need of the UPR^{mt} regulator ATFS-1.

Diet is an important determinant controlling organismal aging [24]. While dietary restriction has long been appreciated in mediating lifespan extension [25, 26], there is a growing recognition that the *type* of diet and genetic background of the host can interact in order to control aging rates. This has been observed in a number of cases in *C. elegans*. For example, a mutation in the *C. elegans* 1-pyrroline-5-carboxylate (P5C) dehydrogenase homolog *alh-6*, which mediates the conversion of P5C to glutamate during proline metabolism in mitochondria, displays reduced lifespan when fed on the *E. coli* strain OP50, but not when fed with the strain HT115 [27]. The reduced lifespan observed for *alh-6* mutants grown on *E. coli* OP50 is due to increased

accumulation of P5C that results in mitochondrial dysfunction. A second example of how gene-diet can affect lifespan is seen with a mutation in the *rict-1* gene, the *C. elegans* homolog of a component of the Target of Rapamycin complex 2 (TORC2). Lifespan of *rict-1* mutants fed *E. coli* OP50 is reduced compared to that observed using the *E. coli* strain HB101 [28]. Interestingly, *rict-1* mutants tend to avoid the HB101 strain more often than OP50 resulting in less feeding and a dietary restriction-induced increase in longevity. More recently, loss of the kinase FLR-4 was shown to increase *C. elegans* longevity when fed *E. coli* HT115 but not OP50, through diet-specific activation of p38 MAPK and xenobiotic gene expression [29]. Our study indicates that a specific genetic background can synergize with a diet of low vitamin B12 to promote lifespan extension via activation of the UPR^{mt}. It is interesting that vitamin B12 restriction was previously shown to reduce, rather than increase, lifespan duration [22]. It is possible that the sensitized *mrpl-2(osa3)* background requires a lesser degree of vitamin B12 restriction that promotes, rather than antagonizes, lifespan. Indeed, the activation of the UPR^{mt} and increase in longevity of *mrpl-2(osa3)* animals required less vitamin B12 restriction (four generations of growth on vitamin B12-deficient *E. coli*) than was previously reported which reduced the lifespan of wild-type animals (following five generations of growth on vitamin B12-deficient *E. coli*) [22]. Also interesting is that a vitamin B12-replete diet of HT115 was previously shown to promote host protection against *P. aeruginosa* infection compared to a vitamin B12-restricted diet of OP50 [20], whereas our study discovered the opposite trend. However, the aforementioned protection occurred in the context of *P. aeruginosa*-mediated liquid-killing which reduces animal survival through the production of iron-binding siderophores [30]. In our current study, reduced vitamin B12 supply allowed *mrpl-2(osa3)* animals to survive longer during *P. aeruginosa* slow-killing which results from pathogen

colonization of the gut [31]. This suggests that the beneficial effects of gene-diet interactions are context-dependent.

We also show that a reduction of function mutation in a mitochondrial ribosome gene converges with methionine restriction to promote lifespan at the level of the UPR^{mt}. Mitonuclear imbalance was previously shown to increase animal longevity which required the UPR^{mt} regulator UBL-5 [3]. Our study supports this finding by demonstrating a requirement of ATFS-1 for the extended lifespan of *mrpl-2(osa3)* fed a low vitamin B12 diet. Also, while an association between methionine restriction and lifespan extension has previously been reported [32], to our knowledge this is the first connection between this pathway and the activation of the UPR^{mt}. While the mechanism behind the activation of the UPR^{mt} resulting from methionine restriction was not explored, we do show a requirement for ATFS-1 in mediating the observed extension in longevity. The association between ATFS-1/ UPR^{mt} and the extended lifespan that is observed with mitochondrial stress remains controversial [5, 12, 18, 33]. Certain conditions that activate the UPR^{mt} are associated with extended lifespan and require ATFS-1 or other regulators of this stress response pathway. This includes mitonuclear imbalance [3], ETC dysfunction [12], and more recently from the loss of two neuronal epigenetic regulators [34]. Contrary to these findings, ATFS-1 had no role in regulating the lifespan increase observed with RNAi knockdown of the cytochrome c oxidase 1 gene *cco-1*, despite it reducing the expression of the UPR^{mt} reporter [5]. Also, ATFS-1 was not required for the lifespan extension observed with transaldolase inhibition despite an activated UPR^{mt} [33]. Furthermore, constitutive activation of ATFS-1 does not extend animal lifespan but rather, accelerates aging [5]. Our finding that ATFS-1 is required for the increased longevity of *mrpl-2(osa3)* animals is in line with previous observations demonstrating a requirement of the UPR^{mt} for mitonuclear imbalance-induced longevity [3]. We have also shown

that mild methionine restriction could also activate the UPR^{mt} and extend lifespan in an ATFS-1-dependent manner. One possibility is that the requirement of ATFS-1 and the UPR^{mt} for longevity is highly context-dependent and thus is only revealed during specific types of mitochondrial stress such as the conditions presented in this study. Furthermore, the regulation of lifespan by the UPR^{mt} may also be dependent on the strength of mitochondrial stress encountered. For example, the matrix peptide exporter HAF-1 regulates the UPR^{mt} under conditions of mild mitochondrial stress but not under elevated levels of dysfunction [9, 35]. Future work will now focus on identifying the mechanism of UPR^{mt} activation and lifespan extension occurring with methionine restriction which may help resolve these inconsistencies further.

Materials and Methods

C. elegans and bacterial strains

C. elegans strains were maintained on nematode growth medium (NGM) using previously established methods [36] and cultured at 20^{o}C. Various previously reported *C. elegans* strains were obtained from the Caenorhabditis Genetics Center (CGC) and include: N2 Bristol [36], *zcIs13*[*hsp-6p*::GFP], *metr-1(ok521), mmcm-1(ok1637)*. Strains identified in this study include: *sucg-1(osa2), mrpl-2(osa3), osa4*, and *pdr-1(osa5).* All mutant strains were backcrossed at least four times prior to use. Transgenic rescue worm strains were as follows: *sucg-1(osa2)* [*sucg-1*+], *mrpl-2(osa3)* [*mrpl-2*+], *pdr-1(osa5)* [*pdr-1*+], N2 [*pdr-1*+], and N2 [*pdr-1*(*osa5*)].

The following bacterial strains were also used in this study: *E. coli* strains OP50, HB101, HT115, and BW25113, as well as *P. aeruginosa* PA14 and *P. aeruginosa* PA14-dsRed. *E. coli* strains were obtained from the CGC and *P. aeruginosa* strains were a gift from Dr. Joao Xavier (MSKCC).

EMS mutagenesis

Approximately 2000 SJ4100 animals were harvested from NGM plates with S-basal, washed twice to remove bacteria and resuspended in 2 ml S-basal. 2 ml of 2X ethyl methyl sulfonate (EMS) solution (60 µM) was added to worm suspension and placed on a rocker for 4 hrs. After mutagenesis, worms were washed three times with S-basal, resuspended in 0.5 ml S-basal and plated onto seeded NGM plates. After overnight incubation, 50 adult worms were singled out into NGM plates and allowed to grow until F2 generation (7 days). F2 worms showing green fluorescence were selected for further study.

Germline transformation

We used germline transformation to rescue the phenotypes associated with *sucg-1(osa2)*, *mrpl-2(osa3)*, and *pdr-1(osa5)* using standard techniques [37]. PCR fragments were generated consisting of the promoter, open reading frame, and 3'UTR of each gene and microinjected at 10 ng/µl along with *Pmyo-2*::mCherry plasmid at 5 ng/µl as a co-injection marker. Promoter lengths used for germline transformation experiments were as follows: *mrpl-2* (533 bp), *sucg-1* (2153 bp), and *pdr-1* (1613 bp). Primer sequences used to PCR amplify each rescue fragment were as follows: *mrpl-2*: ttcacagccagactccaatg and gctatttgccgatttgtcgt, *sucg-1*: gcagctccttctgatcttgg and ggaagggtatgccattttga, *pdr-1*: gcgcctcttcatgattagca and catttgttgctgctgttgct. For [*pdr-1(osa5)*] rescue PCR, *pdr-1(osa5)* genomic DNA was used as a template. At least two independent transgenic lines were used from each transformation to test for rescue.

Microscopy

All fluorescent reporter expression assays were conducted using a Zeiss Observer Z1 upright microscope. Worms were anesthetized using 2.5 mM sodium azide in S-Basal and arranged on agarose pad-lined glass microscopy slides for visualization. ImageJ software was used for quantification of fluorescence intensity. Background fluorescence was subtracted from the intestinal fluorescence and divided by worm size to generate a fluorescence intensity value. All photomicrographs show a collection of representative animals. For quantification, at least 20 worms were scored blindly in three independent replicates.

Mitochondrial activity assays

Oxygen consumption rate (OCR) assay

The OCR assay was performed according to (Zuo et al., 2017) using the MitoXpress Xtra oxygen consumption assay kit (Agilent, USA). Approximately 100-150 worms were recovered from each bacterial diet plate and washed three times with S-basal solution to remove excess bacteria. The worms were then transferred to wells of a 96-well plate in a final sample volume of 90 µl. Then 10µl of the oxygen probe was added to each sample. The wells of the 96 well plate were then covered with two drops of mineral oil and immediately read using a Synergy Neo 2 plate reader using Gen5 software (BioTek, Wisnooski, VT, USA) in a time-resolved fluorescence mode with 380 nm excitation and 650 nm emission filters.

Measurement of ATP production

ATP was quantified using a bioluminescence ATP measurement kit (Thermo Fisher Scientific, Waltham, MA, USA). Worms were collected from NGM plates and washed three times in S-basal to remove bacteria and frozen at -80°C overnight. Before assessment, the samples heated to 95°C for 15 minutes and then cooled on ice for 5 minutes. The samples were then centrifuged at 14,000 x g for 10 min at 4°C and the supernatant used to measure ATP. 10 µl of each sample were transferred into 96-well plates in triplicates. The ATP assay solution was prepared according to the manufacturer's instructions. 90 µl of the assay solution was then added to each sample. The sample wells were read on Synergy Neo 2 plate reader using Gen5 software (BioTek, Wisnooski, VT, USA) with a luminometer filter. An ATP standard curve was generated and the ATP concentration for each sample was calculated based on the standard curve.

Quantification of mitochondrial membrane potential

To assess mitochondrial membrane potential, worms were grown on NGM media seeded with particular *E. coli* diets containing 1.25 nM tetramethylrhodamine ethyl ester (TMRE) at 20^{o}C for 3 days and visualized at the L4 stage.

Measurement of protein oxidation by OxyBlot

The OxyBlot protein oxidation detection kit (Millipore-Sigma, Burlington, MA, USA) was used to measure the level of protein oxidation. Worms were collected from each condition, washed with S-basal to remove bacteria and frozen to -80^{o}C. After one hour, the samples were thawed and 100µl of lysis buffer was added. Worms were homogenized using TissueLyser II (Qiagen, Germantown, MD, USA). The DNP reaction mixture was prepared by adding 35 µg protein for each sample adjusted in 7 µl, 3 µl of 15% SDS and 10 µl of DNP solution. The mixture was kept at room temperature for 15 min, then 7.5 µl of Neutralization buffer was added. The samples were then loaded and run in 10% SDS-PAGE gels. Next, they were transferred to nitrocellulose (Bio-Rad, Hercules, California, USA) and blocked with 5% non-fat milk for 1h. After washing with 1X PBS, the membrane was incubated with the first antibody (1:150) overnight at 4^{o}C and then for 1h with the secondary antibody (1:300) at room temperature. Membranes were incubated with ECL plus detection reagent (Bio-Rad) and scanned using Chemiluminescent scanner (Bio-Rad). Band densities in a given lane were analyzed using ImageJ and added together as previously described [38]. Afterwards, the membranes were incubated with 15% hydrogen peroxide for 30 min at room temperature and treated with actin antibody. OxyBlot values were then normalized to actin for each sample.

Development and fertility assays

Worm development was assessed by first synchronizing animals at the L1 stage and then quantifying developmental stage each day for 3 days. Approximately 100 animals were used for this assay. Developmental stage was scored based on vulva development stage. For the fertility assay, animals at the L4 stage were transferred to fresh seeded plates daily and the number of progenies on each plate counted.

Thrashing assay

Worms were grown on NGM agar plates seeded with each *E. coli* bacterial strain until they reached the L4 stage of development. On days 1, 4, 8 and 12 the rate of animal movement was measured by quantifying their thrashing rate. Individual worms were placed in a 10 ml drop of S-basal on a microscope slide. After one minute of acclimation, the number of bends within 10 seconds were counted for each worm (with a total of 10 worms per experiment) blindly for a total of three biological replicates. One body bend was recorded as one rightward and one leftward body bend. The data was represented as number of thrashes per minute.

Pumping rate

Pharyngeal contractions were recorded for each animal under high magnification using a Zeiss Observer Z1 microscope. Worms were transferred onto a new plate and allowed to acclimate for

a few minutes. Pharyngeal pumping was then counted for 30 seconds for each worm for a total of three biological replicates. The data was represented as pumps per minute.

Vitamin B12 restriction protocol

E. coli OP50 was grown in M9 medium at 37 °C for 3 days. The bacteria were inoculated every 3 days into fresh M9 medium to be used as a food source for *C. elegans [22]*.

To prepare B_{12}-deficient worms, two to three L4 worms from the control plate were transferred onto plates containing B_{12}-deficient M9 medium seeded with B_{12}-deficient *E. coli.* Worms were grown on B_{12}-deficient media for four generations until analysis [22].

Lifespan analysis

All lifespan experiments were performed at 20^{o}C. One hundred animals at the L4 stage were maintained on the *E. coli* strain for the duration of the assay and transferred every 1-2 days until animals no longer produced progeny. Animals were considered dead if they did not respond to touch using the platinum wire. Worms were censored if they escaped the plate or if they ruptured at the uterus. For supplementation of methylcobalamin or adenosylcobalamin, each metabolite was spread over the bacterial lawn to a final concentration of 0.2 µg/ml. Methionine and other amino acids were added to NGM media to a final concentration of 10µM. Doxycycline was added at a concentration of 6 µg/ml. GraphPad Prism version 8 (GraphPad Software, San Diego, California, USA) was used to calculate statistical significance where p-values were generated by the log-rank (Mantel-Cox) test. Statistical analysis was performed as previously described [39]. In order to

achieve sufficient statistical power, three biological replicates were used for each lifespan experiment starting with 100 animals per plate. For each experiment where there were more than two strains, the log-rank test was performed on each strain individually compared to the control strain. Only experiments in which all three biological replicates showed identical statistics were considered. In all cases, p-values <0.05 are considered significant. Each lifespan figure represents one lifespan experiment. All lifespan trials and their statistics are provided in S1 Table.

C. elegans pathogen infection assays

Worms were age-matched at the L4 stage by harvesting eggs using bleach/NaOH treatment of gravid hermaphrodites. Eggs were aliquoted on NGM plates containing *E. coli* (OP50, HT115, HB101, or BW25113) and then 50 L4 worms were transferred to *P. aeruginosa* PA14 infection plates. To prepare infection plates, PA14 was inoculated from a fresh culture plate and grown overnight at 37^{o}C. The following day 15 ml of PA14 overnight culture was spotted onto NGM media plates. Plates were incubated overnight at room temperature and then transferred to 37^{o}C for an overnight incubation and used for the survival assay the following day. Animal deaths were recorded daily every 2 hrs for a 12 hr period each day. Statistical analysis was performed as described for the lifespan assays.

To assess the level of infection, we grew wild-type and *mrpl-2(osa3)* animals on the various *E. coli* diets until the L4 stage at which time animals were transferred to plates containing *P. aeruginosa* expressing RFP. Infection levels were then measured based on the degree of fluorescence emitted in the worm gut lumen.

Determination of vitamin B12 levels

Vitamin B12 levels were obtained using the Vitamin B12 ELISA Kit (Biovision). Around 2000 synchronized worms per biological replicate were grown on *E. coli* OP50 and HT115 plates, washed in S-basal, harvested, and homogenized in lysis buffer. Supernatants were used for determining the vitamin B12 content in samples following manufacturer's instructions.

Determination of methionine levels

Methionine content was determined using the Methionine Fluorescence Assay Kit (Abcam) and each experiment was performed in three biological replicates. Around 500 worms were grown on *E. coli* OP50 and HT115 plates, washed three times in S-basal, and then in 100 µl of Methionine assay buffer. Supernatants were used for determining the methionine content according to the manufacturer's instructions.

RNA sequencing analysis

Trizol extraction method was used to recover total RNA from worms and RNA was purified using Direct-zol RNA Kit (Zymo Research, CA, USA). An Agilent 2100 Bioanalyzer was used to assess RNA integrity. Library construction and sequencing was done by Novogene Inc. (CA, USA). In short, mRNA was enriched using oligo(dT) beads and rRNA removed using the Ribo-Zero kit. mRNA was fragmented, followed by synthesis of first and second strand cDNA synthesis. Then sequencing adapters were ligated and the double-stranded cDNA library completed through size selection and PCR enrichment. The library was sequenced using an Illumina Hiseq 4000 following manufacturer's instructions for paired-end 150-bp reads. The raw data was cleaned by removing

adapter sequences, reads containing poly-N and low-quality reads (Q<30) using Trimmomatic [40]. Tophat v.2.0.9 [41] was used to align clean reads to the *C. elegans* reference genome. The mapped reads from each sample was assembled using Cufflinks v.2.1.1 [41]. HTSeq v.0.6.1 [42] was used to count the number of reads mapped to each gene. In addition, the reads per kilobase million (RPKM) of each gene was calculated based on the length of the gene and the number of reads mapped to it. Differential expression analysis was performed using DESeq2 R package (v.1.10.1) [43]. Relative expression of genes with Benjamini-Hochberg corrected *P*-values (*Padj*)<0.05 were considered to be differentially expressed. Heatmaps were generated with pheatmap in R Studio.

Acknowledments

We would like to thank the *Caenorhabditis* Genetic Center which is funded by the NIH Office of Research Infrastructure (P40 OD010440) for providing some of the worm strains used in this study. Research support was provided by the National Institutes of Health (R35GM128885) and Cancer Prevention & Research Institute of Texas (RR160053) to M.W.P, a CPRIT Scholar in Cancer Research.

References

1. Lionaki E, Gkikas I, Tavernarakis N. Differential Protein Distribution between the Nucleus and Mitochondria: Implications in Aging. Front Genet. 2016;7:162. Epub 2016/10/04. doi: 10.3389/fgene.2016.00162. PubMed PMID: 27695477; PubMed Central PMCID: PMCPMC5025450.

2. Harbauer AB, Zahedi RP, Sickmann A, Pfanner N, Meisinger C. The protein import machinery of mitochondria-a regulatory hub in metabolism, stress, and disease. Cell Metab. 2014;19(3):357-72. Epub 2014/02/25. doi: 10.1016/j.cmet.2014.01.010. PubMed PMID: 24561263.

3. Houtkooper RH, Mouchiroud L, Ryu D, Moullan N, Katsyuba E, Knott G, et al. Mitonuclear protein imbalance as a conserved longevity mechanism. Nature. 2013;497(7450):451-7. Epub 2013/05/24. doi: 10.1038/nature12188. PubMed PMID: 23698443; PubMed Central PMCID: PMCPMC3663447.

4. Mouchiroud L, Houtkooper RH, Moullan N, Katsyuba E, Ryu D, Canto C, et al. The NAD(+)/Sirtuin Pathway Modulates Longevity through Activation of Mitochondrial UPR and FOXO Signaling. Cell. 2013;154(2):430-41. Epub 2013/07/23. doi: 10.1016/j.cell.2013.06.016. PubMed PMID: 23870130; PubMed Central PMCID: PMCPMC3753670.

5. Bennett CF, Vander Wende H, Simko M, Klum S, Barfield S, Choi H, et al. Activation of the mitochondrial unfolded protein response does not predict longevity in Caenorhabditis elegans. Nat Commun. 2014;5:3483. Epub 2014/03/26. doi: 10.1038/ncomms4483. PubMed PMID: 24662282; PubMed Central PMCID: PMCPMC3984390.

6. Shpilka T, Haynes CM. The mitochondrial UPR: mechanisms, physiological functions and implications in ageing. Nat Rev Mol Cell Biol. 2018;19(2):109-20. Epub 2017/11/23. doi: 10.1038/nrm.2017.110. PubMed PMID: 29165426.

7. Qureshi MA, Haynes CM, Pellegrino MW. The mitochondrial unfolded protein response: Signaling from the powerhouse. J Biol Chem. 2017;292(33):13500-6. Epub 2017/07/09. doi: 10.1074/jbc.R117.791061. PubMed PMID: 28687630; PubMed Central PMCID: PMCPMC5566509.

8. Haynes CM, Yang Y, Blais SP, Neubert TA, Ron D. The matrix peptide exporter HAF-1 signals a mitochondrial UPR by activating the transcription factor ZC376.7 in C. elegans. Mol Cell. 2010;37(4):529-40. Epub 2010/03/02. doi: 10.1016/j.molcel.2010.01.015. PubMed PMID: 20188671; PubMed Central PMCID: PMCPMC2846537.

9. Nargund AM, Pellegrino MW, Fiorese CJ, Baker BM, Haynes CM. Mitochondrial import efficiency of ATFS-1 regulates mitochondrial UPR activation. Science. 2012;337(6094):587-90. Epub 2012/06/16. doi: 10.1126/science.1223560. PubMed PMID: 22700657; PubMed Central PMCID: PMCPMC3518298.

10. Sun N, Youle RJ, Finkel T. The Mitochondrial Basis of Aging. Mol Cell. 2016;61(5):654-66. Epub 2016/03/05. doi: 10.1016/j.molcel.2016.01.028. PubMed PMID: 26942670; PubMed Central PMCID: PMCPMC4779179.

11. Durieux J, Wolff S, Dillin A. The cell-non-autonomous nature of electron transport chain-mediated longevity. Cell. 2011;144(1):79-91. Epub 2011/01/11. doi: 10.1016/j.cell.2010.12.016. PubMed PMID: 21215371; PubMed Central PMCID: PMCPMC3062502.

12. Wu Z, Senchuk MM, Dues DJ, Johnson BK, Cooper JF, Lew L, et al. Mitochondrial unfolded protein response transcription factor ATFS-1 promotes longevity in a long-lived

mitochondrial mutant through activation of stress response pathways. BMC Biol. 2018;16(1):147. Epub 2018/12/20. doi: 10.1186/s12915-018-0615-3. PubMed PMID: 30563508; PubMed Central PMCID: PMCPMC6298126.

13. Pellegrino MW, Nargund AM, Kirienko NV, Gillis R, Fiorese CJ, Haynes CM. Mitochondrial UPR-regulated innate immunity provides resistance to pathogen infection. Nature. 2014;516(7531):414-7. Epub 2014/10/03. doi: 10.1038/nature13818. PubMed PMID: 25274306; PubMed Central PMCID: PMCPMC4270954.

14. Jeong DE, Lee D, Hwang SY, Lee Y, Lee JE, Seo M, et al. Mitochondrial chaperone HSP-60 regulates anti-bacterial immunity via p38 MAP kinase signaling. EMBO J. 2017;36(8):1046-65. Epub 2017/03/12. doi: 10.15252/embj.201694781. PubMed PMID: 28283579; PubMed Central PMCID: PMCPMC5391144.

15. Gao K, Li Y, Hu S, Liu Y. SUMO peptidase ULP-4 regulates mitochondrial UPR-mediated innate immunity and lifespan extension. Elife. 2019;8. Epub 2019/01/16. doi: 10.7554/eLife.41792. PubMed PMID: 30642431; PubMed Central PMCID: PMCPMC6355198.

16. Hwang AB, Ryu EA, Artan M, Chang HW, Kabir MH, Nam HJ, et al. Feedback regulation via AMPK and HIF-1 mediates ROS-dependent longevity in Caenorhabditis elegans. Proc Natl Acad Sci U S A. 2014;111(42):E4458-67. Epub 2014/10/08. doi: 10.1073/pnas.1411199111. PubMed PMID: 25288734; PubMed Central PMCID: PMCPMC4210294.

17. Yoneda T, Benedetti C, Urano F, Clark SG, Harding HP, Ron D. Compartment-specific perturbation of protein handling activates genes encoding mitochondrial chaperones. J Cell Sci. 2004;117(Pt 18):4055-66. Epub 2004/07/29. doi: 10.1242/jcs.01275. PubMed PMID: 15280428.

18. Tian Y, Garcia G, Bian Q, Steffen KK, Joe L, Wolff S, et al. Mitochondrial Stress Induces Chromatin Reorganization to Promote Longevity and UPR(mt). Cell. 2016;165(5):1197-208.

Epub 2016/05/03. doi: 10.1016/j.cell.2016.04.011. PubMed PMID: 27133166; PubMed Central PMCID: PMCPMC4889216.

19. Klass MR. Aging in the nematode Caenorhabditis elegans: major biological and environmental factors influencing life span. Mech Ageing Dev. 1977;6(6):413-29. Epub 1977/11/01. PubMed PMID: 926867.

20. Revtovich AV, Lee R, Kirienko NV. Interplay between mitochondria and diet mediates pathogen and stress resistance in Caenorhabditis elegans. PLoS Genet. 2019;15(3):e1008011. Epub 2019/03/14. doi: 10.1371/journal.pgen.1008011. PubMed PMID: 30865620; PubMed Central PMCID: PMCPMC6415812.

21. Watson E, MacNeil LT, Ritter AD, Yilmaz LS, Rosebrock AP, Caudy AA, et al. Interspecies Systems Biology Uncovers Metabolites Affecting C. elegans Gene Expression and Life History Traits. Cell. 2014;156(6):1336-7. Epub 2014/03/13. doi: 10.1016/j.cell.2014.02.036. PubMed PMID: 28898637.

22. Bito T, Matsunaga Y, Yabuta Y, Kawano T, Watanabe F. Vitamin B12 deficiency in Caenorhabditis elegans results in loss of fertility, extended life cycle, and reduced lifespan. FEBS Open Bio. 2013;3:112-7. Epub 2013/06/19. doi: 10.1016/j.fob.2013.01.008. PubMed PMID: 23772381; PubMed Central PMCID: PMCPMC3668511.

23. Cabreiro F, Au C, Leung KY, Vergara-Irigaray N, Cocheme HM, Noori T, et al. Metformin retards aging in C. elegans by altering microbial folate and methionine metabolism. Cell. 2013;153(1):228-39. Epub 2013/04/02. doi: 10.1016/j.cell.2013.02.035. PubMed PMID: 23540700; PubMed Central PMCID: PMCPMC3898468.

24. Fontana L, Partridge L. Promoting health and longevity through diet: from model organisms to humans. Cell. 2015;161(1):106-18. Epub 2015/03/31. doi:

10.1016/j.cell.2015.02.020. PubMed PMID: 25815989; PubMed Central PMCID: PMCPMC4547605.

25. Kapahi P, Kaeberlein M, Hansen M. Dietary restriction and lifespan: Lessons from invertebrate models. Ageing Res Rev. 2017;39:3-14. Epub 2016/12/23. doi: 10.1016/j.arr.2016.12.005. PubMed PMID: 28007498; PubMed Central PMCID: PMCPMC5476520.

26. Fontana L, Partridge L, Longo VD. Extending healthy life span--from yeast to humans. Science. 2010;328(5976):321-6. Epub 2010/04/17. doi: 10.1126/science.1172539. PubMed PMID: 20395504; PubMed Central PMCID: PMCPMC3607354.

27. Pang S, Curran SP. Adaptive capacity to bacterial diet modulates aging in C. elegans. Cell Metab. 2014;19(2):221-31. Epub 2014/01/21. doi: 10.1016/j.cmet.2013.12.005. PubMed PMID: 24440036; PubMed Central PMCID: PMCPMC3979424.

28. Soukas AA, Kane EA, Carr CE, Melo JA, Ruvkun G. Rictor/TORC2 regulates fat metabolism, feeding, growth, and life span in Caenorhabditis elegans. Genes Dev. 2009;23(4):496-511. Epub 2009/02/26. doi: 10.1101/gad.1775409. PubMed PMID: 19240135; PubMed Central PMCID: PMCPMC2648650.

29. Verma S, Jagtap U, Goyala A, Mukhopadhyay A. A novel gene-diet pair modulates C. elegans aging. PLoS Genet. 2018;14(8):e1007608. Epub 2018/08/21. doi: 10.1371/journal.pgen.1007608. PubMed PMID: 30125273; PubMed Central PMCID: PMCPMC6117094.

30. Kirienko NV, Kirienko DR, Larkins-Ford J, Wahlby C, Ruvkun G, Ausubel FM. Pseudomonas aeruginosa disrupts Caenorhabditis elegans iron homeostasis, causing a hypoxic response and death. Cell Host Microbe. 2013;13(4):406-16. Epub 2013/04/23. doi:

10.1016/j.chom.2013.03.003. PubMed PMID: 23601103; PubMed Central PMCID: PMCPMC3641844.

31. Tan MW, Mahajan-Miklos S, Ausubel FM. Killing of Caenorhabditis elegans by Pseudomonas aeruginosa used to model mammalian bacterial pathogenesis. Proc Natl Acad Sci U S A. 1999;96(2):715-20. Epub 1999/01/20. doi: 10.1073/pnas.96.2.715. PubMed PMID: 9892699; PubMed Central PMCID: PMCPMC15202.

32. Lee BC, Kaya A, Gladyshev VN. Methionine restriction and life-span control. Ann N Y Acad Sci. 2016;1363:116-24. Epub 2015/12/15. doi: 10.1111/nyas.12973. PubMed PMID: 26663138; PubMed Central PMCID: PMCPMC5008916.

33. Bennett CF, Kwon JJ, Chen C, Russell J, Acosta K, Burnaevskiy N, et al. Transaldolase inhibition impairs mitochondrial respiration and induces a starvation-like longevity response in Caenorhabditis elegans. PLoS Genet. 2017;13(3):e1006695. Epub 2017/03/30. doi: 10.1371/journal.pgen.1006695. PubMed PMID: 28355222; PubMed Central PMCID: PMCPMC5389855.

34. Yuan J, Chang SY, Yin SG, Liu ZY, Cheng X, Liu XJ, et al. Two conserved epigenetic regulators prevent healthy ageing. Nature. 2020;579(7797):118-22. Epub 2020/02/28. doi: 10.1038/s41586-020-2037-y. PubMed PMID: 32103178.

35. Runkel ED, Liu S, Baumeister R, Schulze E. Surveillance-activated defenses block the ROS-induced mitochondrial unfolded protein response. PLoS Genet. 2013;9(3):e1003346. Epub 2013/03/22. doi: 10.1371/journal.pgen.1003346. PubMed PMID: 23516373; PubMed Central PMCID: PMCPMC3597513.

36. Brenner S. The genetics of Caenorhabditis elegans. Genetics. 1974;77(1):71-94. Epub 1974/05/01. PubMed PMID: 4366476; PubMed Central PMCID: PMCPMC1213120.

37. Kadandale P, Chatterjee I, Singson A. Germline transformation of Caenorhabditis elegans by injection. Methods Mol Biol. 2009;518:123-33. Epub 2008/12/17. doi: 10.1007/978-1-59745-202-1_10. PubMed PMID: 19085141; PubMed Central PMCID: PMCPMC2796118.

38. Yang W, Li J, Hekimi S. A Measurable increase in oxidative damage due to reduction in superoxide detoxification fails to shorten the life span of long-lived mitochondrial mutants of Caenorhabditis elegans. Genetics. 2007;177(4):2063-74. Epub 2007/12/13. doi: 10.1534/genetics.107.080788. PubMed PMID: 18073424; PubMed Central PMCID: PMCPMC2219504.

39. Petrascheck M, Miller DL. Computational Analysis of Lifespan Experiment Reproducibility. Front Genet. 2017;8:92. Epub 2017/07/18. doi: 10.3389/fgene.2017.00092. PubMed PMID: 28713422; PubMed Central PMCID: PMCPMC5492194.

40. Bolger AM, Lohse M, Usadel B. Trimmomatic: a flexible trimmer for Illumina sequence data. Bioinformatics. 2014;30(15):2114-20. Epub 2014/04/04. doi: 10.1093/bioinformatics/btu170. PubMed PMID: 24695404; PubMed Central PMCID: PMCPMC4103590.

41. Trapnell C, Roberts A, Goff L, Pertea G, Kim D, Kelley DR, et al. Differential gene and transcript expression analysis of RNA-seq experiments with TopHat and Cufflinks. Nat Protoc. 2012;7(3):562-78. Epub 2012/03/03. doi: 10.1038/nprot.2012.016. PubMed PMID: 22383036; PubMed Central PMCID: PMCPMC3334321.

42. Anders S, Pyl PT, Huber W. HTSeq--a Python framework to work with high-throughput sequencing data. Bioinformatics. 2015;31(2):166-9. Epub 2014/09/28. doi: 10.1093/bioinformatics/btu638. PubMed PMID: 25260700; PubMed Central PMCID: PMCPMC4287950.

43. Love MI, Huber W, Anders S. Moderated estimation of fold change and dispersion for RNA-seq data with DESeq2. Genome Biol. 2014;15(12):550. Epub 2014/12/18. doi: 10.1186/s13059-014-0550-8. PubMed PMID: 25516281; PubMed Central PMCID: PMCPMC4302049.

Figure Legends

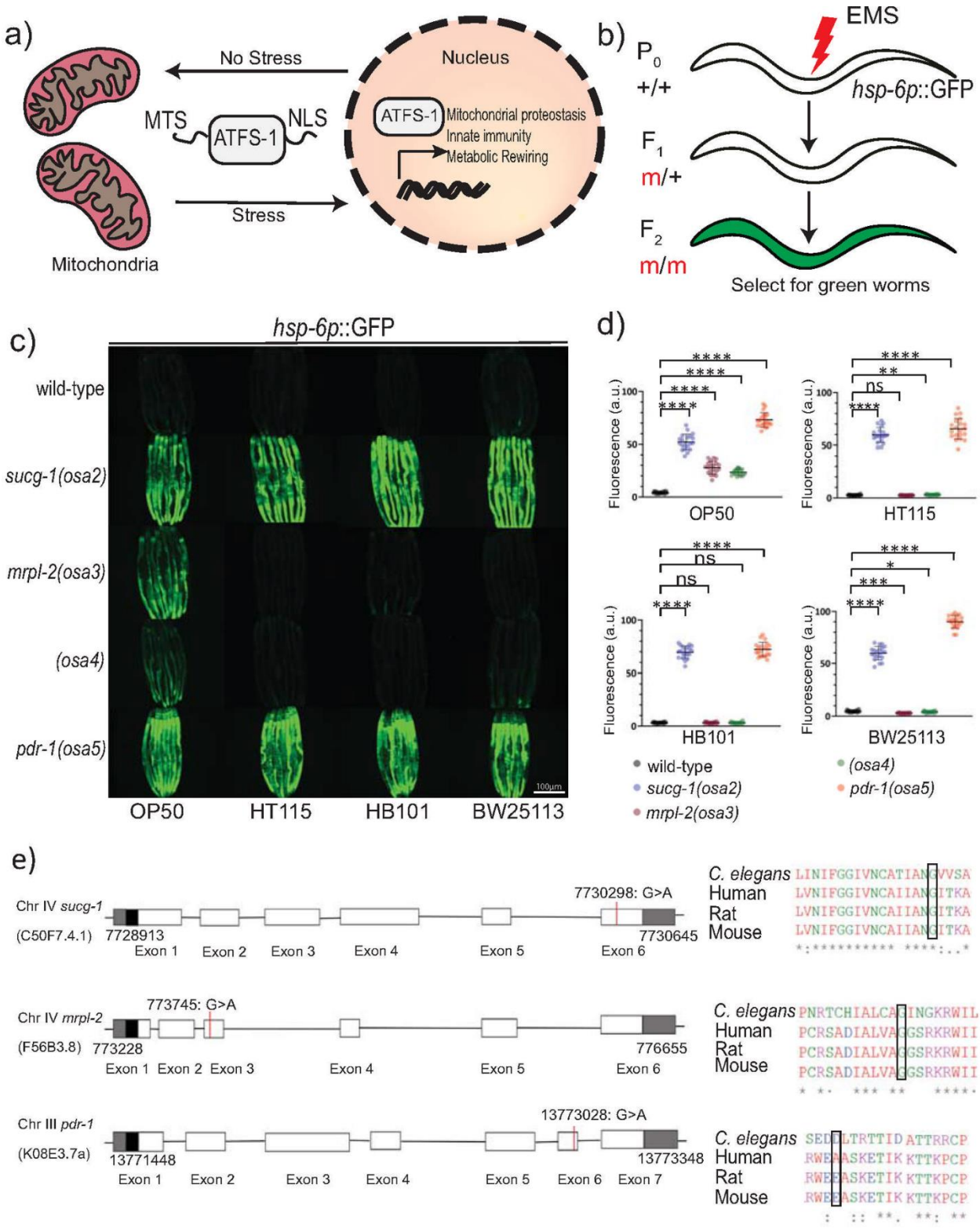

Figure 1. Isolation of novel alleles that activate the UPR^{mt} in diet-dependent and –independent manners.

(A) Schematic of the UPR^{mt} response.

(B) Schematic illustrating the strategy used to isolate mutants that activate the UPR^{mt} using forward genetics.

(C, D) Photomicrographs and quantification of *hsp-6p*::GFP expression for the four isolated mutants fed different diets of *E. coli*. The alleles were named *osa2*, *osa3*, *osa4* and *osa5*. Quantification of fluorescence intensities expressed as arbitrary units (A.U.); (mean $\pm$SD; $n \geq 20$ worms); ns denotes not significant, * denotes $p<0.05$, ** denotes $p \leq 0.01$, *** denotes $p \leq 0.001$, **** denotes $p \leq 0.0001$ (Student's *t* test).

(E) Schematics of gene structure and protein alignment of *sucg-1(osa2)*, *mrpl-2(osa3)*, and *pdr-1(osa5)* with the indicated mutations and amino acid changes.

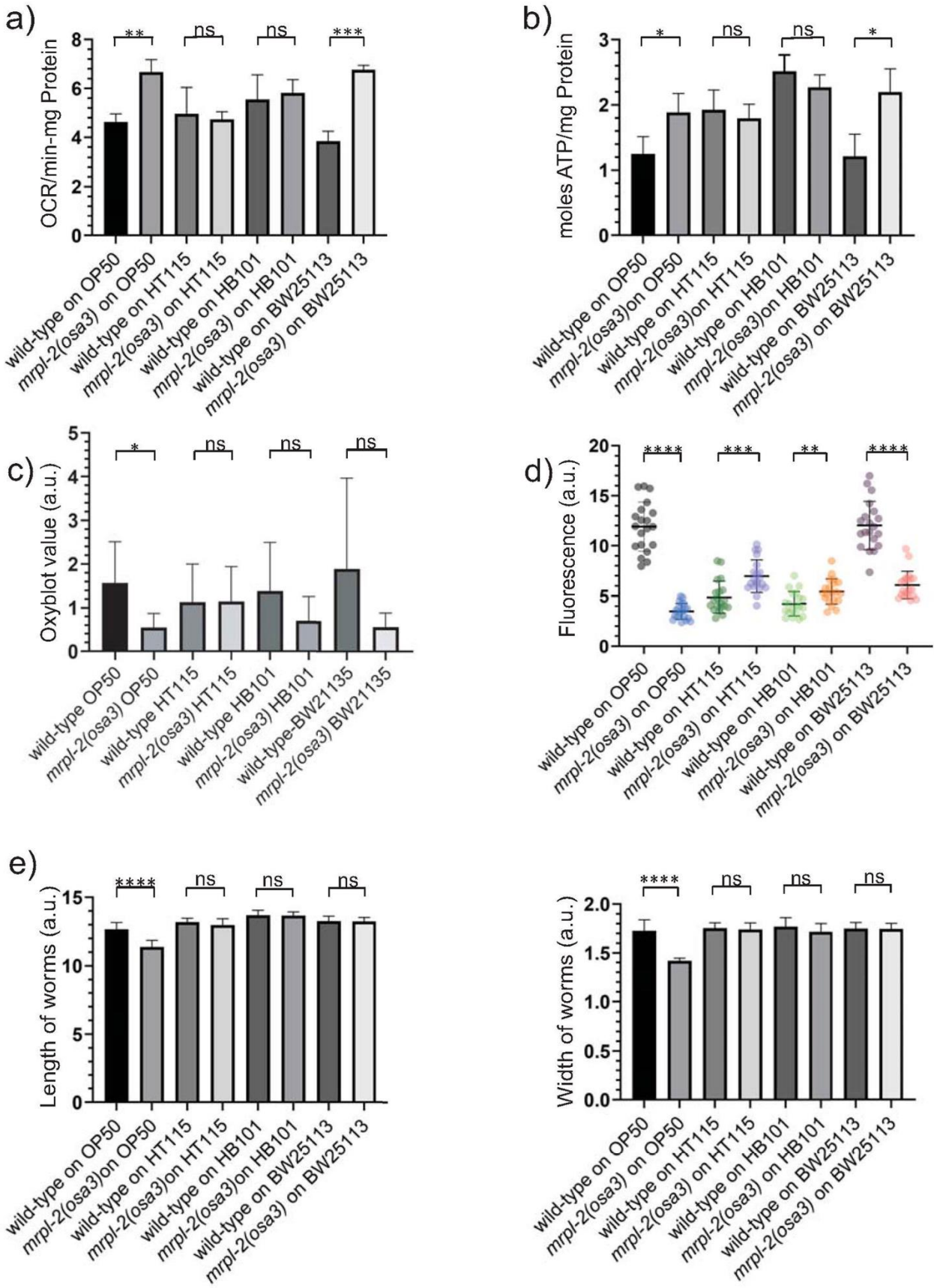
a)
OCR/min-mg Protein
**
ns
ns
***
wild-type on OP50
mrpl-2(osa3) on OP50
wild-type on HT115
mrpl-2(osa3) on HT115
wild-type on HB101
mrpl-2(osa3) on HB101
wild-type on BW25113
mrpl-2(osa3) on BW25113
b)
moles ATP/mg Protein
*
ns
ns
*
c)
Oxyblot value (a.u.)
*
ns
ns
ns
wild-type OP50
mrpl-2(osa3) OP50
wild-type HT115
mrpl-2(osa3) HT115
wild-type HB101
mrpl-2(osa3) HB101
wild-type-BW21135
mrpl-2(osa3) BW21135
d)
Fluorescence (a.u.)
****
***
**
****
e)
Length of worms (a.u.)
****
ns
ns
ns
Width of worms (a.u.)
****
ns
ns
ns

Figure 2. Mitochondrial function is altered in *mrpl-2(osa3)* animals in a diet-dependent manner.

(A) Oxygen consumption rate determination for wild-type and *mrpl-2(osa3)* animals fed *E. coli* OP50, HT115, HB101, and BW25113. Oxygen consumption was normalized to total protein content (mean ±SD; $n = 3$); ns denotes not significant, ** denotes $p \leq 0.01$, *** denotes $p \leq 0.001$ (Student's *t* test).

(B) ATP production quantification for wild-type and *mrpl-2(osa3)* animals fed *E. coli* OP50, HT115, HB101, and BW25113. ATP levels are normalized to total protein content (mean ±SD; $n = 3$); ns denotes not significant, * denotes $p \leq 0.05$ (Student's *t* test).

(C) Oxidative protein modification determination using the OxyBlot assay. OxyBlot values were normalized to actin for each sample and represented as arbitrary units (A.U.). (mean ± SD; n=5); ns denotes not significant, * denotes $p \leq 0.05$ (Student's *t* test).

(D) Mitochondrial membrane potential determination using TMRE and quantification for wild-type and *mrpl-2(osa3)* animals fed *E. coli* OP50, HT115, HB101, and BW25113 reflected as arbitrary units (A.U.). (mean ±SD; $n \geq 20$ worms); ** denotes $p \leq 0.01$, *** denotes $p \leq 0.001$, **** denotes $p \leq 0.0001$ (Student's *t* test).

(E) Animal size quantification of wild-type and *mrpl-2(osa3)* animals fed *E. coli* OP50, HT115, HB101, and BW25113. Animal size is expressed as the length and width of each animal and represented as arbitrary units (A.U.); (mean ±SD; $n \geq 20$ worms); ns denotes not significant, **** denotes $p \leq 0.0001$ (Student's *t* test).

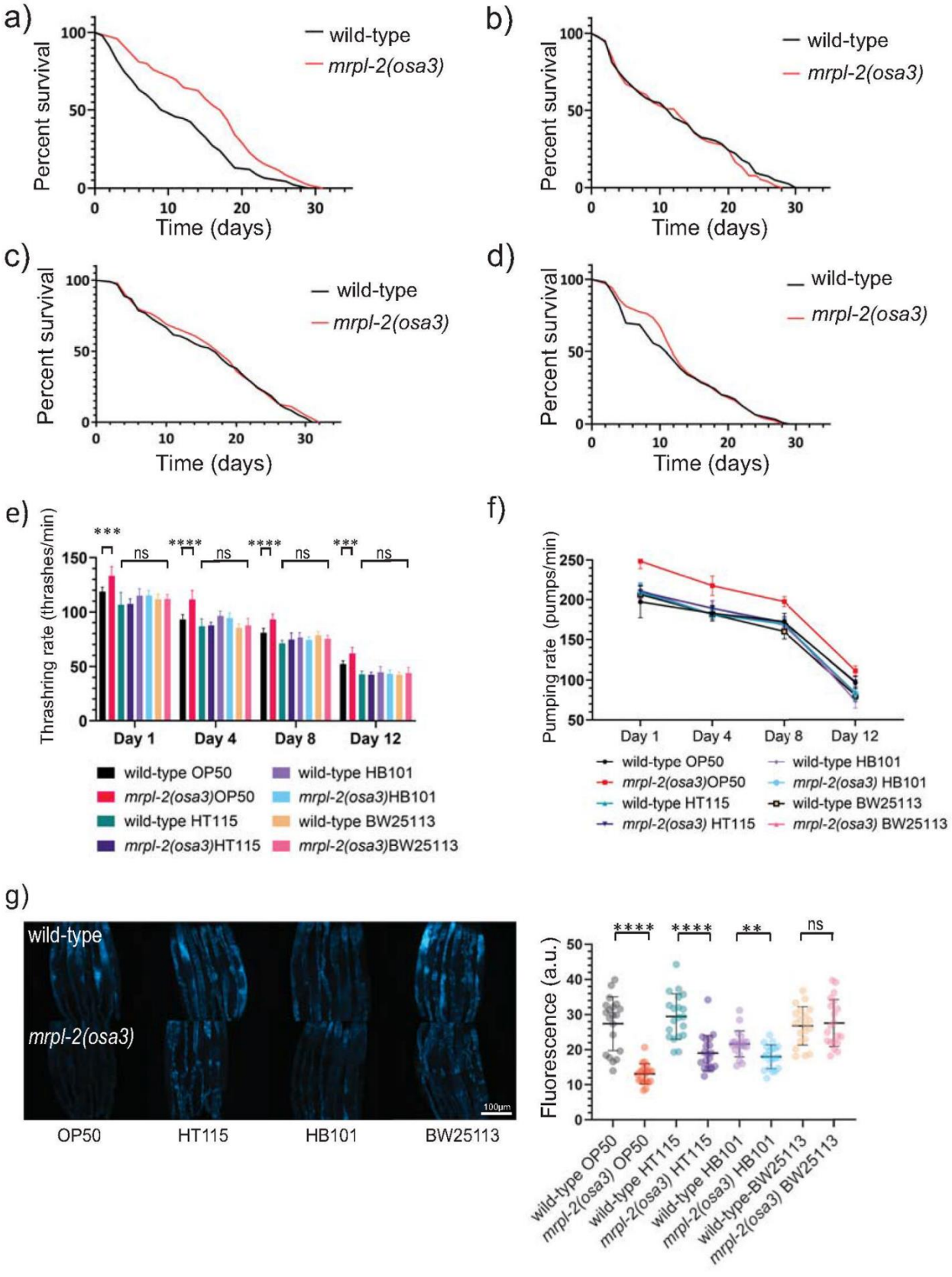
a)
Percent survival
Time (days)
wild-type
mrpl-2(osa3)
b)
Percent survival
Time (days)
wild-type
mrpl-2(osa3)
c)
Percent survival
Time (days)
wild-type
mrpl-2(osa3)
d)
Percent survival
Time (days)
wild-type
mrpl-2(osa3)
e)
Thrashring rate (thrashes/min)
***
ns
****
ns
****
ns
***
ns
Day 1
Day 4
Day 8
Day 12
wild-type OP50
mrpl-2(osa3)OP50
wild-type HT115
mrpl-2(osa3)HT115
wild-type HB101
mrpl-2(osa3)HB101
wild-type BW25113
mrpl-2(osa3)BW25113
f)
Pumping rate (pumps/min)
Day 1
Day 4
Day 8
Day 12
wild-type OP50
mrpl-2(osa3)OP50
wild-type HT115
mrpl-2(osa3) HT115
wild-type HB101
mrpl-2(osa3) HB101
wild-type BW25113
mrpl-2(osa3) BW25113
g)
wild-type
mrpl-2(osa3)
100µm
OP50
HT115
HB101
BW25113
Fluorescence (a.u.)
****
****
**
ns
wild-type OP50
mrpl-2(osa3) OP50
wild-type HT115
mrpl-2(osa3) HT115
wild-type HB101
mrpl-2(osa3) HB101
wild-type-BW25113
mrpl-2(osa3) BW25113

Figure 3. Diet-type determines lifespan in *mrpl-2(osa3)* animals.

(A-D) Lifespans of wild-type and *mrpl-2(osa3)* animals fed *E. coli* (A) OP50, (B) HT115, (C) HB101, and (D) BW25113. See S1 Table for all lifespan assay statistics.

(E) Whole body thrashing rate quantification of wild-type and *mrpl-2(osa3)* animals fed *E. coli* OP50, HT115, HB101, and BW25113. (mean $\pm$SD; $n \geq 10$ worms); ns denotes not significant, *** denotes $p \leq 0.001$, **** denotes $p \leq 0.0001$ (Student's *t* test).

(F) Pharyngeal pumping rate quantification of wild-type and *mrpl-2(osa3)* animals fed *E. coli* OP50, HT115, HB101, and BW25113 (mean $\pm$SD; $n \geq 10$ worms).

(G) Photomicrographs and quantification of gut autofluorescence in wild-type and *mrpl-2(osa3)* animals. Quantification of fluorescence intensities expressed as arbitrary units (A.U.); ns denotes not significant, ** denotes $p \leq 0.01$, **** denotes $p \leq 0.0001$ (Student's *t* test).

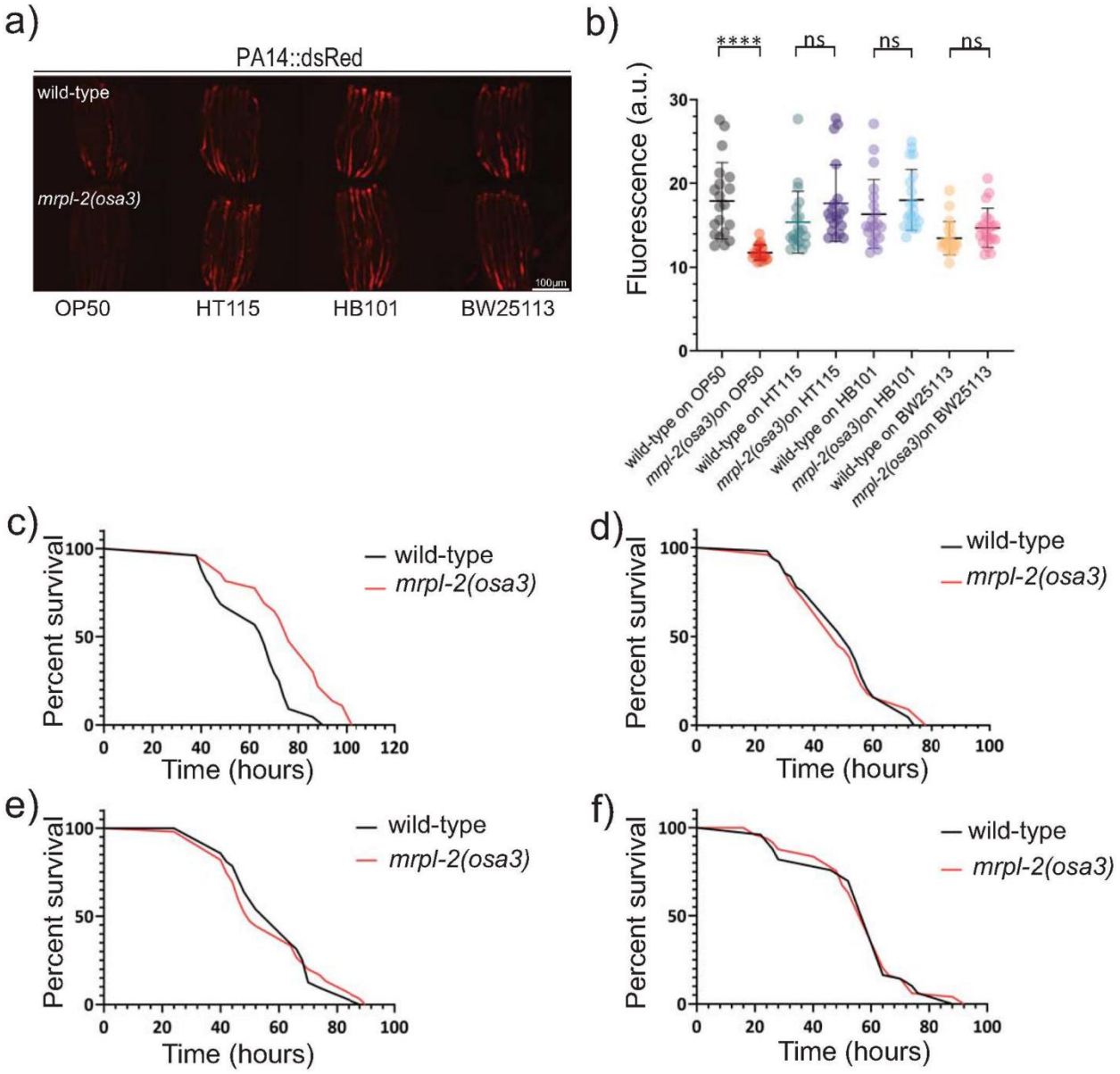

Figure 4. *mrpl-2(osa3)* animals survive longer during infection depending on their prior diet.

(A, B) Photomicrographs and quantification of *P. aeruginosa* PA14-dsRed expression of infected wild-type or *mrpl-2(osa3)* animals previously fed different diets of *E. coli.* Quantification of fluorescence intensities expressed as arbitrary units (A.U.); (mean ±SD; $n \geq 20$ worms); ns denotes not significant, **** denotes $p \leq 0.0001$ (Student's *t* test).

(C-F) Survival analysis of wild-type and *mrpl-2(osa3)* animals infected with *P. aeruginosa*. *E. coli* diets prior to *P. aeruginosa* infection are (C) OP50, (D) HT115, (E) HB101, and (F) BW25113. See S1 Table for all survival assay statistics.

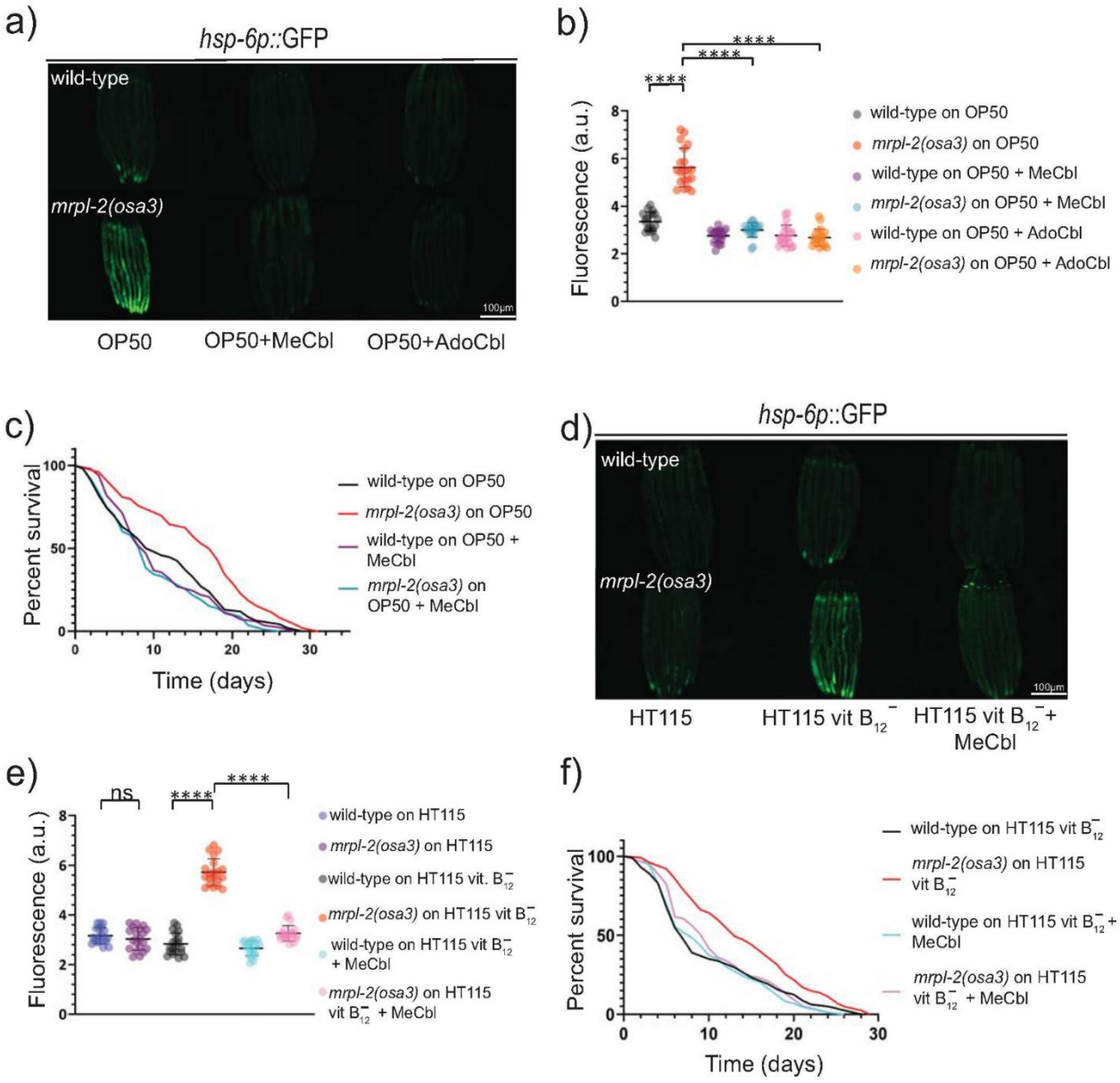

Figure 5. Vitamin B12 levels determine the activation of the UPR^{mt} in *mrpl-2(osa3)* animals under different diets.

(A, B) Photomicrographs and quantification of *hsp-6p*::GFP expression in wild-type and *mrpl-2(osa3)* animals fed *E. coli* OP50 in the presence or absence of 0.2 µg/ml methylcobalamin or adenosylcobalamin. Quantification of fluorescence intensities expressed as arbitrary units (A.U.); (mean ±SD; $n \geq 20$ worms); **** denotes $p \leq 0.0001$ (Student's *t* test).

(C) Lifespans of wild-type and *mrpl-2(osa3)* animals fed *E. coli* OP50 in the presence or absence of 0.2 µg/ml methylcobalamin.

(D, E) Photomicrographs and quantification of *hsp-6p*::GFP expression in wild-type and *mrpl-2(osa3)* animals fed vitamin B12-restricted *E. coli* HT115 in the presence or absence of 0.2 µg/ml methylcobalamin. Quantification of fluorescence intensities expressed as arbitrary units (A.U.); (mean $\pm$SD; $n \geq 20$); ns denotes not significant, **** denotes $p \leq 0.0001$ (Student's *t* test).

(F) Lifespans of wild-type and *mrpl-2(osa3)* animals fed vitamin B12-restricted *E. coli* HT115 in the presence or absence of 0.2 µg/ml methylcobalamin.

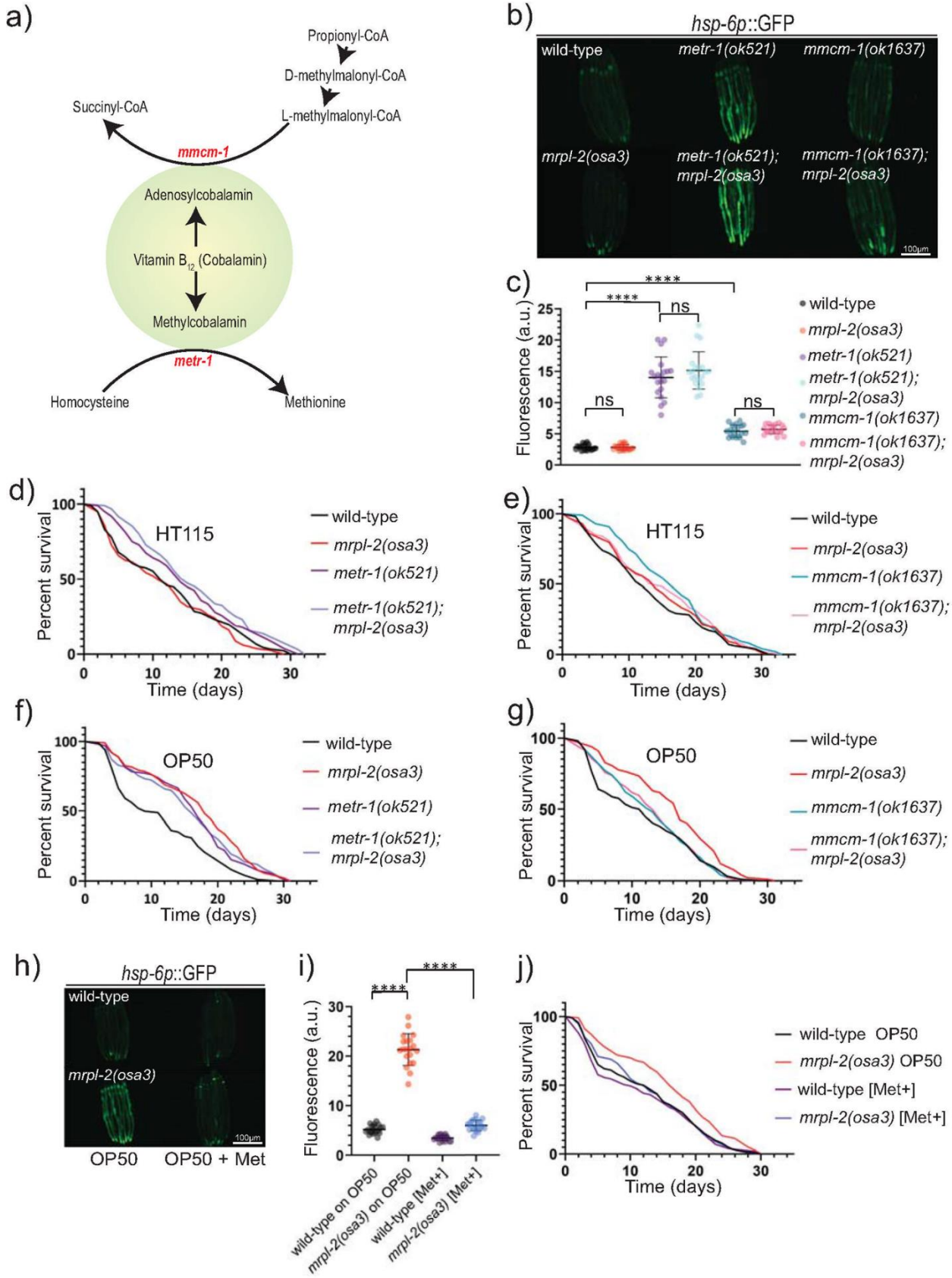
a)
Propionyl-CoA
D-methylmalonyl-CoA
L-methylmalonyl-CoA
Succinyl-CoA
mmcm-1
Adenosylcobalamin
Vitamin B12 (Cobalamin)
Methylcobalamin
metr-1
Homocysteine
Methionine
b)
hsp-6p::GFP
wild-type
metr-1(ok521)
mmcm-1(ok1637)
mrpl-2(osa3)
metr-1(ok521); mrpl-2(osa3)
mmcm-1(ok1637); mrpl-2(osa3)
100µm
c)
Fluorescence (a.u.)
****
****
ns
ns
ns
wild-type
mrpl-2(osa3)
metr-1(ok521)
metr-1(ok521); mrpl-2(osa3)
mmcm-1(ok1637)
mmcm-1(ok1637); mrpl-2(osa3)
d)
HT115
Percent survival
Time (days)
wild-type
mrpl-2(osa3)
metr-1(ok521)
metr-1(ok521); mrpl-2(osa3)
e)
HT115
Percent survival
Time (days)
wild-type
mrpl-2(osa3)
mmcm-1(ok1637)
mmcm-1(ok1637); mrpl-2(osa3)
f)
OP50
Percent survival
Time (days)
wild-type
mrpl-2(osa3)
metr-1(ok521)
metr-1(ok521); mrpl-2(osa3)
g)
OP50
Percent survival
Time (days)
wild-type
mrpl-2(osa3)
mmcm-1(ok1637)
mmcm-1(ok1637); mrpl-2(osa3)
h)
hsp-6p::GFP
wild-type
mrpl-2(osa3)
100µm
OP50
OP50 + Met
i)
Fluorescence (a.u.)
****
****
wild-type on OP50
mrpl-2(osa3) on OP50
wild-type [Met+]
mrpl-2(osa3) [Met+]
j)
Percent survival
Time (days)
wild-type OP50
mrpl-2(osa3) OP50
wild-type [Met+]
mrpl-2(osa3) [Met+]

Figure 6. Methionine supplementation suppresses UPR^{mt} activation in *mrpl-2(osa3)* animals fed a vitamin B12 deficient diet.

(A) Schematic illustration of vitamin B12-dependent metabolic pathways.

(B, C) Photomicrographs and quantification of *hsp-6p*::GFP expression of wild-type, *mrpl-2(osa3)*, *metr-1(ok521)*, *mmcm-1(ok1637)*, *metr-1(ok521); mrpl-2(osa3)*, and *mmcm-1(ok1637); mrpl-2(osa3)* fed an *E. coli* HT115 diet. Quantification of fluorescence intensities expressed as arbitrary units (A.U.); (mean $\pm$SD; $n \geq 20$); ns denotes not significant , **** denotes $p \leq 0.0001$ (Student's *t* test).

(D) Lifespans of wild-type, *mrpl-2(osa3)*, *metr-1(ok521)*, *metr-1(ok521); mrpl-2(osa3)* fed an *E. coli* HT115 diet.

(E) Lifespans of wild-type, *mrpl-2(osa3)*, *mmcm-1(ok1637)*, *mmcm-1(ok1637); mrpl-2(osa3)* fed an *E. coli* HT115 diet.

(F) Lifespans of wild-type, *mrpl-2(osa3)*, *metr-1(ok521)*, *metr-1(ok521); mrpl-2(osa3)* fed an *E. coli* OP50 diet.

(G) Lifespans of wild-type, *mrpl-2(osa3)*, *mmcm-1(ok1637)*, *mmcm-1(ok1637); mrpl-2(osa3)* fed an *E. coli* OP50 diet.

(H, I) Photomicrographs and quantification of *hsp-6p*::GFP expression of wild-type and *mrpl-2(osa3)* fed an *E. coli* OP50 diet in the presence or absence of 10 mM methionine. Quantification of fluorescence intensities expressed as arbitrary units (A.U.); (mean $\pm$SD; $n \geq 20$); **** denotes $p \leq 0.0001$ (Student's *t* test).

(J) Lifespans of wild-type and *mrpl-2(osa3)* fed an *E. coli* OP50 diet in the presence or absence of 10 mM methionine.

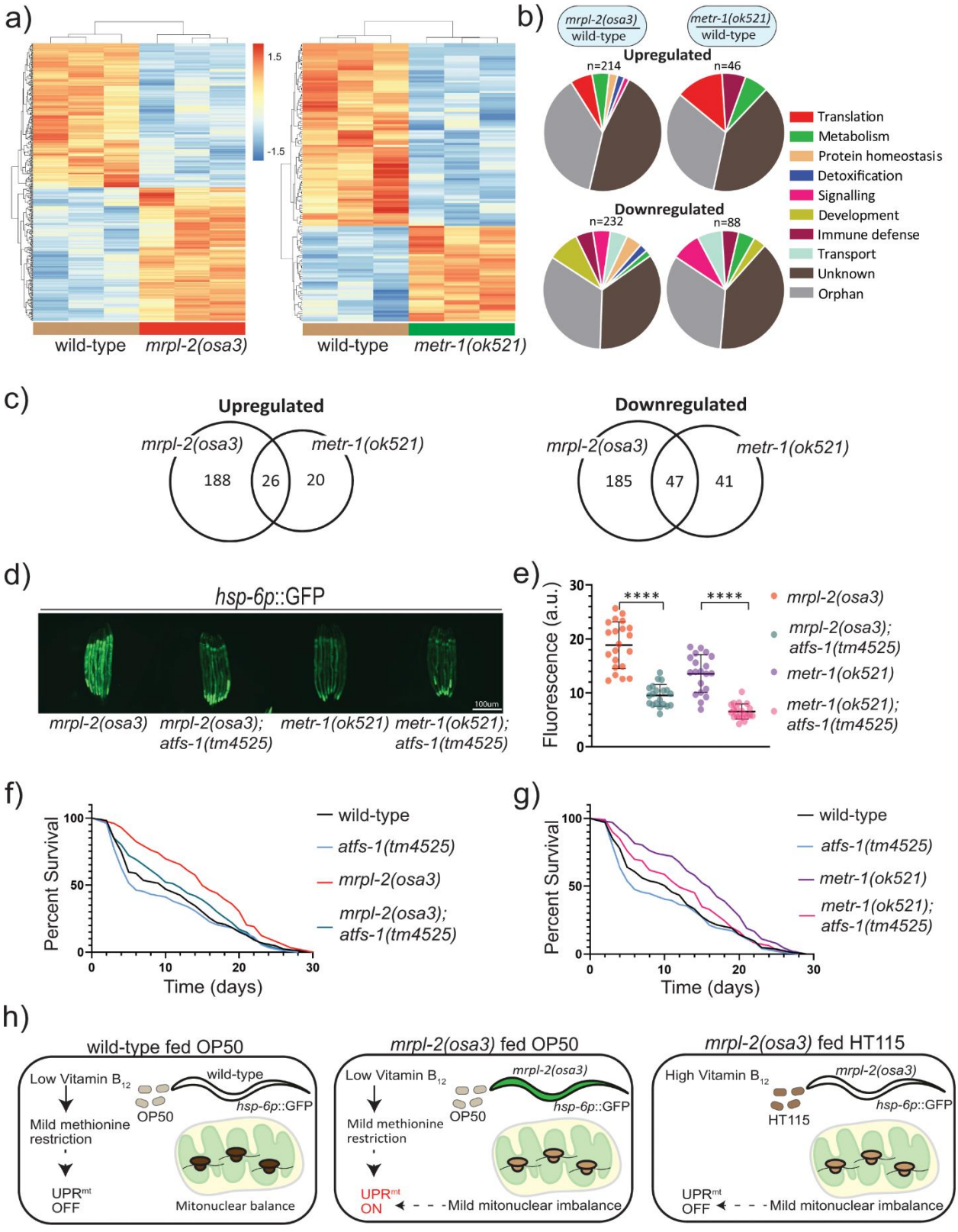
a)
1.5
-1.5
wild-type
mrpl-2(osa3)
wild-type
metr-1(ok521)
b)
mrpl-2(osa3) / wild-type
metr-1(ok521) / wild-type
Upregulated
n=214
n=46
Downregulated
n=232
n=88
Translation
Metabolism
Protein homeostasis
Detoxification
Signalling
Development
Immune defense
Transport
Unknown
Orphan
c)
Upregulated
mrpl-2(osa3)
metr-1(ok521)
188
26
20
Downregulated
mrpl-2(osa3)
metr-1(ok521)
185
47
41
d)
hsp-6p::GFP
100um
mrpl-2(osa3)
mrpl-2(osa3); atfs-1(tm4525)
metr-1(ok521)
metr-1(ok521); atfs-1(tm4525)
e)
Fluorescence (a.u.)
****
****
mrpl-2(osa3)
mrpl-2(osa3); atfs-1(tm4525)
metr-1(ok521)
metr-1(ok521); atfs-1(tm4525)
f)
Percent Survival
Time (days)
wild-type
atfs-1(tm4525)
mrpl-2(osa3)
mrpl-2(osa3); atfs-1(tm4525)
g)
Percent Survival
Time (days)
wild-type
atfs-1(tm4525)
metr-1(ok521)
metr-1(ok521); atfs-1(tm4525)
h)
wild-type fed OP50
Low Vitamin B12
Mild methionine restriction
UPRmt OFF
OP50
wild-type
hsp-6p::GFP
Mitonuclear balance
mrpl-2(osa3) fed OP50
Low Vitamin B12
Mild methionine restriction
UPRmt ON
OP50
mrpl-2(osa3)
hsp-6p::GFP
Mild mitonuclear imbalance
mrpl-2(osa3) fed HT115
High Vitamin B12
HT115
mrpl-2(osa3)
hsp-6p::GFP
UPRmt OFF
Mild mitonuclear imbalance

Figure 7. ATFS-1/ UPR^{mt} mediate the lifespan extension of mitonuclear imbalance and methionine restriction.

(A) Heat maps representing gene expression changes in wild-type, *mrpl-2(osa3)*, and *metr-1(ok521)* fed an *E. coli* OP50 diet. Genes were considered as differentially expressed if there was a significance difference of $p \leq 0.05$ (after Benjamini-Hochberg correction).

(B) Functional categories of differentially expressed genes.

(C) Venn diagram of differentially expressed genes shared between *mrpl-2(osa3)* and *metr-1(ok521).*

(D, E) Photomicrographs and quantification of *hsp-6p*::GFP expression for *mrpl-2(osa3)*, *mrpl-2(osa3)*; *atfs-1(tm4525), metr-1(ok521), and metr-1(ok521); atfs-1(tm4525)* fed a diet of *E. coli* OP50. Quantification of fluorescence intensities expressed as arbitrary units (A.U.); (mean ±SD; $n \geq 20$); **** denotes $p \leq 0.0001$ (Student's *t* test).

(F) Lifespans of wild-type, *mrpl-2(osa3), atfs-1(tm4525),* and *mrpl-2(osa3)*; *atfs-1(tm4525)* fed a diet of *E. coli* OP50.

(G) Lifespans of wild-type, *metr-1(ok521), atfs-1(tm4525),* and *metr-1(ok521)*; *atfs-1(tm4525)* fed a diet of *E. coli* OP50.

(H) Model. Wild-type animals fed a diet of *E. coli* OP50 experience a mild vitamin B12 restriction which reduces methionine synthase activity resulting in a subtle methionine restriction that is insufficient to activate the UPR^{mt}. However, the UPR^{mt} is activated in combination with the mild mitonuclear imbalance of the *mrpl-2(osa3)* reduction of function mutant which results in extended lifespan. In contrast, methionine supply is higher when fed a vitamin B12 replete diet of *E. coli*

HT115, and therefore the mild mitonuclear imbalance of *mrpl-2(osa3)* mutant alone is incapable of inducing the UPR^{mt} in this scenario resulting in animals that display normal aging rates.

SUPPLEMENTARY FIGURES

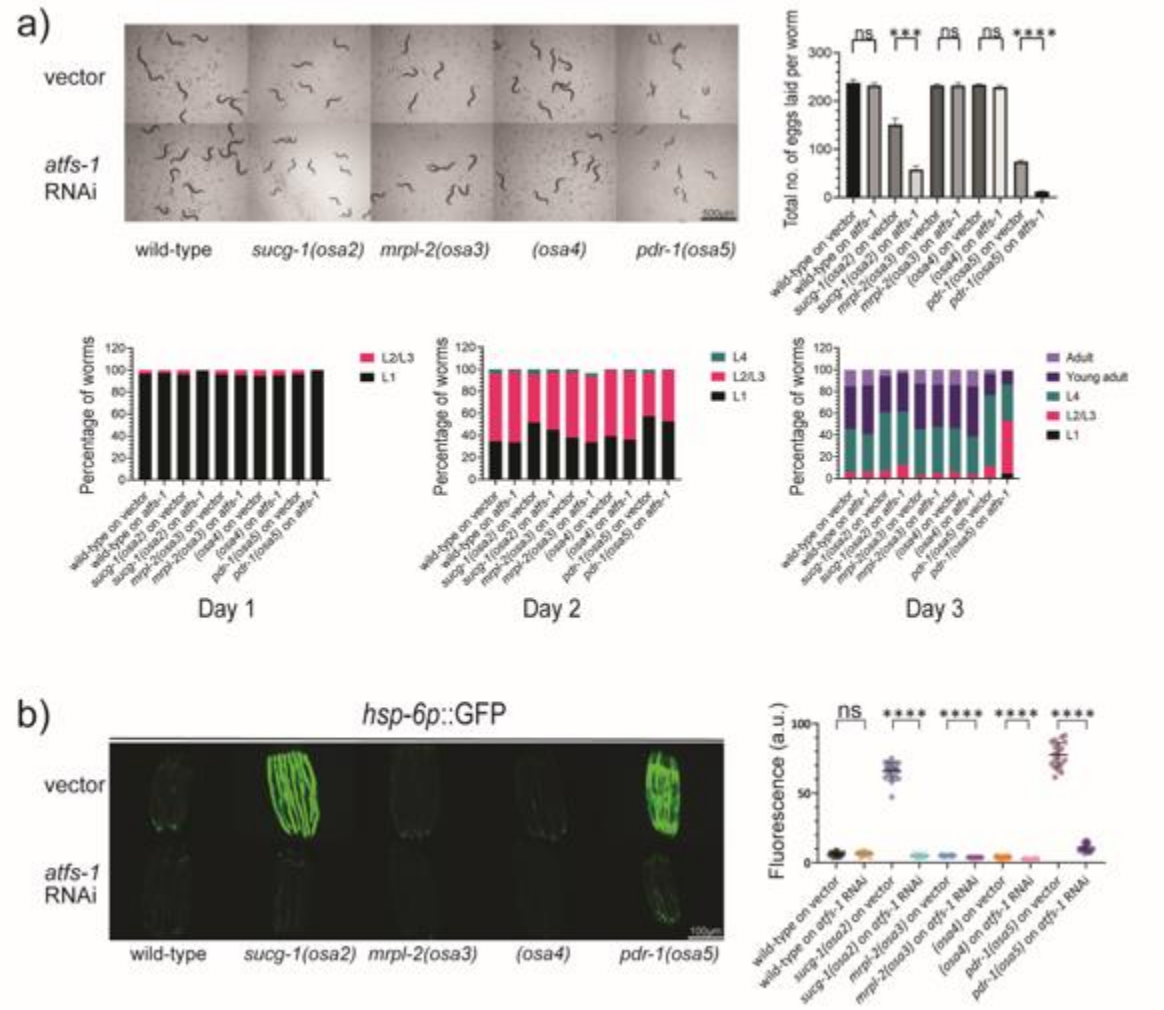

Figure S1. *atfs-1* RNAi impairs development/fertility of *sucg-1(osa2)* and *pdr-1*(*osa5)* but not *mrpl-2(osa3)* or *osa4* animals.

(A) Photomicrographs and quantifications of developmental stage and fertility of wild-type, *sucg-1*(*osa2)*, *mrpl-2(osa3)*, *osa4*, or *pdr-1(osa5)* animals grown on control or *atfs-1* RNAi plates. (mean ±SD; $n \geq 20$); ns denotes not significant, *** denotes $p \leq 0.001$, **** denotes $p \leq 0.0001$ (Student's *t* test).

(B) Photomicrographs and quantification of *hsp-6p*::GFP expression in wild-type, *sucg-1(osa2)*, *mrpl-2(osa3)*, *osa4*, or *pdr-1(osa5)* animals grown on control or *atfs-1* RNAi plates. Quantification of fluorescence intensities expressed as arbitrary units (A.U.); (mean ±SD; $n \geq 20$); ns denotes not significant, **** denotes $p \leq 0.0001$ (Student's *t* test).

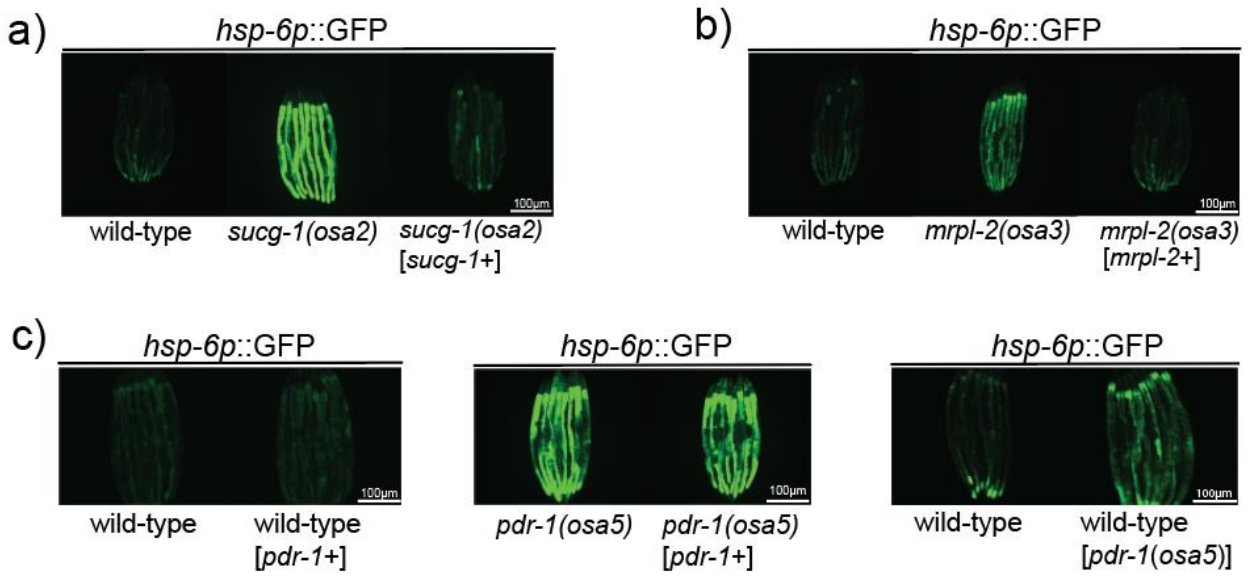

Figure S2. Germline rescue of *sucg-1(osa2)*, *mrpl-2(osa3)* and *pdr-1(osa5)*.

(A) Photomicrographs of *hsp-6p*::GFP expression in wild-type, *sucg-1(osa2)*, and *sucg-1(osa2)* [*sucg-1*+].

(B) Photomicrographs of *hsp-6p*::GFP expression in wild-type, *mrpl-2(osa3)*, and *mrpl-2(osa3)* [*mrpl-2*+].

(C) Photomicrographs of *hsp-6p*::GFP expression in wild-type, wild-type [*pdr-1*+], *pdr-1(osa5)* [*pdr-1*+], and wild-type [*pdr-1*(*osa5*)].

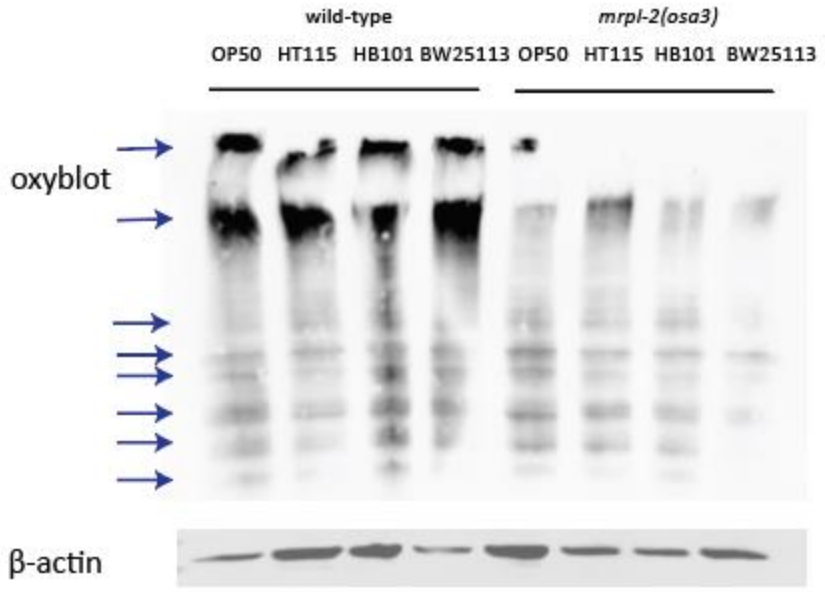

Figure S3. Representative image of the OxyBlot experiment performed for Figure 2C.

OxyBlots were generated as described in the Materials and Methods section. Arrows indicate density peaks that were used in the generation of the OxyBlot value.

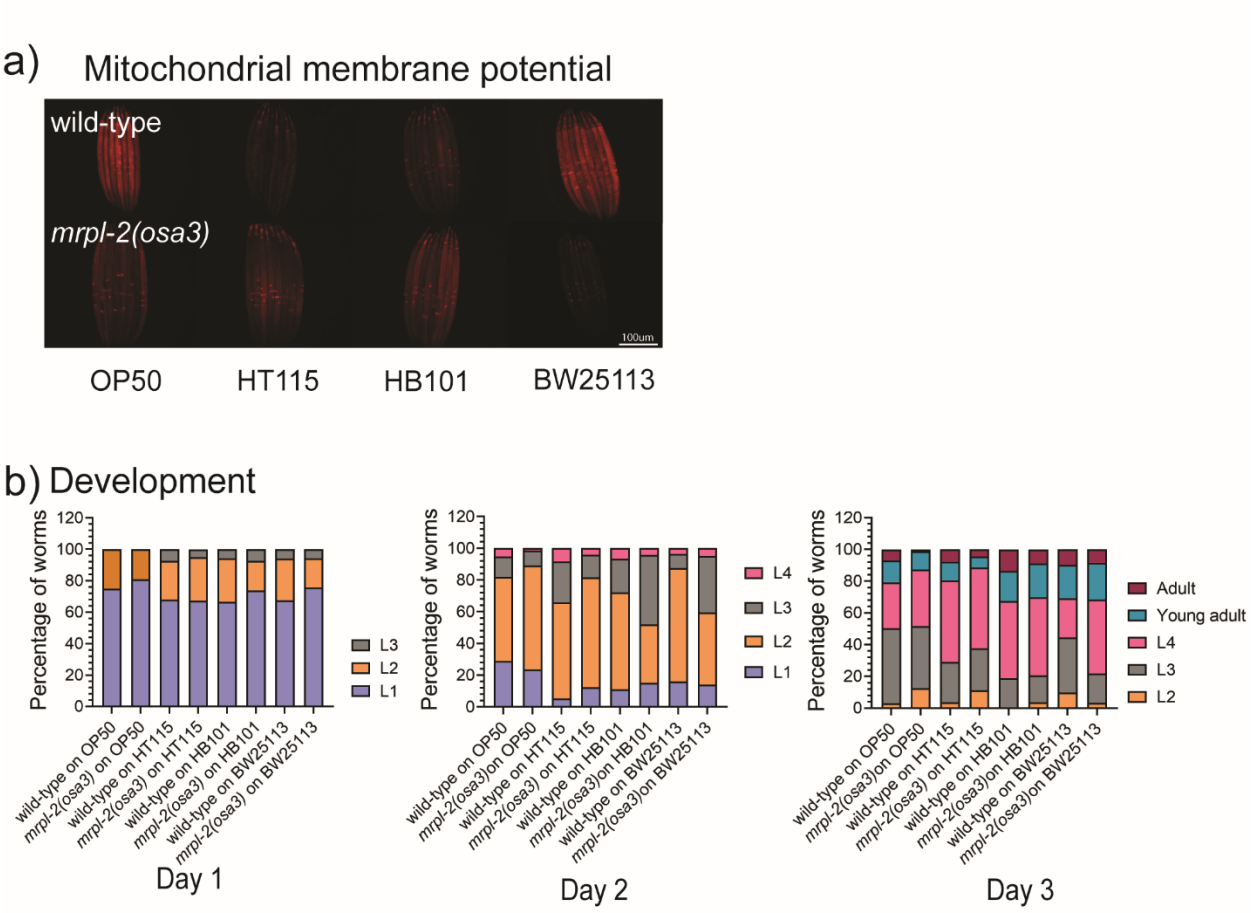

Figure S4. No change in the developmental rates of *mrpl-2(osa3)* animals fed various *E. coli* diets.

(A) Photomicrographs of wild-type and *mrpl-2(osa3)* animals fed *E. coli* OP50, HT115, HB101, and BW25113 and stained with TMRE dye.

(B) Quantification of developmental stages at various time points for wild-type or *mrpl-2(osa3)* animals fed various *E. coli* diets (n = 3).

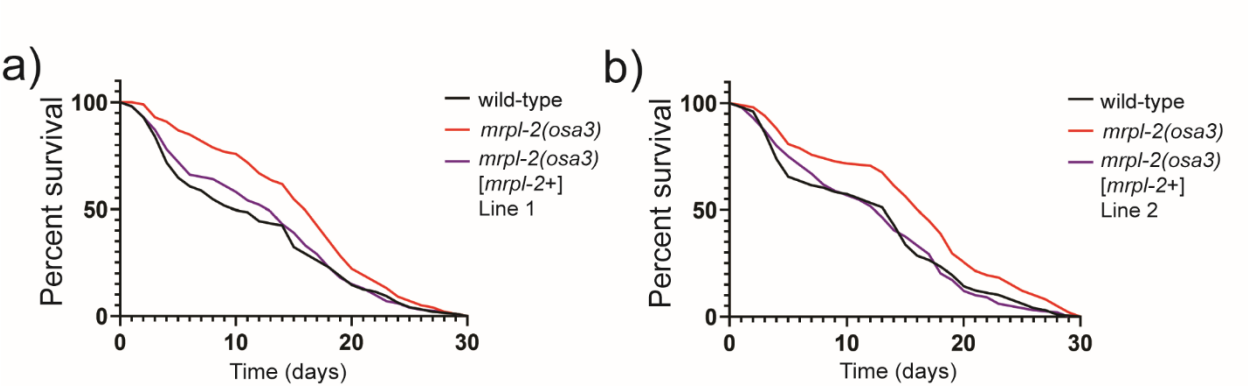

Figure S5. Rescue of *mrpl-2(osa3)* lifespan extension on a diet of *E. coli* OP50 through introduction of a wild-type *mrpl-2* transgene.

(A, B) Lifespans of wild-type, *mrpl-2(osa3), and mrpl-2(osa3)* [*mrpl-2+*] fed a diet of *E. coli* OP50. Independent transgenic line 1 (A) and line 2 (B) are shown.

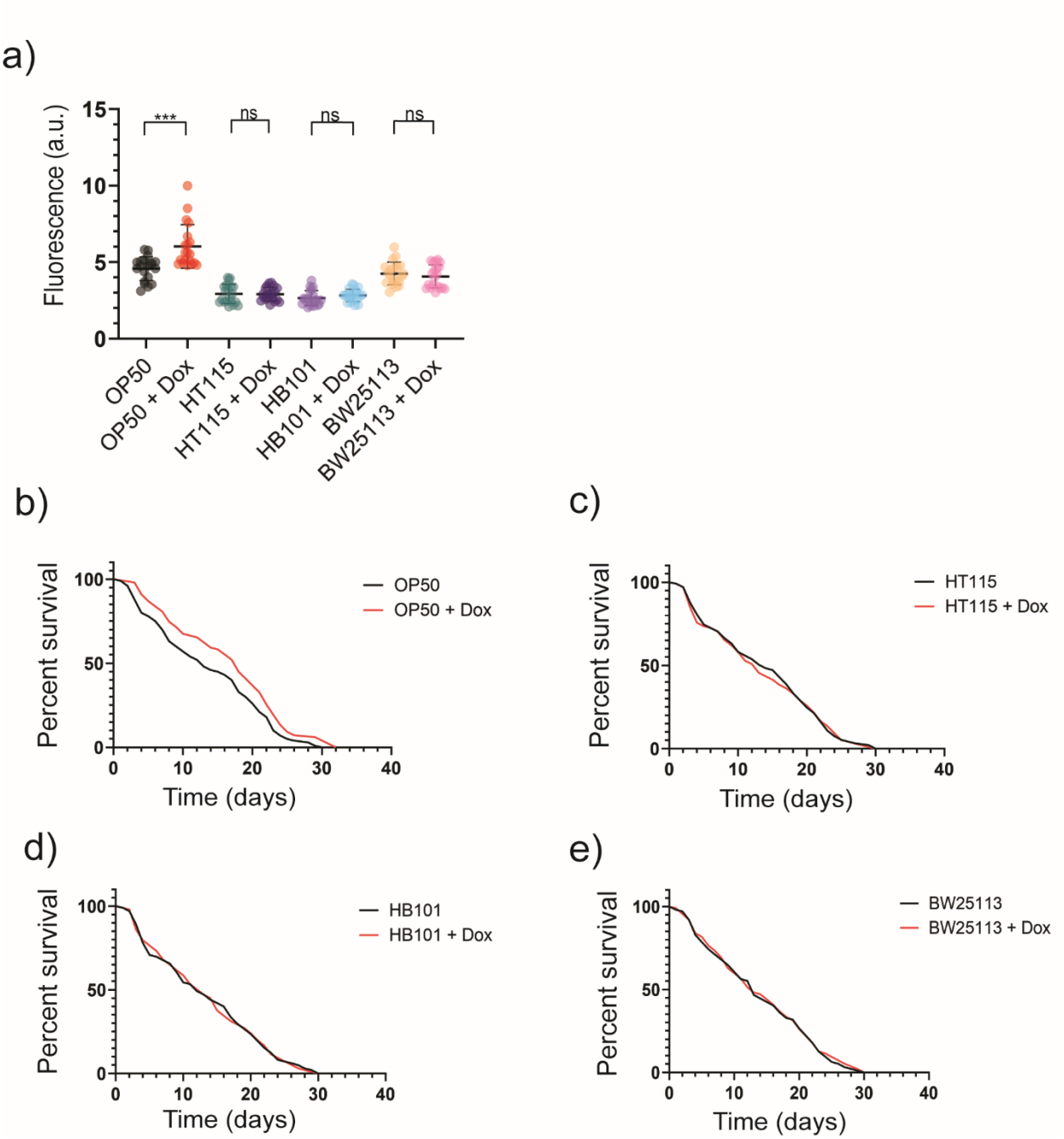

Figure S6. Mild impairment to mitochondrial translation using doxycycline activates the UPR^{mt} and extends wild-type animal lifespan in a diet-dependent manner.

(A) Quantification of *hsp-6p*::GFP expression in wild-type animals fed diets of *E. coli* OP50, HT115, HB101, or BW25113 in the presence or absence of 6 µg/ml doxycycline. Quantification

of fluorescence intensities expressed as arbitrary units (A.U.); (mean ±SD; $n \geq 20$); ns denotes not significant, *** denotes $p \leq 0.001$ (Student's *t* test).

(B-E) Lifespans of wild-type animals fed diets of *E. coli* OP50, HT115, HB101, or BW25113 in the presence or absence of 6 µg/ml doxycycline.

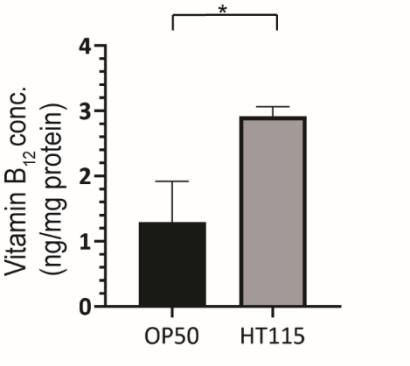

Figure S7. Vitamin B12 levels are lower in animals fed *E. coli* OP50 relative to *E. coli* HT115.

Quantification of vitamin B12 levels in wild-type animals fed *E. coli* OP50 versus HT115 (see Materials and Methods for details). (mean ±SD; $n=3$); * denotes $p \leq 0.05$ (Student's *t* test).

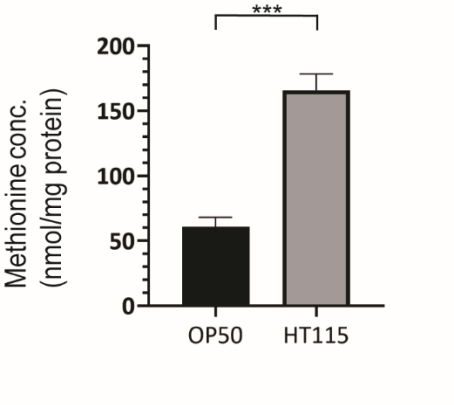

Figure S8. Methionine levels are reduced in animals fed *E. coli* OP50 relative to those fed *E. coli* HT115.

Quantification of methionine levels in wild-type animals fed *E. coli* OP50 versus HT115 (see Materials and Methods for details). (mean $\pm$SD; n=4); *** denotes $p \leq 0.001$ (Student's *t* test).

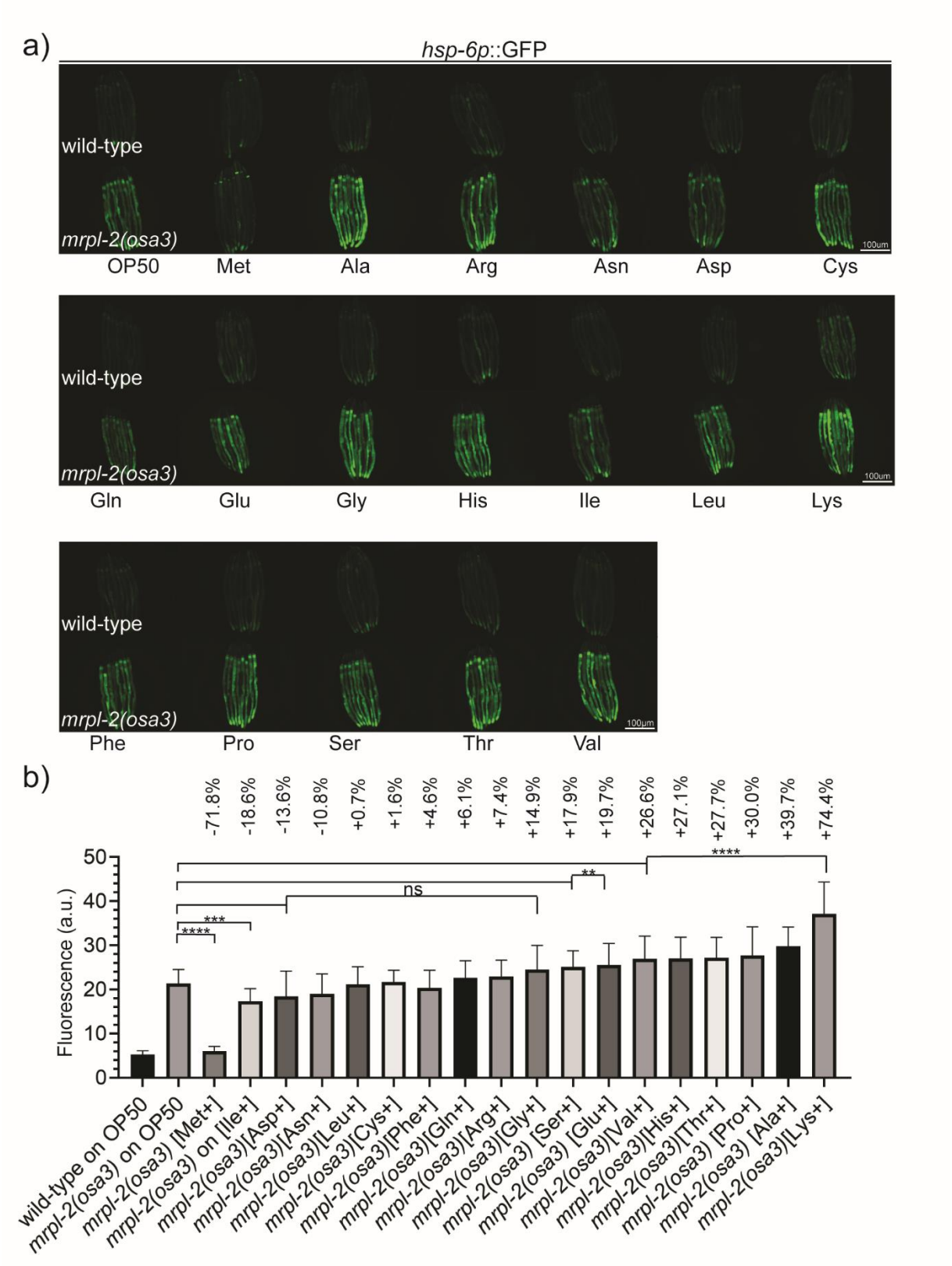
a)
hsp-6p::GFP
wild-type
mrpl-2(osa3)
OP50
Met
Ala
Arg
Asn
Asp
Cys
Gln
Glu
Gly
His
Ile
Leu
Lys
Phe
Pro
Ser
Thr
Val
100um
b)
-71.8%
-18.6%
-13.6%
-10.8%
+0.7%
+1.6%
+4.6%
+6.1%
+7.4%
+14.9%
+17.9%
+19.7%
+26.6%
+27.1%
+27.7%
+30.0%
+39.7%
+74.4%
Fluorescence (a.u.)
0
10
20
30
40
50
****
***
****
ns
**
****
wild-type on OP50
mrpl-2(osa3) on OP50
mrpl-2(osa3) [Met+]
mrpl-2(osa3) on [Ile+]
mrpl-2(osa3)[Asp+]
mrpl-2(osa3)[Asn+]
mrpl-2(osa3)[Leu+]
mrpl-2(osa3)[Cys+]
mrpl-2(osa3)[Phe+]
mrpl-2(osa3)[Gln+]
mrpl-2(osa3)[Arg+]
mrpl-2(osa3)[Gly+]
mrpl-2(osa3) [Ser+]
mrpl-2(osa3) [Glu+]
mrpl-2(osa3)[Val+]
mrpl-2(osa3)[His+]
mrpl-2(osa3)[Thr+]
mrpl-2(osa3) [Pro+]
mrpl-2(osa3) [Ala+]
mrpl-2(osa3)[Lys+]

Figure S9. Methionine supplementation suppresses UPR^{mt} activation in *mrpl-2(osa3)* animals fed a diet of *E. coli* OP50.

(A, B) Photomicrographs and quantification of *hsp-6p*::GFP expression of wild-type and *mrpl-2(osa3)* fed an *E. coli* OP50 diet in the presence or absence of the indicated amino acids at a concentration of 10 mM. Quantification of fluorescence intensities expressed as arbitrary units (A.U.); (mean $\pm$SD; $n \geq 20$); ns denotes not significant, * denotes $p \leq 0.05$, ** denotes $p \leq 0.01$, *** denotes $p \leq 0.001$, **** denotes $p \leq 0.0001$ (Student's *t* test).

SUPPLEMENTARY TABLES

Figure	Replicate	Control Strain (no. of animals scored)	Mean Lifespan (days)	Test Strain (no. of animals scored)	Mean Lifespan (days)	Percent change	*p*-value
							$p>0.05$ = ns
3a	1	wild-type on OP50 (91)	11.16	*mrpl-2(osa3)* on OP50 (95)	15.64	40.14	0.0004
	2	wild-type on OP50 (92)	10.79	*mrpl-2(osa3)* on OP50 (99)	15.57	44.30	0.0182
	3	wild-type on OP50 (94)	11.97	*mrpl-2(osa3)* on OP50 (97)	15.45	29.07	0.0002
3b	1	wild-type on HT115 (95)	12.23	*mrpl-2(osa3)* on HT115 (96)	11.73	-4.09	ns
	2	wild-type on HT115 (95)	11.75	*mrpl-2(osa3)* on HT115 (93)	11.46	-2.47	ns
	3	wild-type on HT115 (98)	13.78	*mrpl-2(osa3)* on HT115 (90)	13.69	-0.65	ns
3c	1	wild-type on HB101 (98)	15.91	*mrpl-2(osa3)* on HB101 (99)	16.69	4.90	ns
	2	wild-type on HB101 (100)	16.42	*mrpl-2(osa3)* on HB101 (98)	16.82	2.44	ns
	3	wild-type on HB101 (91)	17.79	*mrpl-2(osa3)* on HB101 (100)	18.2	2.30	ns
3d	1	wild-type on BW25113 (94)	11.68	*mrpl-2(osa3)* on BW25113 (98)	12.9	10.45	ns
	2	wild-type on BW25113 (94)	11.49	*mrpl-2(osa3)* on BW25113 (95)	12.67	10.27	ns
	3	wild-type on BW21135 (97)	11.44	*mrpl-2(osa3)* on BW25113 (95)	12.92	12.94	ns
5c	1	wild-type on OP50 (94)	10.79	*mrpl-2(osa3)* on OP50 (97)	15.57	44.30	0.0002
	2	wild-type on OP50 (91)	11.16	*mrpl-2(osa3)* on OP50 (95)	15.64	40.14	0.0004
	3	wild-type on OP50 (98)	11.71	*mrpl-2(osa3)* on OP50(96)	15.29	30.57	0.044

	1	wild-type on OP50 (94)	10.79	wild-type on OP50 + MeCbl (89)	9.86	-8.62	ns
	2	wild-type on OP50 (91)	11.16	wild-type on OP50 + MeCbl (85)	10.18	-8.78	ns
	3	wild-type on OP50 (98)	11.71	wild-type on OP50 + MeCbl (100)	11.8	0.77	ns
	1	wild-type on OP50 (94)	10.79	*mrpl-2(osa3)* on OP50 + MeCbl (87)	8.84	-18.07	ns
	2	wild-type on OP50 (91)	11.16	*mrpl-2(osa3)* on OP50 + MeCbl (86)	9.58	-14.16	ns
	3	wild-type on OP50 (98)	11.71	*mrpl-2(osa3)* on OP50 + MeCbl (98)	12.77	9.05	ns
5f	1	wild-type on HT115 vit $B12^-$ (95)	9.75	*mrpl-2(osa3)* on HT115 vit $B12^-$ (93)	13.84	41.95	0.0003
	2	wild-type on HT115 vit $B12^-$ (92)	9.5	*mrpl-2(osa3)* on HT115 vit $B12^-$ (95)	13.4	41.05	0.0015
	3	wild-type on HT115 vit $B12^-$ (98)	9.63	*mrpl-2(osa3)* on HT115 vit $B12^-$ (97)	13.42	39.36	0.0004
	1	wild-type on HT115 vit $B12^-$ (95)	9.75	wild-type on HT115 vit $B12^-$ +MeCbl (98)	9.87	1.23	ns
	2	wild-type on HT115 vit $B12^-$ (92)	9.5	wild-type on HT115 vit $B12^-$ +MeCbl (99)	9.74	2.53	ns
	3	wild-type on HT115 vit $B12^-$ (98)	9.63	wild-type on HT115 vit $B12^-$ +MeCbl (95)	10.33	7.27	ns
	1	wild-type on HT115 vit $B12^-$ (95)	9.75	*mrpl-2(osa3)* on HT115 vit $B12^-$ +MeCbl (90)	10.27	5.33	ns
	2	wild-type on HT115 vit $B12^-$ (92)	9.5	*mrpl-2(osa3)* on HT115 vit $B12^-$ +MeCbl (91)	10.21	7.47	ns
	3	wild-type on HT115 vit $B12^-$ (98)	9.63	*mrpl-2(osa3)* on HT115 vit $B12^-$ +MeCbl (91)	10.36	7.58	ns

6d	1	wild-type (95)	11.75	*mrpl-2(osa3)* (93)	11.46	-2.47	ns
	2	wild-type (98)	13.78	*mrpl-2(osa3)* (90)	13.69	-0.65	ns
	3	wild-type (95)	12.23	*mrpl-2(osa3)* (96)	11.42	-6.62	ns
	1	wild-type (95)	11.75	*metr-1(ok521)* (91)	13.99	19.06	0.0449
	2	wild-type (98)	13.78	*metr-1(ok521)* (93)	15.46	12.19	0.0267
	3	wild-type (95)	12.23	*metr-1(ok521)* (90)	14.51	18.64	0.0315
	1	wild-type (95)	11.75	*metr-1(ok521); mrpl-2(osa3)* (95)	15.91	35.40	0.0033
	2	wild-type (98)	13.78	*metr-1(ok521); mrpl-2(osa3)* (105)	15.74	14.22	0.018
	3	wild-type (95)	12.23	*metr-1(ok521); mrpl-2(osa3)* (90)	15.38	25.76	0.0071
6e	1	wild-type (98)	13.33	*mrpl-2(osa3)* (97)	13.81	3.60	ns
	2	wild-type (99)	13.2	*mrpl-2(osa3)* (98)	14.11	6.89	ns
	3	wild-type (99)	13.62	*mrpl-2(osa3)* (94)	13.86	1.76	ns
	1	wild-type (98)	13.33	*mmcm-1(ok1637)* (97)	16.46	23.48	0.0359
	2	wild-type (99)	13.2	*mmcm-1(ok1637)* (94)	15.81	19.77	0.0108
	3	wild-type (99)	13.62	*mmcm-1(ok1637)* (98)	16.22	19.09	0.0294
	1	wild-type (98)	13.33	*mmcm-1(ok1637); mrpl-2(osa3)* (94)	14.55	9.15	ns
	2	wild-type (99)	13.2	*mmcm-1(ok1637); mrpl-2(osa3)* (100)	13.93	5.53	ns
	3	wild-type (99)	13.62	*mmcm-1(ok1637); mrpl-2(osa3)* (97)	14.97	9.91	ns
6f	1	wild-type (97)	11.19	*mrpl-2(osa3)* (92)	15.98	42.81	<0.0001
	2	wild-type (94)	11.21	*mrpl-2(osa3)* (94)	15.31	36.57	0.0007
	3	wild-type (94)	10.55	*mrpl-2(osa3)* (93)	13.97	32.42	0.0002
	1	wild-type (97)	11.19	*metr-1(ok521)* (92)	15.04	34.41	0.0002
	2	wild-type (94)	11.21	*metr-1(ok521)* (90)	14.92	33.10	0.0003
	3	wild-type (94)	10.55	*metr-1(ok521)* (94)	14.31	35.64	0.0003

	1	wild-type (97)	11.19	*metr-1(ok521); mrpl-2(osa3)* (93)	15.02	34.23	0.0001
	2	wild-type (94)	11.21	*metr-1(ok521); mrpl-2(osa3)* (91)	14.14	26.14	0.0079
	3	wild-type (94)	10.55	*metr-1(ok521); mrpl-2(osa3)* (97)	13.86	31.37	0.0029
6g	1	wild-type (97)	11.19	*mrpl-2(osa3)* (92)	15.98	42.81	<0.0001
	2	wild-type (94)	11.21	*mrpl-2(osa3)* (94)	15.31	36.57	0.0007
	3	wild-type (94)	10.55	*mrpl-2(osa3)* (93)	13.97	32.42	0.0002
	1	wild-type (97)	11.19	*mmcm-1(ok1637)* (98)	13.18	17.78	ns
	2	wild-type (94)	11.21	*mmcm-1(ok1637)* (99)	12.71	13.38	ns
	3	wild-type (94)	10.55	*mmcm-1(ok1637)* (97)	12.49	18.39	ns
	1	wild-type (97)	11.19	*mmcm-1(ok1637); mrpl-2(osa3)* (93)	13.35	19.30	ns
	2	wild-type (94)	11.21	*mmcm-1(ok1637); mrpl-2(osa3)* (98)	12.56	12.04	ns
	3	wild-type (94)	10.55	*mmcm-1(ok1637); mrpl-2(osa3)* (97)	12.96	22.84	ns

Note: for Fig 6f and 6g, experiments were done simultaneously and the data for wild-type and *mrpl-2(osa3)* come from the same biological replicates

6j	1	wild-type on OP50 (100)	12.42	*mrpl-2(osa3)* on OP50 (98)	15.48	24.64	0.0073
	2	wild-type on OP50 (99)	12.5	*mrpl-2(osa3)* on OP50 (98)	15.77	26.16	0.0081
	3	wild-type on OP50 (100)	12.26	*mrpl-2(osa3)* on OP50 (100)	15.45	26.02	0.0096
	1	wild-type on OP50 (100)	12.42	Wild-type on OP50 + Methionine (98)	11.42	-8.05	ns
	2	wild-type on OP50 (99)	12.5	Wild-type on OP50 + Methionine (95)	11.42	-8.64	ns
	3	wild-type on OP50 (100)	12.26	Wild-type on OP50 + Methionine (97)	11.4	-7.01	ns
	1	wild-type on OP50 (100)	12.42	*mrpl-2(osa3)* on OP50 + Methionine (99)	12.35	-0.56	ns

	2	wild-type on OP50 (99)	12.5	*mrpl-2(osa3)* on OP50 + Methionine (96)	12.99	3.92	ns
	3	wild-type on OP50 (100)	12.26	*mrpl-2(osa3)* on OP50 + Methionine (97)	12.56	2.45	ns
7f	1	wild-type (90)	10.26	*atfs-1(tm4525)* (99)	9.98	-2.73	ns
	2	wild-type (93)	10.48	*atfs-1(tm4525)* (96)	9.67	-7.73	ns
	3	wild-type (95)	10.45	*atfs-1(tm4525)* (92)	9.16	-12.34	ns
	1	wild-type (90)	10.26	*mrpl-2(osa3)* (97)	14.58	42.11	0.0012
	2	wild-type (93)	10.48	*mrpl-2(osa3)* (91)	14.49	38.26	0.0012
	3	wild-type (95)	10.45	*mrpl-2(osa3)* (96)	13.84	32.44	0.0018
	1	wild-type (90)	10.26	*atfs-1(tm4525); mrpl-2(osa3)* (98)	12.56	22.42	ns
	2	wild-type (93)	10.48	*atfs-1(tm4525); mrpl-2(osa3)* (100)	12.34	17.75	ns
	3	wild-type (95)	10.45	*atfs-1(tm4525); mrpl-2(osa3)* (98)	11.65	11.48	ns
7g	1	wild-type (90)	10.26	*atfs-1(tm4525)* (99)	9.98	-2.73	ns
	2	wild-type (93)	10.48	*atfs-1(tm4525)* (96)	9.67	-7.73	ns
	3	wild-type (95)	10.45	*atfs-1(tm4525)* (92)	9.16	-12.34	ns
	1	wild-type (90)	10.26	*metr-1(ok521)* (92)	14.66	42.88	0.0013
	2	wild-type (93)	10.48	*metr-1(ok521)* (98)	15.03	43.42	0.0006
	3	wild-type (95)	10.45	*metr-1(ok521)* (95)	14.34	37.22	0.0016
	1	wild-type (90)	10.26	*metr-1(ok521); atfs-1(tm4525)* (98)	12.41	20.96	ns
	2	wild-type (93)	10.48	*metr-1(ok521); atfs-1(tm4525)* (94)	12.57	19.94	ns
	3	wild-type (95)	10.45	*metr-1(ok521); atfs-1(tm4525)* (93)	11.38	8.90	ns

Note: for Fig 7f and 7g, experiments were done simultaneously and the data for wild-type and *atfs-1(tm4525)* come from the same biological replicates

S4a	1	wild-type (100)	11.48	*mrpl-2(osa3)* (98)	15.44	34.49	0.0022
	2	wild-type (98)	11.44	*mrpl-2(osa3)* (99)	15.26	33.39	0.0126
	3	wild-type (95)	11.48	*mrpl-2(osa3)* (98)	15.25	32.84	0.0143
	1	wild-type (100)	11.48	*mrpl-2(osa3)* [*mrpl-2*+] Line 1 (98)	12.37	7.75	ns
	2	wild-type (98)	11.44	*mrpl-2(osa3)* [*mrpl-2*+] Line 1 (100)	12.46	8.92	ns
	3	wild-type (95)	11.48	*mrpl-2(osa3)* [*mrpl-2*+] Line 1 (99)	12.11	5.49	ns
S4b	1	wild-type (98)	12.05	*mrpl-2(osa3)* (98)	15.38	27.63	0.0048
	2	wild-type (98)	11.89	*mrpl-2(osa3)* (99)	15.33	28.93	0.0044
	3	wild-type (99)	11.77	*mrpl-2(osa3)* (99)	14.88	26.42	0.0103
	1	wild-type (98)	12.05	*mrpl-2(osa3)* [*mrpl-2*+] Line 2 (99)	12.24	1.58	ns
	2	wild-type (98)	11.89	*mrpl-2(osa3)* [*mrpl-2*+] Line 2 (98)	12.32	3.62	ns
	3	wild-type (99)	11.77	*mrpl-2(osa3)* [*mrpl-2*+] Line 2 (99)	12.49	6.12	ns
S6b	1	wild-type on OP50 (100)	13.56	wild-type on OP50 + Dox (98)	16.04	18.29	0.014
	2	wild-type on OP50(97)	12.96	wild-type on OP50 + Dox (99)	15.56	20.06	0.008
	3	wild-type on OP50 (95)	13.07	wild-type on OP50 + Dox (99)	15.59	19.28	0.048
S6c	1	wild-type on HT115 (95)	13.19	wild-type on HT115 + Dox (97)	12.97	-1.67	ns
	2	wild-type on HT115 (97)	13.23	wild-type on HT115 + Dox (96)	13.35	0.91	ns
	3	wild-type on HT115 (96)	13.22	wild-type on HT115 + Dox (96)	13.55	2.50	ns
S6d	1	wild-type on HB101 (98)	12.98	wild-type on HB101 + Dox (96)	12.74	-1.85	ns
	2	wild-type on HB101 (98)	13.33	wild-type on HB101 + Dox (97)	12.95	-2.85	ns
	3	wild-type on HB101 (98)	12.94	wild-type on HB101 + Dox (98)	12.32	-4.79	ns

S6e	1	wild-type on BW25113 (96)	13.94	wild-type on BW25113 + Dox (98)	13.52	-3.01	ns
	2	wild-type on BW25113 (96)	12.97	wild-type on BW25113 + Dox (99)	13.56	4.55	ns
	3	wild-type on BW25113 (95)	13.21	wild-type on BW25113 + Dox (96)	13.58	2.80	ns

S1 Table. Summary of lifespan and survival data with statistics.

https://doi.org/10.1371/journal.pgen.1009234.s011 (XLSX)

S2 Table. Summary of RNA sequencing analysis comparing wild-type, *mrpl-2(osa3)*, and *metr-1(ok521)* animals fed *E. coli* OP50.

Chapter 4

Investigating the association between the mechanisms of methionine restriction and UPR^{mt} regulation

Abstract

A known relationship exists between diet and the determination of organismal lifespan. For example, reduced food intake while maintaining nutrition levels has improved aging and aging-related diseases in invertebrates, such as rodents, primates, and humans. Moreover, reduced intake of specific nutrients, like methionine or cysteine, also plays a role in promoting the health of the organism. Extensive lines of evidence from various model organisms demonstrate an association between aging and multiple nutrient-signaling pathways, including mTOR (mechanistic target of rapamycin), insulin/IGF-1-like signaling, and sirtuins in mediating the effects of dietary restriction (DR). We previously discovered that methionine restriction promotes lifespan extension via the mitochondrial unfolded protein response (UPR^{mt}) in *C. elegans*, though the mechanistic basis of this relationship was not identified. We begin an exploration of this mechanism using a forward genetic approach with the hope of identifying specific molecular factors that mediate the activation of the UPR^{mt} resulting from methionine restriction.

Introduction

Methionine is a proteogenic amino acid that is acquired from food and gastrointestinal microbes. During translation, an "initiator" tRNA carries the first amino acid, which is usually methionine. This makes methionine an essential protein synthesis element in prokaryotes and eukaryotes [1, 2]. In addition, methionine also acts as catalytic antioxidants, protecting proteins inside cells [3]. Methionine also serves major roles via its metabolism. Methionine uptake and metabolism are involved in several cellular functions, acting as a precursor for glutamine synthesis and the primary methyl donor for nucleic acid, phospholipid, histone, and protein methylation. It also serves as a pivotal link to the folate cycle during the transsulfuration pathway [4, 5, 6].

Aging is a universal process that affects all organs and causes a decline in their function. Aging causes cellular dysfunction, which perturbs cellular homeostasis, resulting in reduced responsiveness to intracellular stresses, including oxidative stress [7]. However, studies have shown that dietary intervention without causing malnutrition can improve organismal health promote lifespan extension. While it has long been appreciated that dietary restriction (DR) extends lifespan [8], more recent studies indicate that manipulating specific nutrient levels in the diet can also affect aging. For example, reducing methionine from the diet (known as methionine restriction; MR) has been shown to mimic the effects of DR and lifespan extension in various model organisms, including flies, worms, and rodents [9]. Also, in yeast, the reduction in glucose availability downregulates the biosynthesis of methionine, which decreases the overall intracellular methionine concentration and extends lifespan [10]. Research conducted by the Orentriech group first reported that an 80% reduction in methionine levels from the diet increases the lifespan of Fischer 344 rats [11]. Moreover, Richie *et al.* demonstrated that a similar MR level showed a lifespan increase in Fischer rats compared to controls [12].

Similarly, feeding BALB/cJ × C57BL/6J F1 mice food with 65% less methionine increased their lifespan [13]. Lastly, in *C. elegans,* it has been shown that knockdown of SAMS-1/C49F5.1, which encodes methionine adenosyltransferase (MAT), can extend lifespan. MAT is an enzyme that catalyzes the biosynthesis of SAM (S-adenosylmethionine), which is the first step in methionine metabolism. Interestingly, Hansen et al. found that SAMS-1 knockdown did not affect feeding rates (as assessed by pharyngeal pumping) but still resulted in slender worms with reduced fertility and extended longevity [14]. This was further validated by Ching et al., showing that overexpression of SAMS-1 could partially suppress the extended lifespan that resulted from the RNAi knockdown of *sams-1* [15]. Hence, extension in lifespan via reduced MAT activity proposes that limiting methionine synthesis is beneficial for lifespan. Parkhitko et al. hypothesize that lowering the activity of the first enzyme in the methionine cycle can limit the flux through the process, which helps extend lifespan. This may also prevent the accumulation of harmful metabolites through the methionine cycle, which is consistent with the effects of MR [5]. Additionally, metformin, a drug used to treat type 2 diabetes (T2D), can increase lifespan in *C. elegans* when supplemented with their *E. coli* OP50 diet. Metformin impairs microbial folate metabolism and affects the methionine cycle, which causes a decrease in SAM concentration in the worms, which modestly increased the mean lifespan of the worms [16].

Aging is associated with tissue and organ dysfunction and increased occurrences of chronic disorders. Therefore, it is expected that nutritional interventions in MR may offer some benefits to prevent age-related illnesses. For example, Malloy et al. showed that a 0.2% methionine diet reduced visceral fat buildup and improved insulin sensitivity in aging Fischer 344 mice independent of energy restriction [17]. It has also been reported that MR can reduce leptin while increasing adiponectin levels in rats [17]. Leptin is a hormone primarily made by adipocytes, which helps regulate metabolism and energy homeostasis by inhibiting hunger [18]. On the other

hand, adiponectin is a peptide that activates fatty acid oxidation and glucose uptake in skeletal muscle and adipose tissue, which improves insulin sensitivity, increasing energy expenditure throughout the body [19]. Ables et al. also reported that MR protects high-fat diet (HFD)-induced obesity in mice and insulin insensitivity and T2D when they are fed a 0.12% diet of methionine compared to a 0.86% diet methionine diet [20].

Our previous study identified a loss of function mutation in the mitochondrial ribosomal protein large subunit (*mrpl-2*) that could induce UPR^{mt} activation when fed a particular diet. When provided *E. coli* OP50 bacteria with low vitamin $B_{12,}$ it extended lifespan in *mrpl-2(osa3)* worms in a UPR^{mt}-dependent manner [21]. Vitamin B_{12} acts as a cofactor for the metabolic enzymes methionine synthase and methylmalonyl CoA mutase. We discovered that the low vitamin B_{12} diet caused reduced methionine synthase, which converts homocysteine to methionine, resulting in mild methionine restriction. We also found that genetic loss of methionine synthase, *metr-1*, could activate the UPR^{mt} and extend lifespan [21]. Although methionine is mainly obtained through the bacterial diet, a small amount is produced in the host by METR-1 in *C. elegans*. Hence, if METR-1 is impaired, it can create a sensitized condition for methionine restriction [22]. How methionine restriction activates the UPR^{mt} is not known. Therefore, this project aims to identify pathways involved in UPR^{mt}-induced longevity as a result of methionine restriction caused by the loss of METR-1/methionine synthase.

Materials and methods

EMS mutagenesis

Approximately 2000 *metr-1(ok521); hsp-6p*::GFP animals were harvested from NGM plates with S-basal. The worms were washed twice to remove bacteria and resuspended in 2 ml S-basal. 2 ml of 2X ethyl methyl sulfonate (EMS) solution (60 μM) was added to worm suspension and placed on a rocker for 4 hrs. After 4 hours, the worms were washed three times with S-basal, resuspended in 0.5 ml S-basal and plated onto seeded NGM plates. After overnight incubation, approximately 160 adult worms were singled out into NGM plates and allowed to grow until F1 generation (3 days). F1 worms showing no fluorescence were selected for further study.

Microscopy

All fluorescent images were taken using a Zeiss Observer Z1 upright microscope. The worms were anesthetized using 2.5 mM sodium azide in S-Basal and transferred to an agarose pad-lined glass microscopy slides for visualization. ImageJ software was used for the quantification of fluorescence intensity. The background fluorescence was deducted from the intestinal fluorescence and divided by the area to produce a fluorescence intensity value. Thus, all photomicrographs show a collection of representative animals. For quantification, 20 worms were scored blindly in three independent replicates.

Results and Future Directions

Forward genetic mutagenesis screen identifies novel alleles that repress the metr-1(ok521)-induced UPR^{mt}

Our previous study showed a correlation between methionine restriction caused by loss of METR-1/methionine synthase and the activation of the UPR^{mt} [72]. We wanted to investigate the mechanistic basis of this pathway activation using a forward genetics suppressor screen. Briefly, *metr-1(ok521)*; *hsp-6p*::GFP were exposed to the mutagen EMS which generated many random mutations in the genome (Figure 1). We then selected animals in the F1 generation that no longer activated the UPR^{mt} reporter *hsp-6p*::GFP or were reduced compared to controls. We first identified 99 F1 worms from the screen that showed lower fluorescence levels than the parent *metr-1(ok521); hsp-6p*::GFP. However, of these 99 mutants, only 75 were fertile, while 36 did not breed true suppressors. Therefore, our final screening result generated 39 independent, viable mutants that displayed lower *hsp-6p*::GFP expression compared to the *metr-1(ok521); hsp-6*::GFP parent strain (mutant alleles *osa9-osa47*) (Figure 2).

We hypothesized that the activation of the UPR^{mt} by *metr-1(ok521)* methionine restriction might be specific to this condition. We, therefore, tested whether our identified suppressors (*osa9-osa47*) could also suppress the UPR^{mt} in the presence of other mitochondrial stresses. Thus, we exposed all suppressors to paraquat, a reagent that disrupts mitochondrial respiration causing mitochondrial dysfunction and activation of the UPR^{mt}. Interestingly, all identified suppressors showed activation of the UPR^{mt} reporter *hsp-6p*::GFP in the presence of paraquat (data not shown). This suggests that the suppressors of *metr-1(ok521)* induced UPR^{mt} activation may be specific for the condition of methionine restriction.

Upon identification of these suppressors, the next step would be the identification of the causative allele. We will next backcross the strain with the parent *metr-1(ok521)* background multiple times to reduce the number of unlinked mutations. Next, we will perform SNP (single nucleotide polymorphism) mapping to narrow the chromosome and region containing the causative allele [23, 24]. This will be followed by whole-genome sequencing [25, 26] to identify all mutations in this region, focusing on those mutations in open reading frames that result in a change in the amino acid. Lastly, we will perform CRISPR/Cas9 genome editing on candidate genes to see if they can phenocopy the originally isolated mutant suppressor (i.e., reduced the *hsp-6p*::GFP expression in the *metr-1(ok521)* background).

References

[1] H. Lodish, A. Berk, S. Zipursky and e. al., "Stepwise Formation of Proteins on Ribosomes.," in *Molecular Cell Biology*, 4th edition ed., New York, W. H. Freeman, 2000, p. Section 4.5.

[2] R. L. Levine, L. Mosoni, B. S. Berlett and E. R. Stadtman, "Methionine residues as endogenous antioxidants in proteins," *Proceedings of the National Academy of Sciences USA*, vol. 93, p. 15036– 15040, 1996.

[3] S. Luo and R. L. Levine, "Methionine in proteins defends against oxidative stress," *FASEB Journal*, vol. 23, p. 464– 472, 2009.

[4] Z. Li, F. Wang, B. Liang and e. al., "Methionine metabolism in chronic liver diseases: an update on molecular mechanism and therapeutic implication.," *Sig Transduct Target Ther*, vol. 5, no. 280, 2020.

[5] A. Parkhitko, P. Jouandin, S. Mohr and N. Perrimon, "Methionine metabolism and methyltransferases in the regulation of aging and lifespan extension across species," *Aging Cell*, vol. 18, no. 13034, 2019.

[6] S. Sanderson, X. Gao, Z. Dai and .. e. al., "Methionine metabolism in health and cancer: a nexus of diet and precision medicine," *Nat Rev Cancer*, vol. 19, p. 625–637, 2019.

[7] M. Kitada, Y. Ogura, I. Monno, J. Xu and D. Koya, "Effect of Methionine Restriction on Aging: Its Relationship to Oxidative Stress," *Biomedicines*, vol. 9, no. 2, 2021.

[8] P. Kapahi, M. Kaeberlein, M. Hansen, "Dietary restriction and lifespan: Lessons from invertebrate models," *Ageing Res Rev.*, vol. 39, p. 3–14, 2017.

[9] B. C. Lee, A. Kaya and V. N. Gladyshev, "Methionine restriction and life-span control.," *Annals of the New York Academy of Sciences*, vol. 1363, p. 116–124, 2016.

[10] K. Zou, S. Rouskin, K. Dervishi, M. McCormick, A. Sasikumar, C. Deng, Z. Chen, M. Kaeberlein, R. Brem, M. Polymenis and e. al., "Life span extension by glucose restriction is abrogated by methionine supplementation: Cross-talk between glucose and and methionine and implication of methionine as a key regulator of life span," *Science Advances*, vol. 6, no. 32, 2020.

[11] N. Orentreich, J. Matias, A. DeFelice and J. Zimmerman, "Low methionine ingestion by rats extends life span.," *J. Nutr.*, vol. 123, no. 2, p. 269–274, 1993.

[12] J. J. Richie, Y. Leutzinger, S. Parthasarathy, V. Malloy, N. Orentreich and J. Zimmerman, "Methionine restriction increases blood glutathione and longevity in F344 rats," *FASEB J.*, vol. 8, p. 1302–1307, 1994.

[13] R. Miller, G. Buehner, Y. Chang, J. Harper, R. Sigler and M. Smith-Wheelock, "Methionine-deficient diet extends mouse lifespan, slows immune and lens aging, alters glucose, T4, IGF-I and insulin levels, and increases hepatocyte MIF levels and stress resistance," *Aging Cell* , ,, vol. 4, p. 119–125, 2005.

[14] M. Hansen, A. L. Hsu, A. Dillin and C. Kenyon, "New genes tied to endocrine, metabolic, and dietary regulation of lifespan from a Caenorhabditis elegans genomic RNAi screen," *PLos genetics*, vol. 1, p. 119– 128, 2005.

[15] T.T. Ching, A.B. Paal, A. Mehta, L. Zhong, A.L. Hsu, "drr-2 encodes an eIF4H that acts downstream of TOR in diet-restriction-induced longevity of C. elegans.," *Aginig Cell*, vol. 9, p. 545– 557, 2010.

[16] F. Cabreiro, C. Au, K. Leung, N. Vergara-Irigaray, H. Cochemé and T. e. a. Noori, "Metformin Retards Aging in C. elegans by Altering Microbial Folate and Methionine Metabolism," *Cell*, vol. 153, no. 1, pp. 228-239, 2013.

[17] V. Malloy, R. Krajcik, S. Bailey, G. Hristopoulos, J. Plummer and N. Orentreich, "Methionine restriction decreases visceral fat mass and preserves insulin action in aging male Fischer 344 rats independent of energy restriction," *Aging Cell*, vol. 5, p. 305–314, 2006.

[18] M. Klok, S. Jakobsdottir and M. Drent, "The role of leptin and ghrelin in the regulation of food intake and body weight in humans: a review," *Obes Rev.*, vol. 8, no. 1, pp. 21-34, 2007.

[19] K. Kraynak, J. Levine and D. Abbott, "Insights Gained From Marmoset Endocrine Research," in *The Common Marmoset in Captivity and Biomedical Research*, American College of Laboratory Animal Medicine, 2019, pp. 525-542.

[20] G. Ables, C. Perrone, D. Orentreich and N. Orentreich, "Methionine-Restricted C57BL/6J Mice Are Resistant to Diet-Induced Obesity and Insulin Resistance but Have Low Bone Density," *PLoS ONE*, vol. 7, no. 12, p. e51357, 2012.

[21] M. Amin, S. Mahmud, J. Dowgielewicz, M. Sapkota and M. Pellegrino, "A novel gene-diet interaction promotes organismal lifespan and host protection during infection via the mitochondrial UPR.," *PLOS genetics*, vol. 16, no. 12, 2020.

[22] F. Cabreiro, C. Au, K. V.-I. N. Leung, H. Cocheme, T. Noori and e. al, "Metformin retards aging in C. elegans by altering microbial folate and methionine metabolism," *Cell*, vol. 153, no. 1, p. 228–39, 2013.

[23] M.W. Davis, M. Hammarlund, T. Harrach, P. Hullett, S. Olsen, E.M. Jorgensen, "Rapid single nucleotide polymorphism mapping in C. elegans," *BMC Genomics*, vol. 6, no. 118, 2005.

[24] D. Fay and A. Bender, "Genetic mapping and manipulation," in *The C. elegans Research Community, WormBook*, , Department of Molecular Biology, University of Wyoming, Laramie, Wyoming 82071-3944 , 2006.

[25] B. Meier, S. L. Cooke, J. Weiss, A. P. Bailly, L. B. Alexandrov, J. Marshall, K. Raine, M. Maddison, E. Anderson, M. R. Stratton, A. Gartner and P. J. Campbell, "C. elegans whole-genome sequencing reveals mutational signatures related to carcinogens and DNA repair deficiency," *Genome Res*, vol. 24, no. 10, p. 1624–1636, 2014.

[26] L. Hillier, G. Marth, A. Quinlan and e. al., "Whole-genome sequencing and variant discovery in C. elegans," *Nat Methods*, vol. 5, p. 183–188, 2008.

Figures

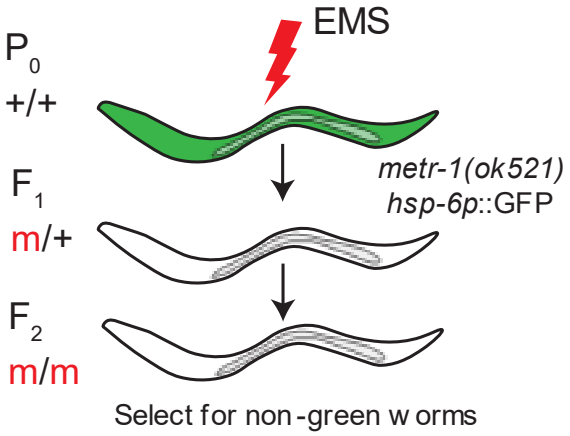

Figure 9 Schematic of the EMS screen for the metr-1(ok521); hsp-6::GFP worms

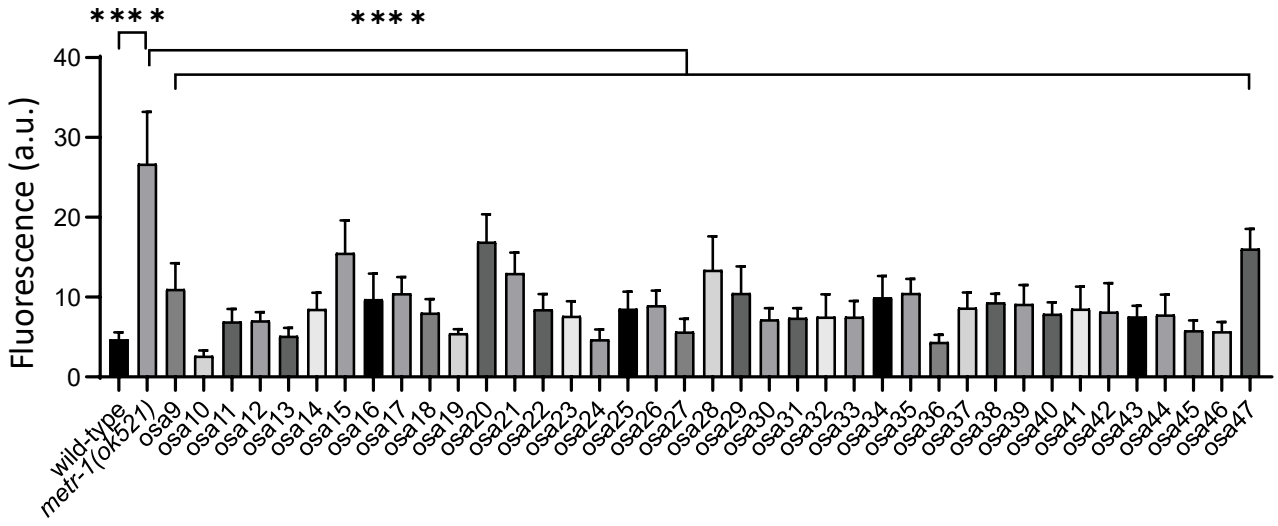

Figure 10 Fluorescence levels of the *osa* worms compared to *metr-1(ok521)* worms.